

FINAL REPORT

A Wireless Platform for Energy Efficient
Building Control Retrofits

ESTCP Project EW-200938

JULY 2012

Satish Narayanan
Sorin Bengea
Yiqing Lin
Russell Taylor
Draguna Vrabie
Shui Yuan
United Technologies Research Center

Stephen Killough
Teja Kuruganti
Wayne Manges
Kenneth Woodworth
Oak Ridge National Laboratory

Francesco Borrelli
Anthony Kelman
University of California Berkeley

This document has been cleared for public release



REPORT DOCUMENTATION PAGE*Form Approved
OMB No. 0704-0188*

The public reporting burden for this collection of information is estimated to average 1 hour per response, including the time for reviewing instructions, searching existing data sources, gathering and maintaining the data needed, and completing and reviewing the collection of information. Send comments regarding this burden estimate or any other aspect of this collection of information, including suggestions for reducing the burden, to the Department of Defense, Executive Services and Communications Directorate (0704-0188). Respondents should be aware that notwithstanding any other provision of law, no person shall be subject to any penalty for failing to comply with a collection of information if it does not display a currently valid OMB control number.

PLEASE DO NOT RETURN YOUR FORM TO THE ABOVE ORGANIZATION.

1. REPORT DATE (DD-MM-YYYY)		2. REPORT TYPE		3. DATES COVERED (From - To)	
4. TITLE AND SUBTITLE				5a. CONTRACT NUMBER	
				5b. GRANT NUMBER	
				5c. PROGRAM ELEMENT NUMBER	
6. AUTHOR(S)				5d. PROJECT NUMBER	
				5e. TASK NUMBER	
				5f. WORK UNIT NUMBER	
7. PERFORMING ORGANIZATION NAME(S) AND ADDRESS(ES)				8. PERFORMING ORGANIZATION REPORT NUMBER	
9. SPONSORING/MONITORING AGENCY NAME(S) AND ADDRESS(ES)				10. SPONSOR/MONITOR'S ACRONYM(S)	
				11. SPONSOR/MONITOR'S REPORT NUMBER(S)	
12. DISTRIBUTION/AVAILABILITY STATEMENT					
13. SUPPLEMENTARY NOTES					
14. ABSTRACT					
15. SUBJECT TERMS					
16. SECURITY CLASSIFICATION OF:			17. LIMITATION OF ABSTRACT	18. NUMBER OF PAGES	19a. NAME OF RESPONSIBLE PERSON
a. REPORT	b. ABSTRACT	c. THIS PAGE			19b. TELEPHONE NUMBER (Include area code)

Table of Contents

List of Figures	4
Acronyms	6
ACKNOWLEDGMENTS	7
1.0 INTRODUCTION	10
1.1 BACKGROUND.....	10
1.2 OBJECTIVE OF THE DEMONSTRATION	11
1.3 REGULATORY DRIVERS.....	11
2.0 TECHNOLOGY DESCRIPTION	11
2.1 TECHNOLOGY OVERVIEW	11
2.2 TECHNOLOGY DEVELOPMENT.....	13
2.2.1 WIRELESS SENSOR NETWORK.....	13
2.2.2 MODEL-BASED PREDICTIVE SUPERVISORY CONTROLLER	15
2.2.2.1 Occupancy Estimation and Forecast Algorithms	15
2.2.2.2 HVAC Models.....	16
2.2.2.3 Building Thermodynamic Model	17
2.2.2.4 Model Predictive Control Algorithm	18
2.3 ADVANTAGES AND LIMITATIONS OF THE TECHNOLOGY.....	19
3.0 PERFORMANCE OBJECTIVES	20
4.0 FACILITY/SITE DESCRIPTION.....	26
4.1 FACILITY/SITE SELECTION	26
4.2 FACILITY/SITE LOCATION AND OPERATIONS	30
4.3 SITE-RELATED PERMITS AND REGULATIONS	30
5.0 TEST DESIGN	31
5.1 CONCEPTUAL TEST DESIGN	31
5.2 BASELINE CHARACTERIZATION	32
5.3 DESIGN AND LAYOUT OF TECHNOLOGY COMPONENTS.....	34
5.3.1 SYSTEM COMMUNICATION ARCHITECTURE.....	34
5.3.2 HIERARCHICAL CONTROL ARCHITECTURE.....	35
5.3.3 HVAC RETROFITS	36
5.4 OPERATIONAL TESTING	37
5.5 SAMPLING PROTOCOL	37
5.6 SAMPLING RESULTS	38
6.0 PERFORMANCE ASSESSMENT	38
6.1 PERFORMANCE COMPARISON BETWEEN PRE- AND POST-RETROFIT MODES	38
6.2 PERFORMANCE COMPARISON BETWEEN POST-RETROFIT AND OPTIMIZATION MODES	41
7.0 COST ASSESSMENT.....	51

7.1	COST MODEL	52
7.2	COST DRIVERS	54
7.3	COST ANALYSIS AND COMPARISON	54
8.0	IMPLEMENTATION ISSUES	58
9.0	REFERENCES	58
	APPENDICES	60
	Appendix A: Points of Contact	60
	Appendix B: Health and Safety Plan (HASP)	60
	Appendix C: EMC ² Report Concerning ISM Band Electromagnetic Site Survey and Characterization Interference Tests Conducted at the Construction Engineering Research Laboratories Champaign, IL	62
	Appendix D: Development of Occupancy Estimation and Forecast Algorithms	99
	Appendix E: Development of HVAC Models	106
	Appendix F: Development of Building Thermodynamic Model.....	115
	Appendix G: Development of Model Predictive Control Algorithm	117
	Appendix H: Procedure for Computation of Quantitative Performance Objective Metrics.....	120

List of Figures

Figure 1. Schematic of the Supervisory Control System Technology.....	12
Figure 2. Wireless Landscape	14
Figure 3. Flowchart illustrating occupancy estimation and forecasting data processing	16
Figure 4. Signal flow chart of the HVAC component models (variables in green are from forecasts or external subsystems, and those in orange are manipulated by the MPC algorithm). 17	
Figure 5. Illustration of three inter-dependent states of ARX zonal temperature model.....	18
Figure 6. CERL Facility in Champaign, IL	27
Figure 7. CERL Building 1 Layout with Highlighted Colored Areas Considered	29
Figure 8. CERL Building 2 Layout with Highlighted Colored Areas Considered	29
Figure 9. CERL facility indicated on 1998-2007 interval average temperature map	31
Figure 10. System Communication Architecture.....	33
Figure 11. Hierarchical Control Architecture	35
Figure 12. Multi-zone unit schematics.....	36
Figure 13. Occupancy related sensor installation location	36
Figure 14. Operational testing sequence.....	38
Figure 15. Ambient temperature (top) and relative humidity (bottom) during the pre- (left plots) and post-retrofit (right plots) modes; on x-axis: calendar days in July 2011 (shaded areas are weekends which are excluded from energy savings comparison)	39
Figure 16. Average zonal load conditions during the pre- and post-retrofit modes	40
Figure 17. Average set points for cold and hot deck discharge air temperatures and supply flows	40
Figure 18. Illustration of HVAC energy consumption for the pre- and post-retrofit modes	40
Figure 19. Average difference between set points and actual space temperature values for pre- and post-retrofit.....	40
Figure 20. Ambient temperature for MPC (blue) and post-retrofit day (green)	41
Figure 21. The total HVAC energy (electrical and thermal) consumption.....	41
Figure 22. The zone temperatures and differences between thermostat and space temperatures for MPC data	42
Figure 23. Illustration of zone temperatures and differences between thermostat and space temperatures for post-retrofit mode data.....	42
Figure 24. Illustration of the HVAC unit power consumption by component for the MPC data. 43	
Figure 25. Illustration of HVAC unit power consumption by component for post-retrofit data.. 43	
Figure 26. Summary of HVAC system energy use (top) and peak power consumption (bottom) for 2011 demonstration tests.....	45
Figure 27. Total power for MPC Day Feb 13, 2012	48
Figure 28. Total power for MPC Day Feb 16, 2012.....	49
Figure 29. Summary of HVAC system energy use (top) and peak power consumption (bottom) measurements from final demonstration tests in Feb. 2012.	50
Figure 30. Summary for the post retrofit and MPC modes, from demonstration tests in Feb. 2012, illustrating the system operation changes accomplished by the optimization algorithm.....	51
Figure 31. Summary for the post retrofit and MPC modes, from demonstration tests in Feb. 2012, illustrating the MPC performance in tracking occupant space temperature relative to zone set point T_{SP} during occupied hours (see left) and maintaining indoor CO_2 levels (see right).	51
Figure 32. Comparison of Wired vs. Wireless as network size increases	57
Figure 33. Cost Savings Using Wireless as network size increases	57

List of Tables

Table 1. Performance Objectives	20
Table 2. Criteria and ranking of the two options in Building II (Color code: green—high preference; yellow—medium preference; orange—not preferable)	30
Table 3. The HVAC system retrofits for all three modes of operation evaluated	32
Table 4. Retrofit items in the demonstration area.....	33
Table 5. List of Sensors to be installed in the demonstration area	33
Table 6. Experimental data and performance summary for MPC days in 2011, summarizing average energy and peak power consumption, indoor and ambient conditions (the relative peak power <i>decrease</i> is negative meaning that the peak power increased).	44
Table 7. Experimental data and performance calculations for MPC day Feb 13, 2012	46
Table 8. Experimental data and performance calculations for MPC day Feb 14, 2012	46
Table 9. Experimental data and performance calculations for MPC day Feb 15, 2012	47
Table 10. Experimental data and performance calculations for MPC day Feb 16, 2012	47
Table 11. Experimental data and performance calculations for MPC day Feb 17, 2012	47
Table 12. Cost Model for Wireless Sensor Network	52
Table 13. Post-retrofit to MPC comparison for four scenarios.....	56
Table 14. Wired versus Wireless comparison.....	56

Acronyms

AHU	Air Handling Unit
ASHRAE	American Society of Heating, Refrigerating and Air-Conditioning Engineers
DoD	Department of Defense
DDC	Direct Digital Control
EMCS	Energy Management and Control Systems
GHz	Giga Hertz
HVAC	Heating, Ventilation and Air Conditioning
IPMVP	International Performance and Measurement Verification Protocol
IAQ	Indoor Air Quality
ISA	The International Society of Automation
LBNL	Lawrence Berkeley National Laboratory
MHz	Mega Hertz
MPC	Model Predictive Control
MZU	Multi-zone unit
OPC	Open connectivity
ORNL	Oak Ridge National Laboratory
PC	People Counter
PIR	Passive Infrared (Sensor)
RA	Return Air
RF	Radio Frequency
UCB	University of California, Berkeley
UIUC	University of Illinois at Urbana Champaign
UTRC	United Technologies Research Center
VAV	Variable Air Volume
VFD	Variable Frequency Drive
WSN	Wireless Sensor Network

ACKNOWLEDGMENTS

ERDC-CERL and the University of Illinois provided a demonstration site and technical support. This includes CERL CFE branch researchers David Schwenk, Joseph Bush, and Andrew Friedl along with CERL-DPW staff Ron Huber and Clint Wilson, the CERL IT staff, and University of Illinois Facilities and Services maintenance staff Bob Wright and Gary Osborne. Notably CERL CFE researchers authored the original sequence of control, assisted with the construction scope of work. The CERL researchers, DPW staff, and University of Illinois staff provided onsite assistance with various maintenance and troubleshooting activities and advice and assistance with operation and support of the building automation system servers.

Alpha Controls, the controls contractor, including Mike Boogemans, Ravi Ramrattan, Jason Vogelbaugh and others, provided an enormous amount of support installing and maintaining the building automation system for the original retrofit as well and during the technology demonstration period.

Finally, the team and authors gratefully acknowledge the financial support and technical guidance provided by the SERDP/ESTCP Office under the leadership of leadership Drs. Jeff Marqusee and Jim Galvin as well as the support provided by Mr. Jonathan Thigpen (HGL) throughout the project period of performance. A thorough review and constructive comments and suggestions provided by Mr. Glen DeVillie (HGL) for the final report are also highly appreciated.

EXECUTIVE SUMMARY

An advanced energy management and control system in an existing building in the Construction and Engineering Research Laboratory (CERL) for Army at Urbana-Champaign (IL) was demonstrated. The medium-size office building underwent a retrofit of the heating, ventilation and air conditioning (HVAC) system and controls employing a technology called optimal Model Predictive Control (MPC) which offers significant potential for saving energy by providing a means to dynamically optimize various sub-systems, such as fans, cooling and heating coils, to take advantage of building utilization and weather patterns, and utility rate structures. The primary objectives of this project are to demonstrate: (1) energy efficiency gains achievable in small- to medium-sized buildings with MPC-based whole-building optimal control and (2) reduction in first costs achievable with a wireless sensor network (WSN)-based building HVAC control system compared to a conventional wired system. The second objective is key because first cost is a barrier to wider application of advanced HVAC control and 70% of the first cost is attributed to installation (wiring) and commissioning.

The UTRC-led team, partnered with Army-CERL facility staff and researchers at the Oak Ridge National Laboratory and University of California Berkeley, tested as a proof-of-concept the on-line implementation of model-based predictive and optimal control of the HVAC system in a 7000 sq. ft. portion of the CERL building. The system was retrofitted with a commercial off-the-shelf open protocol building automation system. The existing controls operated the HVAC system continuously during the day, maintain fixed temperature set points in the AHU heating and cooling deck discharges and use a fixed outdoor air fraction for ventilation in the building. The MPC approach aimed to increase system efficiency by continuous adjustment of system schedule of operation, heating and cooling set points and fresh air levels brought into the building, based on predicted and measured occupancy levels, internal loads and weather forecasts. System and indoor environment measurements of supply air temperatures and airflows, occupancy, zonal temperature, relative humidity and CO₂ levels were used to learn relevant HVAC equipment, thermal and occupancy models on line and to configure control design. Sub-metering was used to establish baseline energy consumption and to verify performance improvements. To reduce installation cost, wireless sensors were utilized wherever possible, particularly for occupancy sensing and thermal comfort. The WSN self-configures routing of data through a gateway to a central control computer that hosts the algorithms.

A multi-variable optimization problem to minimize energy consumption and cost while guaranteeing zonal comfort over a 3 hour predictive horizon was formulated and solved periodically on line. The algorithms were integrated with the building automation system and evaluated experimentally in July 2012 to February 2013 period at the demonstration site. A 55-65% reduction in HVAC system energy use was demonstrated while improving occupant comfort. Of this, nearly 35% improvement was achieved via off-line adjustments of the system schedule of operation and heuristic adjustments of the heating and cooling coil set points. This post retrofit state of the building HVAC system involved implementation of direct digital controls and a basic building automation system. The additional improvement, of 60-80% relative to the post-retrofit heuristic implementation, was accomplished by on line dynamic optimization of the building. A 10-15% installation cost reduction was accomplished due to the use of a robust wireless sensor network versus a fully wired network. The advanced control

system and algorithms was monitored by UTRC and CERL facility management team until Apr. 2012. Following this testing and evaluation period, the CERL facility management team reverted back to the post retrofit mode in anticipation of further upgrades to the remainder of the facility.

It should be noted that the present implementation of optimal controls was for a specific form of central building HVAC system involving a dual deck configuration. Such systems are prevalent in older buildings, of which there are many in the DoD stock, and are more prone to energy waste from system duct losses and leakages, compared to single deck HVAC systems (deployed more commonly now). This could explain some of the large energy savings accomplished when going from a pneumatic control approach for 24/7 operation to a direct digital controls (DDC) mode operation (considered as a post-retrofit baseline for optimal control mode). Furthermore, a more fine tuned DDC mode control strategy involving reset of the cooling and heating deck set points based on outside weather, rather than a seasonal setting (as employed in the demonstration site), would have captured some of the savings achieved by the optimal scheme. Finally, much of the optimal control mode performance data was obtained for heating season operation, although some cooling mode data was captured between July-Sep 2012, primarily for pneumatic and DDC modes of operation. More detailed assessments and analysis for different variants of the central HVAC system and of baseline DDC mode control approaches are needed to ascertain the variability in the energy use and peak power reduction benefits across DoD stock.

The model-based control methodology pursued here can be extended to hydronic heating and cooling systems where variable speed technologies are becoming prevalent and robust, but multivariable optimal control methodologies are lacking. The building HVAC control technology is applicable to small- and medium-sized buildings, which represent a significant portion of the Department of Defense (DoD) building stock. The demonstrated energy savings of more than 60% reduction in HVAC system energy use is estimated to lead to nearly 20% building level energy use reduction (assuming conservatively that HVAC systems constitute 30% of total building energy use). This represents significant progress toward the 30% gains in energy efficiency beyond 2003 levels mandated by Executive Order 13423. Renovations and retrofits are driven toward a 20% savings goal relative to pre-retrofit 2003 levels, and by this measure the improvements demonstrated in the present program represent the potential to meet the goal via broader scale implementation of optimal control technology alone.

Key challenges were identified in the additional cost to install the wireless sensor network, particularly the skill level and familiarity required by the contractor to deploy them. This adversely impacted the installed cost gains that were accomplished through the use of a wireless sensor infrastructure. Furthermore, the unfamiliarity with and related perceived risk in the maintenance for the optimal control platform, which utilizes Matlab and optimization toolboxes, was an impediment to longer term, sustained deployment of the promising technology at the demonstration site. Finally, technical challenges remain in the scalability and level of automation required to obtain relevant dynamic system models, and for the configuration and commissioning of the optimal control algorithms with the building management system.

1.0 INTRODUCTION

1.1 BACKGROUND

The Energy Policy Act (EPACT) of 1992, Energy Independence and Security Act (EISA) of 2007 (Title IV, Subtitle C) and Executive Order 13423 [1] mandate the DoD to measure and to improve facility energy efficiency by 30% beyond 2003 levels. For new construction, the memorandum of understanding for Federal Leadership on High Performance and Sustainable Buildings, the goal is to achieve ASHRAE standards for energy performance, namely 30% lower energy consumption relative to ASHRAE 90.1. Renovations alone are driven toward a 20% decrease in energy use relative to pre-renovation baseline of 2003. For the foreseeable future, the largest opportunity to reduce energy consumption shall come from retrofits and renovations to DOD's *existing* 343,867 buildings. DOD facilities in FY 2007 averaged 104,416 BTU/Sq. ft., an improvement over the baseline (136,744 BTU/Sq. ft. in FY 1985 for standard buildings and 213,349 BTU/Sq. ft. for industrial and lab facilities) but it still lags the national average (see CBECS [2]) of 91,000 BTU/ Sq. ft. (for 2003).

A promising technology for realizing energy efficiency is whole-building optimal control, which has the potential to reduce building energy consumption by 3-10% (0.5-1.7 of the 17 quads of energy consumed by US commercial buildings) [3]. This technology does so by continuously adjusting HVAC ventilation rates and temperature set-points to match building occupancy and weather loads. While such loads dominate the energy usage in office/administrative, lodging/barracks, warehouse, retail and many other buildings, other specialized buildings such as hospitals, data centers and dining facilities are dominated by other process loads, which are typically not controllable since they're essential for the mission critical services they provide. In contrast, the majority of existing buildings are designed and operated based on a maximum occupancy and a worst-case "design day" leading to excessive ventilation and air conditioning. However, a barrier to broad deployment of this technology to the existing building stock is the high first cost of building HVAC control systems. On average, installation (largely wiring and sensor addressing) and commissioning of building control systems account for 70% of the installed costs and the result is a one to ten year simple payback for optimized building controls [3]. What is needed is a scalable, robust building control platform consisting of sensing, computation, and actuation that is suitable for retrofit applications - especially facilities not served by a building management system - at an installed cost significantly below what is common today.

In this program, United Technologies Research Center (UTRC), in partnership with the Oak Ridge National Laboratory (ORNL), and the University of California, Berkeley (UCB) is developing a control platform and demonstrating both the first cost and operational cost benefits of whole-building optimal HVAC control. The system consists of 1) A Wireless Sensor Network (WSN) interfaced via an industry-standard communications protocol to a commercially available, networked HVAC control system, and 2) An optimal control algorithm that reduces wasteful energy consumption and interfaces to existing building HVAC equipment. The demonstration is targeted at small and medium sized buildings and was conducted at the U.S. Army Corps of Engineers Construction Engineering Research Laboratory (CERL) [4], located in Champaign, IL, USA (point of contact: Mr. Dave Schwenk.) The CERL site is ideal for this demonstration. It includes medium sized mixed-use buildings approximately 20-40 years in age

served by both a central plant and also a diverse range of Rooftop Units (RTUs) and split air conditioning systems. Its age, mixed use (office and laboratory), and diversity of HVAC systems makes it typical of buildings that are well suited to a controls retrofit. Moreover, Champaign IL offers weather diversity enabling testing under a broad range of conditions, and the CERL site shall help facilitate transition since the demonstration is aligned with its mission.

1.2 OBJECTIVE OF THE DEMONSTRATION

The specific technical objectives of the demonstration are 1) to develop and deploy a wireless sensor network (WSN) based HVAC control system to a technology maturity level that would enable commercialization leading to wide-scale deployment; 2) to demonstrate that the control system can reduce peak electrical demand by 10% and monthly summer energy consumption by 15% while meeting required indoor environment comfort requirements; 3) to demonstrate a 50% reduction in the costs of system installation, relative to that for a fully wired retrofit solution. The system will be operated over a twelve month period to both mature the technology and measure its performance across a wide range of operating conditions.

The proposed research will also investigate and identify the key barriers for deployment of WSN for advanced building automation and will address the issues for reproducible deployment of the technology.

1.3 REGULATORY DRIVERS

The Energy Policy Act (EPACT) of 1992, Energy Independence and Security Act (EISA) of 2007 (Title IV, Subtitle C) and Executive Order 13423 mandate the DOD to measure and to improve facility energy efficiency by 30% beyond 2003 levels. EO 13514 requires reducing energy intensity in agency buildings. EO13423 is more specific and requires DoD to “improve energy efficiency and reduce greenhouse gas emissions of the agency, through reduction of energy intensity by (i) 3% annually through the end of fiscal year 2015, or (ii) 30% by the end of fiscal year 2015, relative to FY03, and ensure that (i) new construction and major renovation comply with the Guiding Principles, and (ii) 15% of the existing Federal capital asset building inventory of the agency as of the end of FY15 incorporates the sustainable practices in the Guiding Principles.

2.0 TECHNOLOGY DESCRIPTION

2.1 TECHNOLOGY OVERVIEW

The technology consists of two main elements: 1) A Wireless Sensor Network interfaced via an industry-standard communications protocol to a commercially available, networked HVAC control system, and 2) An optimal control algorithm that reduces wasteful energy consumption and interfaces to existing building HVAC equipment. These two elements are detailed in the following sub-sections.

Wireless Sensor Networks have been used for environmental monitoring in applications ranging from civil infrastructure (bridges, roadways, building structures) to outdoor environmental modeling. Use of WSNs for closed loop HVAC control in buildings is innovative. The WSN

provides three distinct advantages when compared to a wired system. First, it reduces installation costs relative to a baseline wired system by eliminating the need to run signal and power wires to each sensor and also by its ability for self configuration. On average 70% of the installed costs for an HVAC control system are for installation and commissioning. Second, the flexible and optimal sensor placement enables more effective control. Sensor placement could be adjusted during operation as a troubleshooting measure, and sensors can be added or removed as the building usage evolves. Third, the elimination of wires may be a critical advantage and cost reduction means for retro-commissioning in old buildings or those where access is expensive (due to issues such as asbestos removal or management). A detailed cost comparison between wired and wireless implementation of the sensor network is performed in Section 7.0 to assist future implementations.

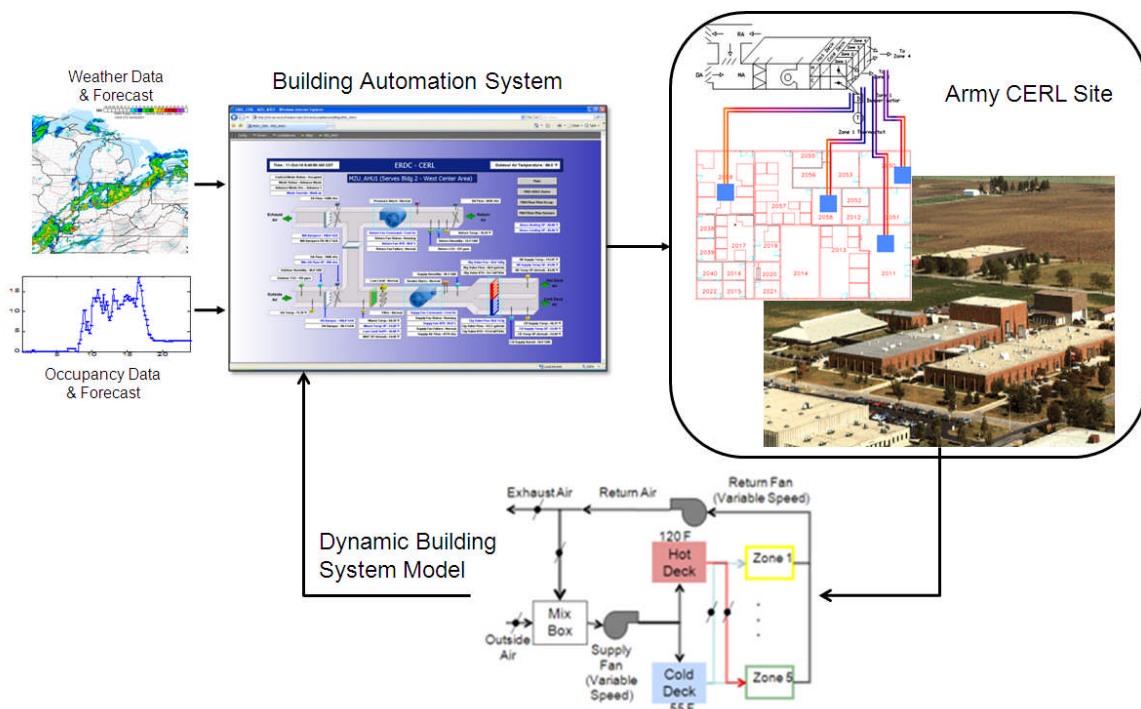


Figure 1. Schematic of the Supervisory Control System Technology

A reliable and secure WSN is used to provide majority of the monitoring capabilities for the project. The technology readiness level (TRL) of the WSN technology used for this project started at TRL 5 at the beginning of the project and extended to TRL 6-7 towards the end of the project. WSN is used to measure temperature, relative humidity, CO₂, passive infrared red, flow, and pressure. The WSN is self configured by routing packets automatically across the network and adjusting network parameters (routing information) as the conditions within the building changes, providing a degree of robustness. Interoperability is the key enabler to retro-commissioning in existing buildings. A gateway is used to make WSN transparent to the existing building automation system. The installer would only have to map the physical address of each node to the logical address of each node. Wireless sensors do provide specific maintenance and security management requirements including battery replacement. Low-power, low-duty cycle radio technology used in the project have projected lifetime up to 3 years. IEEE 802.15.4-based

wireless modules are used for the deployment. AES-128-bit encryption is part of the standard. A determination of whether this met all the relevant DoD security requirements has not formally been made in this program. The demonstration system is not built to include DOD information security requirements like FIPS 140-2. The demonstration system, while not formally qualified, is roughly at FIPS 140-2 Level 1, but can be extended to include higher-level requirements. This would require incorporation of the cryptographic and physical protection mechanisms as defined by the relevant standards. The WSN system is architected in a way to provide fallback to non-optimal operation in case any failures arise in the network.

A model-based predictive supervisory controller (MPC), illustrated in Figure 1, adjusts outside air ventilation rates (i.e. the *outside air ratio*) and zonal temperature set points within comfort and Indoor Air Quality (IAQ) constraints (prescribed by ASHRAE 62.1) to minimize a weighted combination of energy consumption and peak energy demand over a 4-8 hour horizon. The algorithm is executed continuously, constantly monitoring internet-available weather predictions (outside air temperatures, humidity levels, wind velocity and solar level) and indoor environmental conditions, estimating and predicting building occupancy levels, and adjusting the present and future values of outside air ratio (while meeting the ASHRAE 62.1 requirements) and supply temperature and flow set-points to ensure that the building operates within comfort and indoor air quality (IAQ) constraints (determined by CO₂, temperature, and humidity levels), while minimizing the energy cost function. The control is at a *supervisory* level, meaning it determines reference values for local feedback loops, but does not affect the zonal temperature feedback loops themselves, which remain in place to regulate temperature. The cost function can be adjusted to emphasize peak (maximum) power demand or energy consumption over time (the integral of power over time) and can also be adjusted to modify comfort or IAQ constraints such as maximum allowable CO₂, providing a degree of flexibility to building operation. The resulting supervisory control law effectively exploits passive energy storage in both envelope and air. In contrast, conventional HVAC controls are only *reactive*, using feedback to drive set points to fixed values (although there may be set-backs based on a schedule) and do not exploit energy storage optimally. The technology is applicable to a wide variety of buildings that are served by systems ranging from built-up systems to “Roof Top Units” (RTUs) provided the outside air ratio, system temperature and flow set points, and zonal temperature set points are available and adjustable parameters. The methodology of load estimation and predictive model-based performance optimization is also applicable to the control of district systems, such as for cooling and heating, although many of the sub-systems and thermal load models would be quite different from those encountered in building-level HVAC systems.

2.2 TECHNOLOGY DEVELOPMENT

2.2.1 WIRELESS SENSOR NETWORK

Wireless sensor networks provide an attractive retro-commissioning opportunity in existing buildings. Wide variety of wireless networks exist that can be used to instrument buildings. Figure 2 shows the options in wireless networks. The x-axis represents the data rate and the y-axis represents the power consumption and cost/complexity.

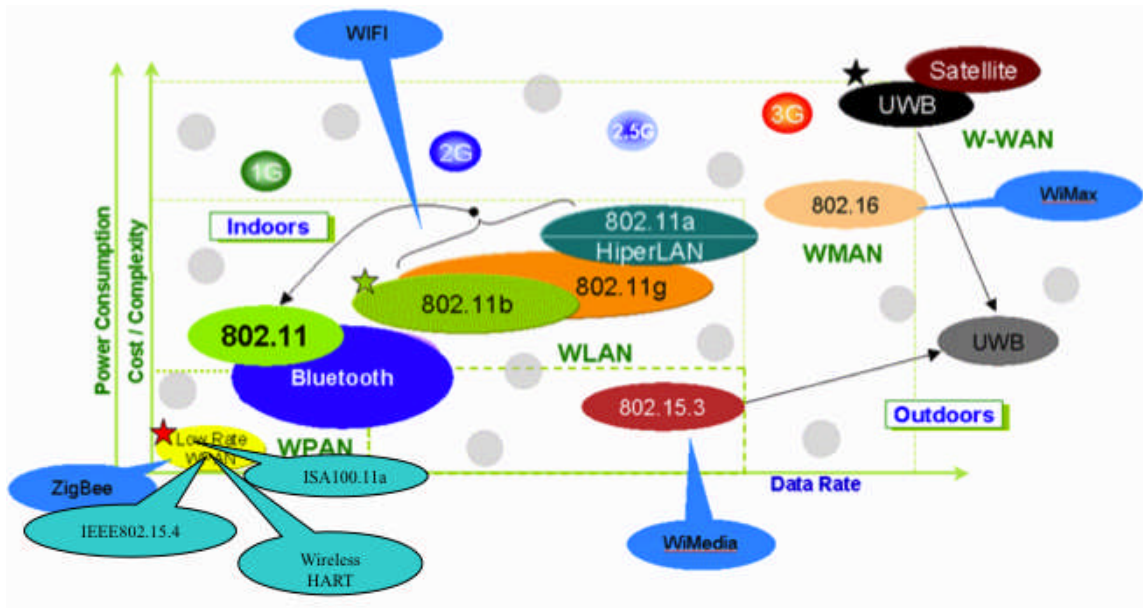


Figure 2. Wireless Landscape

The key metrics to identify the wireless networks for building monitoring applications include:

1. Low-data rate
2. Long battery life
3. Low-cost of deployment and operation
4. Unlicensed frequency of operation
5. Co-existence with existing building wireless networks
6. Interference resistant
7. Secure network operation

The above-mentioned characteristics correspond to the lower left corner of Figure 2. IEEE 802.15.4 standard provides the best platform for monitoring application with in buildings. Two different wireless networks are used at the facility:

1. IEEE 802.15.4-based 2.4GHz wireless network for temperature, humidity, CO₂, airflow, and pressure. SpinWave wireless sensor network is used for the project. The network is based on IEEE 802.15.4 with specific optimizations to improve the network performance including adaptive channel hopping.
2. Directional people counter sensors required for optimal occupancy estimation are not commercially available in the 2.4GHz band. A 900MHz frequency hopping spread spectrum technology is used to obtain these measurements. Data is fed in to the control computer using a separate gateway (other than 2.4.GHz) to provide application level interoperability.

The CERL facility was surveyed for radio-frequency (RF) signals detrimental to the performance of wireless sensors within the building. The goal of the survey was to determine propagation characteristics and RF attenuation within the building. Two modes of survey were performed: receive-only and transmit-receive. The surveys were conducted in the demonstration area of the CERL site over a period of a few days by ORNL team staff with a specialized instrumentation cart for rapid and mobile characterization of wireless sensor networks in enclosures. Standard testing protocols and procedures for such deployment exist. The key conclusion was that the

receive-only, transmit-receive and propagation signal characteristics had high signal-to-noise ratios in both bands of transmission, namely 2.4GHz and 900MHz. The two networks ultimately deployed were 1) the 900MHz network set up as a star network, and 2) the 2.4GHz network setup as a cluster tree mesh network connected by three repeaters with higher duty-cycles than sensor nodes. To ensure that the wireless network operates robustly with low maintenance cost beyond the project completion, the wireless repeaters were plug-powered (and located where there was ease of access to plug-power to minimize installation cost). In addition, 26% of wireless-communication sensors were powered from line power available in close proximity (and for which the wiring installation cost was minimal). Further details and site specific measurement results that justify the above choices and conclusions are provided in Appendix C.

2.2.2 MODEL-BASED PREDICTIVE SUPERVISORY CONTROLLER

The key ingredients of the supervisory control algorithm are indoor and ambient thermal load models that can be used to estimate system demand dynamically and to provide forecasts to optimize system operation. The indoor loads are primarily driven by occupancy and the external loads are driven by weather. In addition to these, dynamic system models of the relevant equipment are needed to determine the operational state of the building HVAC system and the energy cost implications or changes that might be made to the system operation under multiple scenarios considered in the optimization algorithm. Indoor zone thermal models are required to estimate and forecast comfort impacts of potential optimal control commands and ensure that occupant temperature and CO₂ constraints are met at all times. Finally, optimization techniques used to perform dynamic manipulation of system set points and operation variables to reduce energy consumption while maintaining comfort are needed. In the following section, the above enabling technologies and methods to realize optimal supervisory controls for the retrofitted building HVAC system are described.

2.2.2.1 Occupancy Estimation and Forecast Algorithms

The occupancy model provides real-time occupancy estimation and forecast. Specifically, given the set of real-time sensor measurements up-to-date, an occupancy estimation model estimates the number of occupants in each zone at the current time step. Based on the estimates and historical occupancy patterns collected offline, an occupancy-forecast model predicts the numbers of occupants in each zone for a set of future time steps.

The diagram below illustrates the main modules of the occupancy estimation and forecast. As a first step, sensor measurements over an extended time period are collected. With this set of measurements and prior knowledge on occupancy patterns such as unoccupied hours, the occupancy estimation model is run to estimate the occupancy levels for the given time period. A statistical model is then generated based on this set of estimates, which serves as the historical occupancy patterns for real-time forecast.

During real-time daily operation, occupancy estimator is run using real-time sensor measurements to estimate the number of occupants at the current time. Then based on the statistical model of the historical patterns and the real-time estimates, occupancy forecast model predicts the occupancy levels.

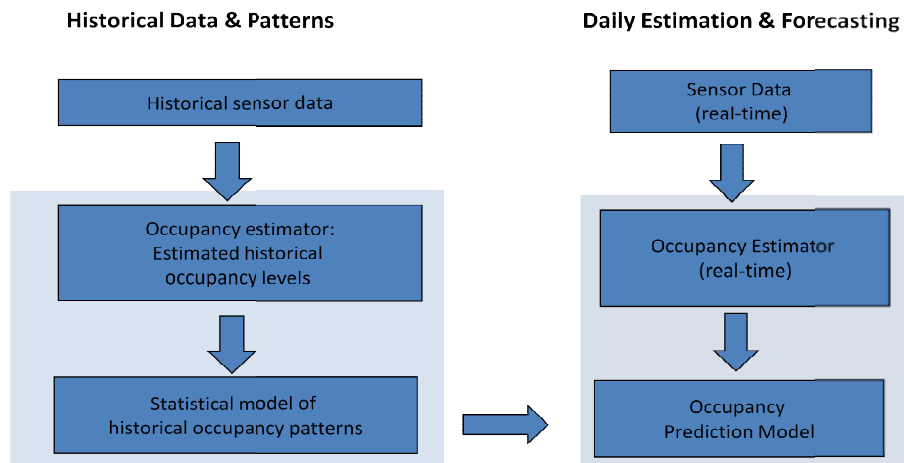


Figure 3. Flowchart illustrating occupancy estimation and forecasting data processing

Occupancy estimator model

Occupancy estimator model provides an estimated number of occupants in each zone based on the sensor measurements collected. A constrained quadratic optimization model is formulated to derive estimates that are most consistent with the collection of sensor data and prior knowledge on occupancy patterns.

The challenge in occupancy estimation is that there is not one type of sensor data alone that can provide accurate occupancy level information. Motion sensors usually have high accuracy, but only provide limited information on whether there are people in a room or not. It has been found that CO₂ sensors have a strong correlation with occupancy level in a room. However, there is a delay in CO₂ level change in response to occupancy level change. In addition, CO₂ level will be affected by other factors such as supply air flow into the room. Therefore, it is difficult to establish an accurate mapping between CO₂ level and occupancy level. Finally, people counter sensors are often used at the entrance of a room to count the number of people entering and leaving. For each instance, the sensor accuracy is high, usually greater than 95%. However, as the number of people in the room at each time step is the summation of people entering and leaving for a period of time. The estimation error will accumulate and becomes significant as the length of time period increases.

For accurate occupancy estimation, an optimization model based on constrained quadratic programming was developed. The model is based on the formulation in [16]. Further refinement was made to the process of CO₂ measurements and the addition of motion sensors. Details of the implementation of occupancy estimation and forecast algorithms are described in Appendix D.

2.2.2.2 HVAC Models

The HVAC component models are critical for control design because their operational constraints and efficiency maps affect the control input selection that ultimately impacts the overall energy consumption and thermal comfort. The main HVAC unit components modeled for control design are: supply and return fans; heating and cooling coils. Due to their faster dynamics

relative to the building temperature dynamics (time responses are an order of magnitude lower) the HVAC component models are built as static models where the previous values of both their inputs (valve positions or fan speeds) and outputs (flows and discharge air temperatures) are considered to have a significantly lower impact than the current inputs. The procedure used to build these models consists of the following steps: (i) execute functional tests on the actual system by generating combinations of valve and fans speeds and therefore controlling the individual components to operate regimes; (ii) use the data from the functional tests to calibrate models with pre-selected structures; (iii) use another portion of the measurements to validate the calibrated models by generating statistics on their prediction errors. A common challenge in building these models, as is the case for any application domain models, is the desired level of accuracy which is a result of a well-known trade-off between computational complexity and performance benefits. Based on previous experience, the team selected as validation error threshold a value of 20%. Another major challenge in building the models is that their inputs can be only variables that are either controlled or forecasted and this is a result of the predictive feature of the control algorithm. This challenge was overcome by adequately selecting the inputs and outputs of each model block as is illustrated in Figure 4.

The models illustrated in Figure 4 and the mentioned design procedures are described in more details in Appendix E.

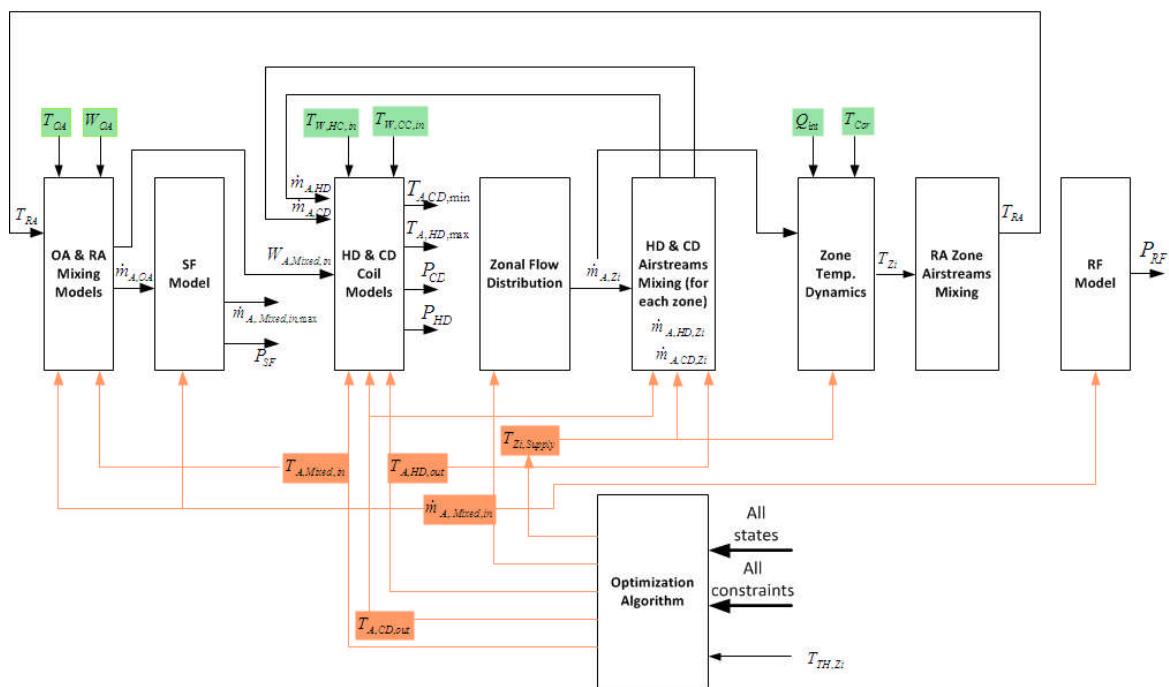


Figure 4. Signal flow chart of the HVAC component models (variables in green are from forecasts or external subsystems, and those in orange are manipulated by the MPC algorithm)

2.2.2.3 Building Thermodynamic Model

The building model is used to predict the temperature in the considered zones over a future period of time for given zone supply flows, supply temperatures, thermal loads and ambient

conditions. This is the only dynamic model used for control design and is critical for maintain thermal comfort and improving energy efficiency. Two approaches were considered for modeling the temperature dynamics.

1. Thermal networks, a classical approach based on similarities with electrical circuit networks. All the wall surface and space temperature states were modeled increasing the size of the model to 96 states. During the calibration and validation steps for this model it was observed that the validation error is larger than expected. This was the result of a combination of model error and load estimation errors.

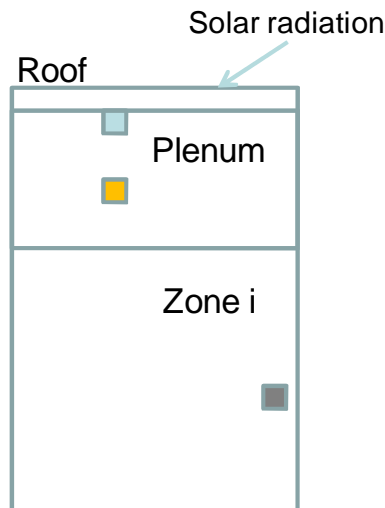


Figure 5. Illustration of three inter-dependent states of ARX zonal temperature model.

2. Simplified models based on classical Auto-Regressive with Exogenous (ARX) term models. This was considered as a simpler alternative to the thermal networks in view larger sensor set needed to validate former. For each zone, the ARX model has three interdependent states depicted in Figure 5: inner-roof surface temperature, plenum temperature and space temperature. The inter-dependence between the adjacent zone temperatures was not considered for this model because the dynamics of the convection heat transfer to a zone from the HVAC unit is significantly larger than the conductive part from other zones with similar space temperature.

The building thermodynamic model is described in Appendix F.

2.2.2.4 Model Predictive Control Algorithm

The following describes the predictive control algorithm formulation and solution approach.

- a) **Cost function and constraints.** The cost function is an abstraction or generalization of the actual utility cost and captures a weighted combination of peak electrical usage (usually over one month, but for our purposes, over a single day) plus the total energy consumed in a time period. Included here are the utility rate structure, which reflect lower energy prices depending on time-of day, or time-varying rate structure depending on grid electrical demand. A user-selectable weight allowed for modifications of the cost to place emphasis on reducing electrical peak demand over average energy usage, which is important in certain

parts of the country. The constraints are equations and inequalities that are coded as software to represent equipment or comfort constraints.

- b) **An optimizer** is software that computes the minimum of the cost function as a function of the manipulated variables (set points and ventilation rates), subject to the constraints captured by the dynamic model and also the physical and equipment constraints. The optimizer in effect uses the simulation model and cost function iteratively to compute optimized control trajectories for a three hour predictive horizon for building zonal temperature and outside air ratio, to minimize the cost function capturing electrical power consumption and electrical peak demand. The algorithm was executed on fifteen minute time intervals and produced optimized set points to be applied for the next four to eight hour time period. The time period was based on the time constant of the building and could be adjusted in practice. The resulting optimization problem was nonlinear and non-convex. We employed state-of-the-art nonlinear optimizers based both on interior point methods.

The optimization problem formulation, solution approach and challenges encountered during its implementations are detailed in Appendix G.

2.3 ADVANTAGES AND LIMITATIONS OF THE TECHNOLOGY

The advantages of the WSN over a wired installation include optimal sensor placement, significantly reduced installation costs (especially retrofit), increased sensing locations, and reduced cost of additional sensing (scalability). The limitations of WSN include time-varying nature of the RF channel requiring site-specific optimization, optimal configuration management over time, and training of the facility operational personnel and maintenance of WSN. This project addresses the limitations and provides guidance and tools to reduce the uncertainties involved. The steps taken to ensure robust network operation are summarized below:

1. Understand the ambient RF environment. While we performed a thorough RF measurements, minimal understanding of the existing networks and frequencies of operation is required to exploit the frequency and spatial diversity
2. Incorporate temporal channel mobility. Each node in the network deployed at CERL constantly monitors the 16 channels in the 2.4GHz band (as channelized in IEEE 802.15.4) and identifies the 4 channels with least interference from sources like microwave ovens etc. The network hops across these channels to maximize performance.
3. Address spatial density by mains powered wireless repeaters which extend the network range and reduce the transmit power on each node improving network lifetime
4. The key limitation of a successful wireless network deployment is interoperability with building automation systems. We addressed this by using a gateway capable of translating 802.15.4 packets in to LonWorks addressable "points"
5. Ensure that network installed is compliant with site IT requirements and constraints. Broader compliance issues related to information assurance requirements for DoD sites were not explored in the program at this early technology feasibility assessment phase.

Robust and accurate occupancy estimation algorithms are useful for estimating internal loads in buildings and the ventilation load. Motion detectors, routinely used for local lighting control, are not typically integrated into the HVAC system controls and they cannot determine the exact *number* of occupants. While temperature and CO₂ sensors provide better but indirect measures of actual occupancy, the slow sensor response makes them more suitable for following trends at

long-time scales (on the order of several tens of minutes to hours). A faster method (on the order of few minutes) is needed to respond quickly to rapid changes in occupancy. Moreover, such sensors can be grossly inaccurate without frequent calibration. Recent studies show that the minimal required outdoor air intake flow (averaged hourly) from CO₂-based demand-controlled ventilation is about 28% more than direct people-count based ventilation control. A multi-sensor data and model driven procedure is proposed here for accurate occupancy estimates and for prediction. Despite their stochastic nature, occupant traffic patterns recur over multiple time scales (hours, days, months, and seasons). Simple representations of such patterns can be adaptively learned and combined with real-time accurate and robust estimates of occupancy distributions in buildings. Augmented with other sources of information, such as from known schedules, occupancy levels can be predicted in a probabilistic fashion. The challenge is to do so accurately and cost effectively, i.e. without requiring full building coverage with accurate sensors. An occupancy estimation error of < 10% using cameras, CO₂ sensor, and PIR sensors combined with learned historical facility usage information was shown recently by UTRC, which is substantially improved when compared to that from using CO₂ or video sensors alone.

Model Predictive Control (MPC) strategies have been used successfully in applications with large time delays, large number of set-points and constraints. As opposed to currently implemented rule-based control policies with fixed set-point, schedules and sequences that react to differences between desired and actual values of zonal temperatures and CO₂ values, predictive strategies use weather forecasts and occupancy patterns for predicting loads over future four to eight hours time horizon and use the passive energy stored in the building envelope and air. In addition to more accurate set-point tracking, this approach results in lower energy consumption and peak power values. To accurately predict the loads, predictive algorithms rely on physics-based models for water-to-air thermal energy transfers and efficiency maps for HVAC equipment. A significant limitation of this approach, the accuracy of these models is critical for improving energy efficiency and set-points tracking. The large number of sensor measurements will help mitigate this risk by calibrating the models' parameters. Another limitation is the number of optimization variables; a large number of variables and constraints can result in long search time for the optimization algorithm to converge to the optimal solution. Selecting appropriate values for the optimization horizon length and update frequency of the actuator inputs will mitigate this risk.

3.0 PERFORMANCE OBJECTIVES

For the proposed demonstration of a wireless control platform for energy efficient building HVAC retrofits, Table 1 below provides a summary of the specific objectives, metrics, data used to compute the metric, the success criteria actual performance metrics computed using measurements.

Table 1. Performance Objectives

Performance Objective	Metric	Data Requirements	Success Criteria	Measured Performance
Quantitative Performance Objectives				

Decrease energy consumption - kWh (<i>Energy</i>)	Difference between optimized and baseline control policies in total energy consumption	Electric metering data for fans; Btu metering data for chilled water and hot water	≥ 15% reduction in HVAC energy consumption	Objective exceeded ¹ : 60-85% (results shown in Figure 29)
Decrease peak power – kW (<i>Demand</i>)	Difference between optimized and baseline control policies in peak electrical & cooling power consumption	Electric metering data for fans; Btu metering data for chilled water	≥ 10% reduction in peak power	Objective met ² : 10-34% (results shown in Figure 29 and discussed on pages 49-51)
Decrease carbon emissions (<i>Green house gas</i>)	Difference between optimized and baseline control policies in equivalent CO ₂ emissions for the total energy consumption	Same as for energy consumption metric; typical CO ₂ emissions value for electricity and natural gas	≥ 10% reduction in CO ₂ emissions compared with current profile	Objective exceeded: >60%
Reduce sensor installation cost (<i>Costs</i>)	Difference between the cost of installation & commissioning of wired and wireless sensors	Quotes from two contractors covering material, installation, and commissioning costs for wired and wireless sensors	=50% reduction in costs	Objective not met: reduction of 15% estimated, with potential reduction of up to 40% for larger network/facility. Relatively poor contractor experience base also led to higher installation risk/cost.

¹ Performance data gathered extensively for transition and heating season when operating the optimal control technology mode. Cooling season data only available for pneumatic (pre-) to DDC (post-) retrofit conversion.

² Only heating thermal power was considered for this objective due to availability of only Winter season experimental data for the refined optimization algorithm.

Maintain/Improve temperature regulation (<i>Comfort</i>)	Difference between optimized and baseline control policies cumulative zonal temperature deviation (from set points) during periods of occupancy, evaluated weekly	Zone temperature measurements and set-points, zone occupancy status (estimated from sensor data)	Metric with optimized control policy \leq Metric with baseline control policy	Objective met; the average temp. difference from set points is: <ul style="list-style-type: none"> • 2-5[°C] for baseline • 0.5-1[°C] for Optimized
Minimize occupancy estimation error (<i>Models</i>)	Mean percentage error between actual and estimated occupancy levels	Occupancy sensor data and ground truth/simulated occupancy data	$\leq 20\%$ estimation error	Objective met: $\leq 15\%$
Qualitative Performance Objectives				
Maintainability	Maintenance effort for proposed system (WSN and MPC)	Records of component maintenance/replacement and system downtime (frequency and duration) for proposed and baseline systems;	Expected maintenance effort similar to existing wired sensors and baseline control system	The WSN for final MPC implementation is a subset of the original network deployed, and associated maintenance costs are nominal (also see SIR estimate).
Ease of use	Ability of CERL facilities staff to operate/tune the proposed controller and maintain WSN after reasonable training	Feedback from CERL facility staff/management on ease of operation and maintenance	Trained facility staff is able to maintain the WSN and operate/tune the new controller. Minimal call backs to team following project completion.	CERL staff is familiar with post retrofit control system and provided documentation. There have been no call backs. MPC system was removed. Lack of familiarity with Matlab and associated software maintenance hindered MPC adoption.

It should be noted that the “baseline control policy” referred here is not the true baseline system with pneumatic controls but an equivalent and representative strategy implemented on LonWorks digital controllers after HVAC equipment & control retrofits. Literature shows that

there is about 10% reduction in energy consumption when shifting from pneumatic to digital controls, all other things being same [11]. Project scheduling constraints preclude the installation of the measurement system before the control system retrofit from pneumatic to digital. The 15% reduction in energy consumption mentioned in Table 1 is from a baseline control strategy that uses DDC and not pneumatic controllers. This reduction would be higher if we compare the optimized control strategy with a baseline control strategy that uses pneumatic controllers.

The optimal control strategy is the proposed control strategy using WSN and MPC. Each performance objective listed in Table 1 above is described in detail below.

Quantitative Performance Objectives

1. *Reduce energy consumption*

Data Used – 1) kWh meter for fan at the AHU, 2) Btu meters for chilled water at the AHU cooling coil (CC), 3) Btu meters for hot water at the AHU heating-coil (HC). The data were trended at fifteen minute intervals.

Criterion – Total energy consumption savings $\geq 15\%$

The primary purpose of the demonstration was to reduce the HVAC energy consumption in the selected section of a building. The total HVAC energy consumption comprised of the electrical energy use (mainly by the Air-handling Unit - AHU fans) and the thermal energy use from the utility streams (chilled water & hot water).

For the section of the building selected for this project, the data related to AHU electrical energy consumption (due to fan), cooling energy consumption (due to cooling coil), and heating energy consumption (due to AHU heating-coil and) were collected for several days at a time over a period of 9 months, alternating between baseline and optimal control strategy. In addition, outside temperature, people count, zone temperatures, thermostat set-points, and outside air (OA) quantity were tracked. These are the independent variables used to generate the baseline energy consumption values for same conditions as those during the optimal control policy. The energy consumption is the sum of each time step fan, cooling coil, and heating coil energy consumption aggregated over the time frame of the experiment and was not normalized on weather.

2. *Decrease peak electrical power:*

Data Used – 1) MMBtu/hr of heating measured at each time step with Btu meters converted to equivalent electric power using typical boiler efficiency of 0.8 kW/ton (information provided by CERL facility manager). The data was trended at fifteen minute intervals.

Criterion – Electric demand savings $\geq 10\%$

The objective was to understand the reduction in peak AHU electrical power (attributed to AHU fan and cooling) as a result of the new control strategy developed. Due to availability of only Winter season data for the refined optimization algorithm, only the peak heating

thermal power reduction was addressed for this performance objective. The peak electrical power consumption for the fans was relatively small and not included in this estimate.

For the section of the building selected for this project, the data related heating thermal power was collected for several days at a time over a period of 9 months, alternating between normal and optimal control strategy. In addition, the weather parameters, people count, temperature, and OA quantity were tracked.

3. *Reduce carbon emissions*

Data Used: 1) kW at each time step using power meters at the fan; 2) MMBtu/hr of cooling measured at each time step with Btu meters converted to equivalent electric power using typical chiller efficiency value of 0.8kW/ton, 3) Btu meters for hot water for the AHU heating-coil converted to natural gas usage using average boiler plant efficiency of 0.75 (as provided by the CERL facility manager), and 4) CO₂ emission factors for electricity and natural gas published by energy information administration.

Criteria – CO₂ reduction \geq 10%

The objective was to understand the reduction in carbon emissions as a result of the new control strategy developed.

For the section of the building selected for this project, the data related to AHU electrical usage and heating gas usage was collected for several days at a time over a period of 9 months, alternating between baseline and optimal control strategy. In addition, the weather parameters, people count, temperature, and OA quantity were tracked.

4. *Decrease in sensor installation cost:*

Data Used – Wireless and wired sensor, installation, and commissioning costs.

Criterion – Cost savings \geq 50%

The objective here was to understand the reduction in sensor network installation (material, labor, commissioning) costs due to use of wireless sensors.

For the section of the building selected, the data related to costs of wireless sensors and their installation and commissioning was compared with the costs of equivalent wired sensor network and its installation. Quotes were obtained for wired and wireless sensor systems.

5. *Maintain/improve temperature regulation:*

Data Used – Temperature measurements and set-points for each of the five thermal zones with baseline control operation and operation with optimized controls; Occupancy information (binary) for each of the five zones from occupancy sensors.

Criterion – Temperature_error_optimized_control \leq Temperature_error_baseline

The objective here was to ensure that energy efficiency gains were achieved without sacrificing temperature regulation in the demonstration.

For each of the five thermal zones in the area selected for this demonstration, the temperature regulation error during the periods of occupancy were measured and aggregated over multiple test windows. The temperature regulation performance (during the period of occupancy) were compared for operation with baseline and optimized control strategy.

6. *Minimize occupancy estimation error*

Data Used – 1) CO2 sensor data at each time step; 2) PIR sensor data indicating the time when there is motion in its detection area; 3) IR people counter data counting the number of people entering and leaving an area for each time step; 4) Occupancy level in the test area served as ground truth data. Each time step is fifteen minutes.

Criterion – Mean percentage error between actual and estimated occupancy levels should be no greater than 20%. The mean percentage error (MPE) is defined as

$$\text{MPE} = \frac{1}{n} \sum_{t=1}^n \frac{f_t - a_t}{a_t}$$

where a_t is the actual occupancy level, and f_t is the estimated value.

The objective was to understand the improvement of occupancy estimation accuracy as a result of the occupancy estimation model used in this project.

For the section of the building selected for this project, sensor data related to occupancy were collected for several days at a time over a period of 9 months, including CO2 sensors, PIR sensors and IR people counters. In addition, ground truth data on occupancy was collected to evaluate the estimator performance. Due to the difficulty in collecting a large amount of ground truth data, simulated occupancy data that are representative of the test area occupancy was used in addition to ground truth data for evaluating estimator performance.

Qualitative Performance Objectives

1. *Maintainability*

Data Used – 1) Record of maintenance schedule for the WSN and wired sensors, 2) record of system downtime for the proposed system, 3) obtain information on typical system downtime for baseline system from CERL facility.

Criterion – Expected maintenance effort for proposed optimal strategy and wireless network system shall be similar to existing wired sensors and baseline control system.

The wireless platform implemented had no downtime and required only minimal component maintenance/replacement. Since its installation in Fall 2010 until the date of this report, only one transceiver failed (for a CO2-sensor node) and was replaced at no cost by the manufacturer (it was covered by warranty). Its replacement effort was also minimal,

consisting simply in mechanical replacement; the node integration in the wireless network was plug-and-play.

The maintainability of the MPC algorithm cannot be estimated at this time due to limited operational information. The most refined version of the MPC algorithm operated for one week in February during occupied hours with minimal intervention. On one occasion, communication between the project platform and the BAS server was lost for unknown reasons and was reset on time. However, more operational data is needed from all seasons and loads in order to make a qualitative estimate of the algorithm robustness and the required maintenance effort.

2. *Ease of Use*

Data Used – Feedback from CERL facility management on the operation and maintenance procedures outlined during the training and conducted during the demonstration phase.

Criterion – With the provision of training, documentation, and involvement of CERL facility staff during the demonstration phase, we expect minimal call backs to the team after project completion.

Due to the minimal maintenance required for the WSN and its excellent performance throughout the project the CERL Facilities were not solicited to operate or re-configure the WSN. In one particular case when the transceiver for the CO₂-sensor node mentioned above failed, the diagnosis was relatively easy (based on erroneous sensor data observed in BAS Graphics screen) and the node was replaced. It would be expected however, that in case of other failures--such as failures of a repeater or the gateway to BAS network) the intervention of a skilled technician would be required.

Throughout its development and refinement stages, the MPC algorithm was developed as a stand-alone software with very intuitive inputs (such as occupied hours, comfort limits, etc) and it operated autonomously for most of the demonstration week in Feb 2012. However, due to the limited available time and lack of familiarity with the Matlab environment in which this algorithm was developed, CERL Facilities did not adopt the technology. A friendlier interface, created and integrated directly in BAS Graphics screen, would have probably been conducive for technology transition.

4.0 FACILITY/SITE DESCRIPTION

4.1 FACILITY/SITE SELECTION

The proposed demonstration was conducted at the U.S. Army Corps of Engineers– Construction Engineering Research Laboratory (CERL), located in Champaign, IL, USA (point of contact: Mr. David Schwenk); see Figure 6. The proposed site/facility is representative of DoD facilities from three perspectives: (i) weather diversity (i.e. with hot, humid summer months, cold winters and distinct transition/shoulder seasons); (ii) existing HVAC equipment condition; (iii) building size (7000 sq. ft. space) and usage (mixed with offices, conference rooms, cubicles and a cafeteria having different occupancy, schedules and terminal HVAC systems).

First, the four-season weather pattern makes possible the testing of retrofitted HVAC system and optimized algorithms in a broad range of ambient conditions, and therefore the season-based energy performance benefits can be extrapolated to a wide range of sites across US. For example, energy savings estimated based on experiments performed in the summer season can be used as reliable predictors for average expected benefits for any facility located in areas with similar temperatures and humidity conditions (assuming similar occupancy patterns, and baseline and retrofits conditions). Second, the condition of existing HVAC equipment is representative for DoD sites with twenty to forty years in age. The condition of the equipment makes possible the implementation of retrofits, demonstrating potential performance improvements vs. cost trade-offs. These trade-off results offer DoD a better understanding of the magnitudes of retrofits beneficial to a wide range of sites. Third, the occupancy patterns and usage mix of office, cubicles, conference area and common area is typical for a building, making possible direct extrapolation of performance benefits to a large subset of DoD buildings.

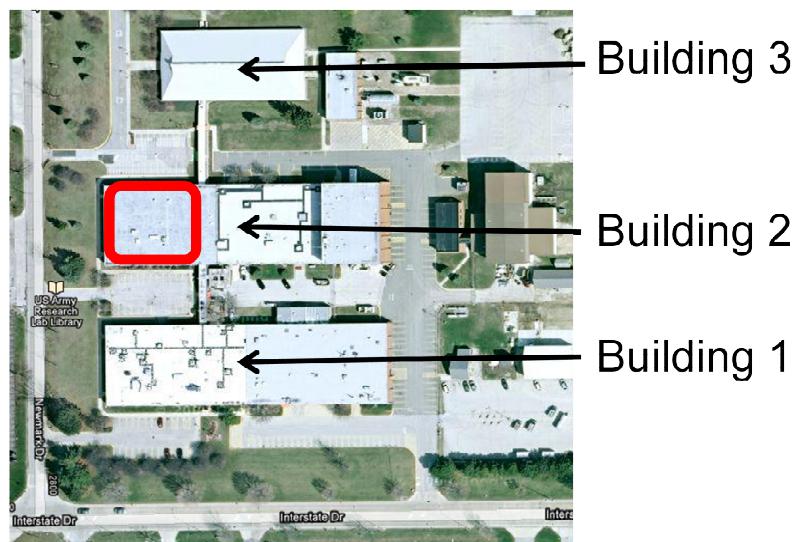


Figure 6. CERL Facility in Champaign, IL

In addition to the above site/facility selection criteria, other considerations, both advantageous and disadvantageous, are:

- The energy retrofit activities align with CERL's mission for reducing the site energy consumption and facilitating the integration of advanced technologies for the HVAC systems.
- A disadvantage against the demonstration of the full savings benefits for typical sites, both in terms of energy and peak power consumption, is the presence of a thermal storage unit that reduces the day-time peak power electrical consumption, and thus is not representative for an average facility. It is therefore expected that the electrical power consumption will be reduced to a larger extent (than demonstrated at CERL site) for facilities not equipped with thermal storage. To generate energy performance estimates for typical sites (not equipped with thermal storage) the performance analysis will use measurement data to estimate reduction directly in the peak thermal power and use typical chiller efficiency value to estimate potential peak electrical power savings.

For selecting a particular area within the three buildings for HVAC system retrofits, advanced control algorithm implementation and demonstration, several criteria were considered based on previous experience of the team members and CERL personnel feedback. These criteria are:

- Availability of Outside Air (OA): This was critical for demonstrating applicability of optimized control schedules for maintaining the comfort within the IAQ constraints.
- Presence of multiple zones: The energy savings potential is larger for areas with larger number of zones, due to a larger potential for using the adjacent-zone thermodynamic interdependencies to increase comfort while decreasing energy consumption.
- Number the rooms per zone: The potential for increasing the comfort reduces as the usage diversity and number of rooms per zone increases.
- Region connectivity and number of entrances in the area: The region connectivity - area of the wall shared between zones - provides similar benefits as presence of multiple zones, while smaller number of entrances increases the occupancy estimation accuracy.
- Diversity of space usage: A representative area for DoD sites which includes a mix of office spaces, conference rooms, and lab space.
- Chilled water source: Scalable energy savings, that can be easily extrapolated to other DoD sites, can be provided if there is no thermal storage present in the chilled water loop. However, CERL facilities include an ice storage unit that services all buildings.
- Near-future planned major retrofits: The building areas selected for retrofit for this project cannot interfere with any near or longer term retrofits or space re-planning/reassigning by CERL facility management.
- Presence of LonWorks communication network: Existing projects at CERL include development and installation of a Building Automation System on a Wonderware platform.

Initially, a coarse selection of areas was made and the resulting options are illustrated in Figure 7 and 8. Building 1 areas have been excluded due to the presence of large open spaces and due to

some areas being planned for near-term retrofits and usage change. Two promising options resulting from the initial pass of selection criteria were - (i) the west side of Building 2, served by Multi-Zone unit, and (ii) the combination of areas served by AHUs 7 & 9 & 12. In the second stage, the team ranked the two areas using above mentioned selection criteria (Table 2). Based on the team ranking of these criteria for the aforementioned two options, the selected demonstration area is the west side of Building 2, an area served by the Multi-Zone unit and consisting of offices, conference room, and cafeteria.

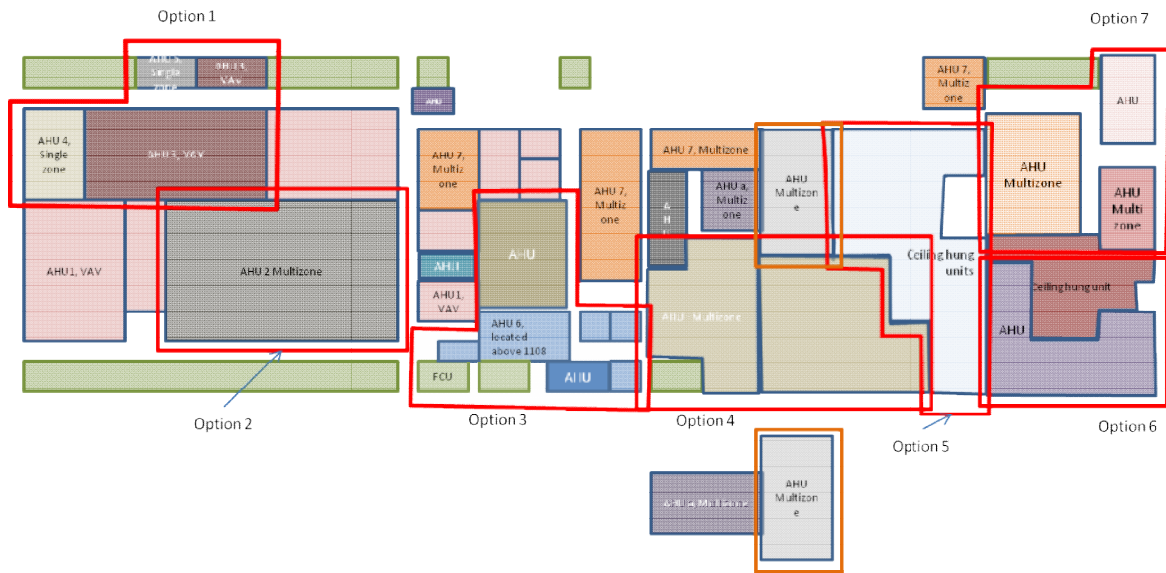


Figure 7. CERL Building 1 Layout with Highlighted Colored Areas Considered

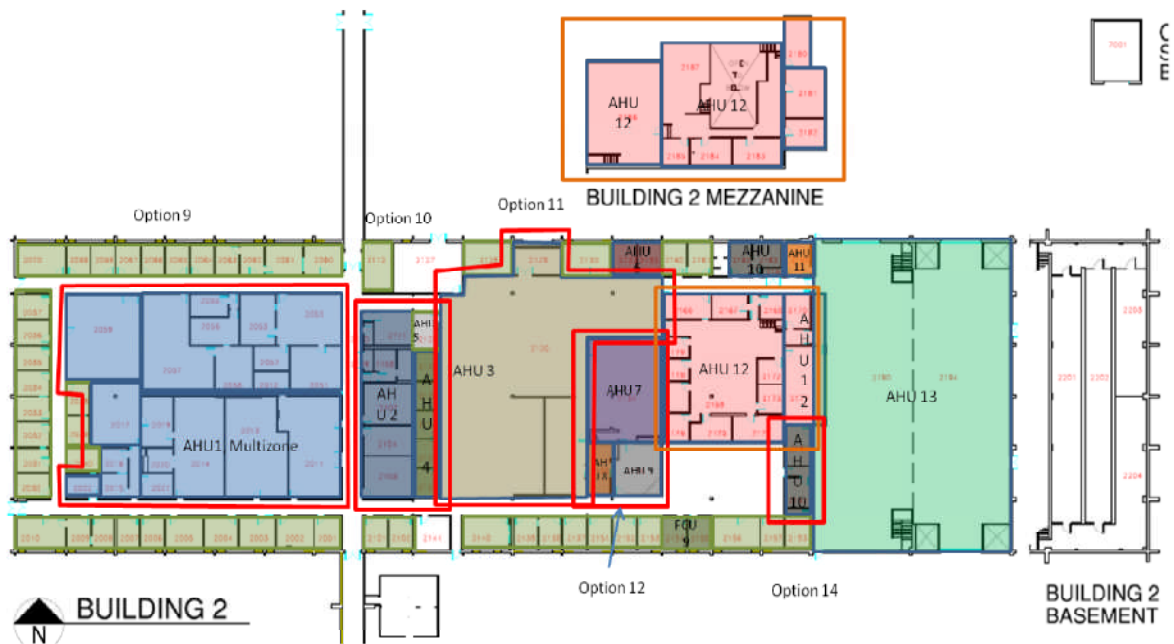


Figure 8. CERL Building 2 Layout with Highlighted Colored Areas Considered

Table 2. Criteria and ranking of the two options in Building II (Color code: green—high preference; yellow—medium preference; orange—not preferable)

Criteria	Option 9 (Bldg 2, AHU MZU)	Option 12 & 13 (Bldg 2, VAV)
OA control		
More than 1 zone		
Fewer rooms per zone (max actuation authority)		
Connected region & small # of entrances		
Diversity of space usage (office, conf room, lab)		
Not served by ice storage		
No major renovation/retrofit planned in the next 2 years		
Existing LonWorks network		

4.2 FACILITY/SITE LOCATION AND OPERATIONS

The demonstration area is served by a constant volume multi-zone system, serving five zones. The HVAC equipment in the demonstration area is controlled using pneumatic actuators that maintain the occupant-selected thermostat temperatures by controlling position of dampers (outside air, supply, return and zone air-flow), and temperature set-points in hot deck and cold deck coils. Facility wide, CERL is upgrading the control equipment to digital controllers and integrating it in a LonWorks communication network that enables both automatic monitoring (near-term) and control (long-term) of the HVAC components. Wonderware software is being installed as part of the upgrading activities currently in progress at CERL (in parallel to this project activity). The existing control schedule is fixed, and independent of weather forecast and occupancy. Due to the lack of adequate instrumentation, integrated controllers and monitoring systems, it is unclear to what extent the IAQ constraints were being met in the pre-retrofit condition, or what the current energy consumption of the system was.

4.3 SITE-RELATED PERMITS AND REGULATIONS

The facility selected for demonstration is owned by the University of Illinois at Urbana Champaign (UIUC) and leased by the Construction Engineering Research Laboratory. The building retrofits required were reviewed with CERL to ensure consistency with CERL and DoD standards for procurement through sub-contractors, installation and commissioning, using an existing controls sub-contractor Alpha Controls who was previously approved for CERL site work. UIUC building standards were also followed to the extent possible while being consistent with project schedule and budget constraints. Any deviations from UIUC standards were reviewed with CERL. The subcontractor performing the retrofits was responsible for obtaining required local permits and ensuring compliance with building HVAC codes. Necessary approvals for installing and programming the BAS and required IT approvals were obtained in close coordination with CERL facility and IT. The remote VPN connection required for the demonstration experiments were approved by CERL facility and IT and a separate computer from CERL was provided to UTRC team to conduct experiments remotely from UTRC location in East Hartford, CT. ORNL obtained the required approvals from CERL for installing RF devices on-site. The frequency band and protocols used for wireless communication were

reviewed with the designated IT and security officials at CERL as part of the approval process. There were no major obstacles encountered in the BAS and WSN installation due to early and close engagement with CERL research, facility management and IT staff. Typical lead times for the required approvals that concerned IT were on the order of 1 month, but could be longer depending on other on site commitments.

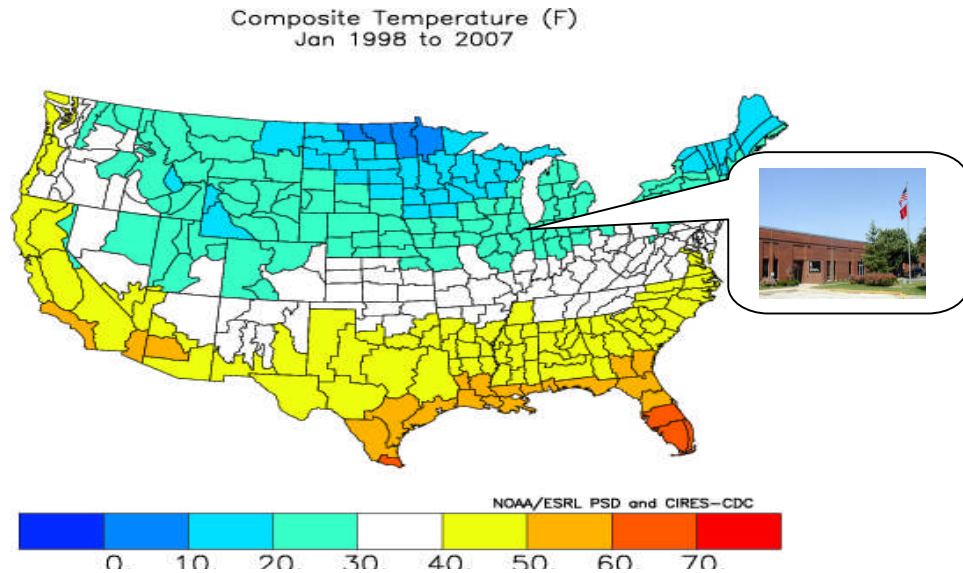


Figure 9. CERL facility indicated on 1998-2007 interval average temperature map

5.0 TEST DESIGN

5.1 CONCEPTUAL TEST DESIGN

The overall experiment consisted of three controls modes that were implemented for various periods of time (days to weeks). These operational modes are:

- 1) Baseline, or Pre-Retrofit, control strategy – this strategy mimics the control strategy that the demonstration system used when it was actuated by a pneumatic system. The HVAC system set points were constant with some seasonal adjustment.
- 2) Normal, or Post-retrofit, control strategy – updated control strategy that takes advantage of the DDC controls and retrofits, and uses heuristic rules for controlling set points. This is a state-of-the-art field implementation that has been also monitored since the system was retrofitted and slightly adjusted to improve performance.
- 3) Advanced, or Optimal, control strategy – the advanced model predictive control strategy that is proposed in this project.

When operating in mode two, the set-points will be generated by the DDC. In modes one and two, the local controls will accept supervisory commands issued by MATLAB regarding which option to run. A LonWorks direct digital control network system will monitor all the energy meters and control points. A wireless network was deployed throughout the demonstration area to collect information on temperature, RH, CO₂, and occupancy.

Table 3. The HVAC system retrofits for all three modes of operation evaluated

Mode	Pneumatic (Baseline)	DDC (Nominal)	MPC (Optimized)
Volume	Constant	Variable	Variable
Actuation type	Pneumatic	DDC	DDC
Instrumentation	Pneumatic, thermostats	T (air and water-side); CO ₂ ; RH; airflow; BTU; kWh	Bi-directional people counters; averaging zone discharge air temp. and relative humidity; additional space temperature sensors
Set point schedule	Constant; same set points as pneumatic actuation; seasonal adjustments;	Reactive; heuristic-rule based	Predictive; optimization-based

5.2 BASELINE CHARACTERIZATION

The baseline control strategy mimicked the existing control strategies against which the post-retrofit and optimal control strategies were compared. Figure 10 shows the current zone and system schematics. The control strategy consists of operating the multi-zone system continuously twenty-four seven, varying the supply temperature to each of the zones by mixing hot and cold air as required, with fixed damper position for outside air. The hot and cold deck dampers are connected to a single shaft. Table 4 shows the list of sensors that will be deployed to monitor the demonstration area during all the three test phases. The following data (with a fifteen-minute sampling interval) was measured to estimate the baseline performance:

1. Cooling coil thermal energy (MMBtu)
2. Heating coil thermal energy (MMBtu)
3. Supply and return fan energy consumption (kWh)

In addition, the independent variables related to weather (temperature), occupancy (people count, CO₂, PIR, and PC), outside air flow, and system operation status were tracked.

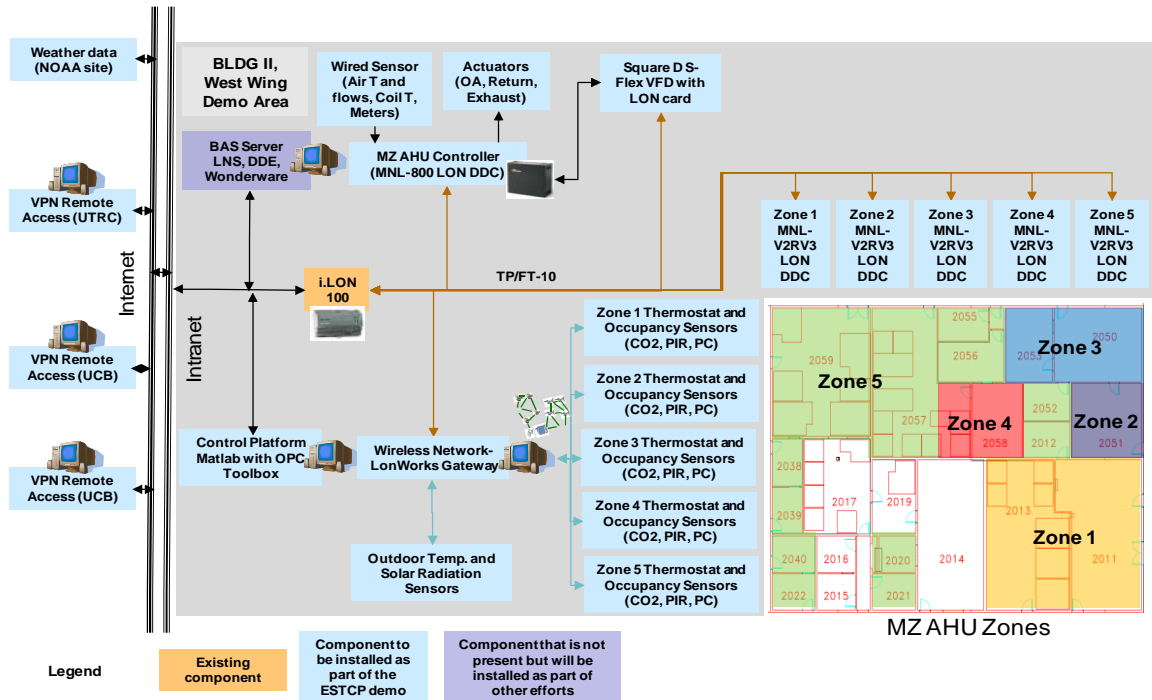


Figure 10. System Communication Architecture

The retrofit tasks for the baseline retrofit are described in Table 4. The retrofit was implemented by Alpha Controls and Services in the time period May-August, 2010.

Table 4. Retrofit items in the demonstration area

Task No.	Description
1.	MZU controllers retrofit, from pneumatic to DDC, and integration to existing LonWorks network
2.	Zone airflow controllers retrofit and integration
3.	Variable frequency drive installation and integration for SF and RF
4.	Control sequences implementation in Building Management System software
5.	Zone 1 and Zone 3 re-ducting and electrical valves installation
6.	Sequence of operation generation for baseline and post-retrofit controllers
7.	Testing, Adjusting & Balance (TAB)

Table 5. List of Sensors to be installed in the demonstration area

Level	Category	Type	Count
Space	Temperature/RH	Wireless	7
			13
	Pressure differential (for diffusers)	Wireless*	3
	CO2	Wireless*	4

	PIR	Wireless*	10
	PC	Wireless	20
Zone	Thermostat	Wired	5
		Wireless	1
	CO2	Wireless*	5
System	Electric Meter	Wired	2
	Air flow meter	Wired	3
	Pressure differential (zones)	Wireless*	5
	Temperature/RH	Wireless	12
	CO2 in supply/return	Wireless*	2
	Btu meter	Wireless*	2
Environment (Outside)	Temperature/RH	Wireless	1
	CO2	Wireless*	1

*any wired sensor that generates 4-20mA signal can be converted to wireless

5.3 DESIGN AND LAYOUT OF TECHNOLOGY COMPONENTS

5.3.1 SYSTEM COMMUNICATION ARCHITECTURE

The overall architecture of the controls platform and its integration with the existing LonWorks network was shown in Figure 10. The DIACAP (DoD Information Assurance Compliance Process) was not part of the project, and a workaround (as an exception) was used instead to conduct the demonstration. The implemented architecture was built on and integrated with CERL's LonWorks-based system consisting of:

- LonWorks communication architecture consisting of a network controller, i.LON 100, and TP/FT-10 cabling. All the local controllers for the MZU unit and zones communicate via this network. They receive updated set point values and system status commands and send updated sensor values.
- Wonderware BAS and LNS server that are currently installed under separate projects at CERL. The communication between Wonderware and LNS server is based on the OPC protocol, and this decision was made to ensure compatibility with the communication protocol with the optimization platform described in Section 5.3.2.
- OPC server installed on the BAS server enables primarily communication between the two levels of the supervisory control architecture detailed in Section 5.3.2, the BAS server and the optimization computer on which an OPC client is installed. All the sensor, actuator and set points are mapped accordingly between the server and client to ensure a consistent communication. Although there is no comprehensive information about this communication network for this application, and the project team has not been aware of a similar implementation as part of similar efforts, the OPC-based communication was robust as demonstrated throughout the optimization algorithm implementation period.

- Wireless platform consisting of gateway between the Wireless Sensor Network and the LNS server. The gateway will enable the real-time sensor measurements to be communicated to the LNS server and to the optimization platform.
- Laptops at UTRC, UCB and ORNL sites were connected remotely to the optimization and wireless platforms for uploading and analyzing data, and to update the algorithms.

5.3.2 HIERARCHICAL CONTROL ARCHITECTURE

The system architecture described above was designed to enable the implementation of the supervisory control architecture with two main layers, as illustrated in Figure 11:

- Optimization platform where the predictive algorithms will reside. The optimization software is based on MATLAB, an engineering computing software, and additional third-party state-of-the-art optimization. The platform operates on-line and communicates with the Wonderware BAS and LNS server via OPC. The optimization algorithm uses sensors measurements and generates optimized set-points.
- MZU and zone controllers that implement the set-point received from either the BAS or the MATLAB platform. These local control loops are realized by controlling the following actuators: Variable Frequency Drives; OA and RA damper actuators; airflow damper actuators; proportional electrical valves controlling the flows in the hot and cold deck coils.

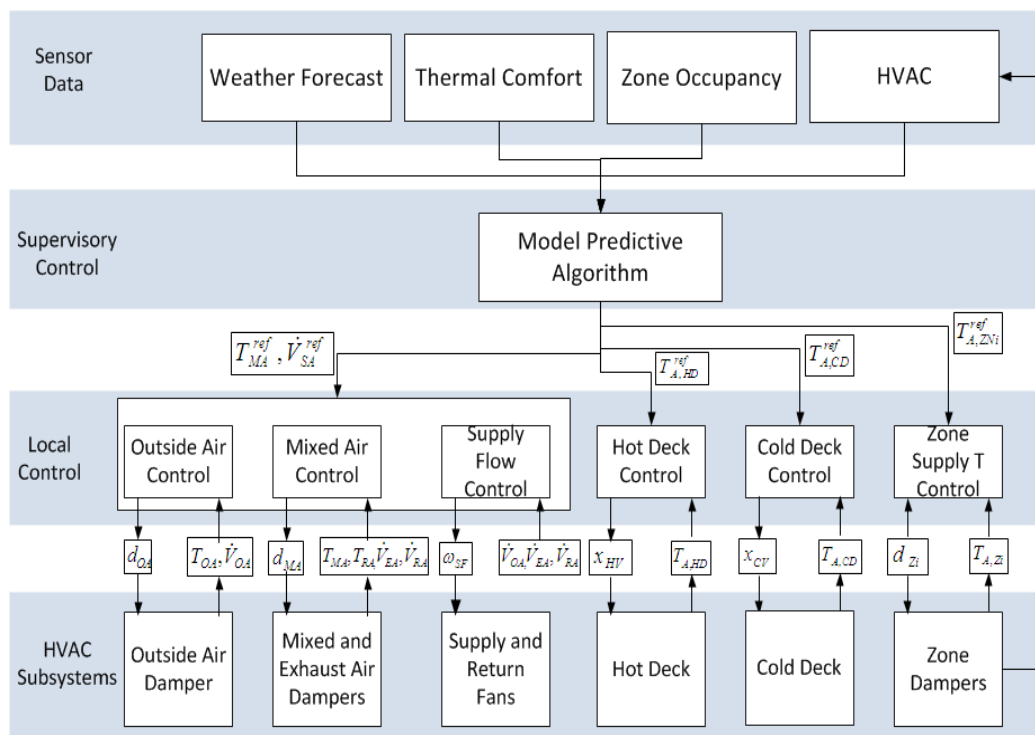


Figure 11. Hierarchical Control Architecture

5.3.3 HVAC RETROFITS

The major retrofits consists of the upgrade of current pneumatic controls to direct digital controls and Variable frequency drive installation and integration for supply and return fans. This allows for significant controllability of the system and helps in realizing the potential of the optimal control strategy. Figure 10. System Communication Architecture

The retrofit tasks for the baseline retrofit are described in Table 4. The retrofit was implemented by Alpha Controls and Services in the time period May-August, 2010.

4 shows all the retrofits items for the demonstration area. **Figure 10. System Communication Architecture**

The retrofit tasks for the baseline retrofit are described in Table 4. The retrofit was implemented by Alpha Controls and Services in the time period May-August, 2010.

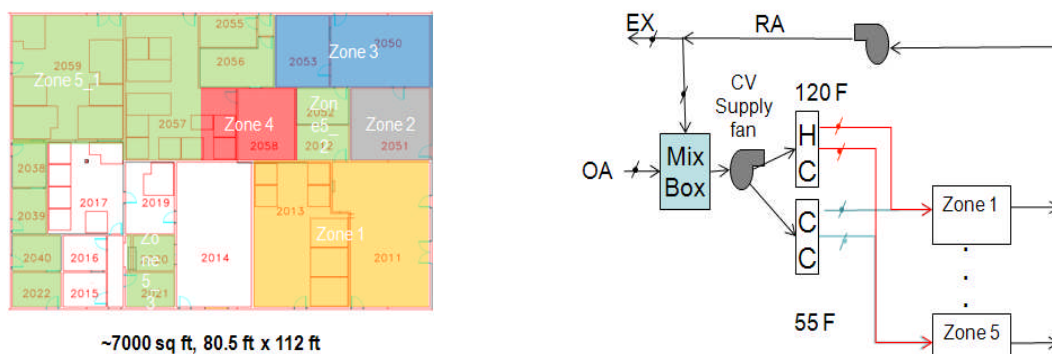


Figure 12. Multi-zone unit schematics

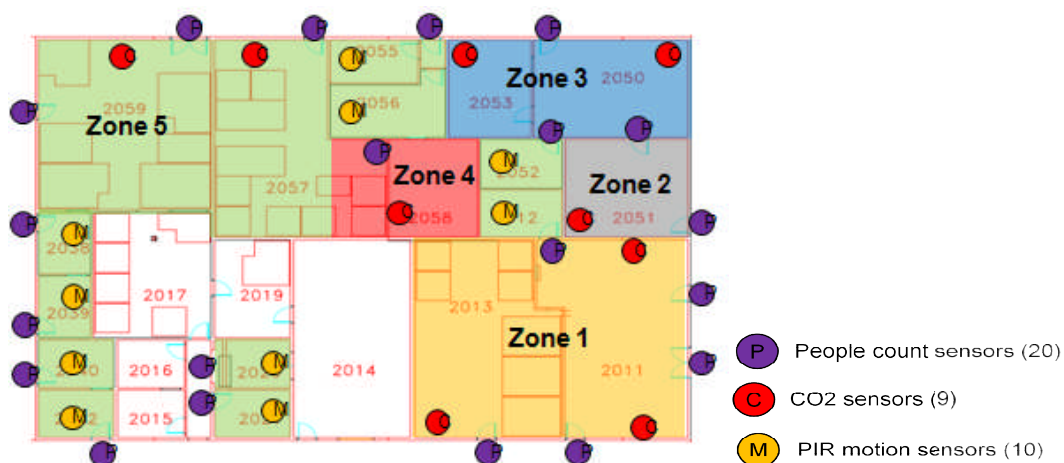


Figure 13. Occupancy related sensor installation location

The sensor requirements are driven by the performance assessment needs (thermal and electric power meters), occupancy and thermal modeling needs. Temperature sensors are located in all the surrounding corridors, ceiling space, and adjacent rooms that are not included in the

demonstration area. These are used for establishing the boundary conditions in the thermal model. CO₂ sensors are useful for both demand control ventilation as well occupancy measurement. The installation details and exact locations were determined on site with the subcontractor who installed and calibrated the equipment. The installation of low and medium priority sensors were determined by budget constraints. Figure 12 illustrates the HVAC system and demonstration site schematically. Figure 13 displays the occupancy measurement sensor network, which was used for model validation and subsequently (a subset) for the control tests.

5.4 OPERATIONAL TESTING

For the retrofits, the contractor commissioned the system to operate in the post-retrofit mode, installed the required software to enable communication with the WSN and with the optimization computer, and programmed the set point overrides for various modes mentioned in Section 5.1. The team conducted tests to check the integration of all the system components and communication between them. Tests were conducted to understand the performance of occupancy related sensors and the wireless sensor network. Before beginning the data collection for the three control modes, the MPC was tuned. This involved collecting data for about two weeks for calibrating the building model thermal states and energy consumption estimation.

Occupancy sensor tests at UTRC and CERL – For the demonstration site, infrared motion sensors, CO₂ sensors and the people counter sensors were deployed in occupied spaces, public passageways, and entrances and exits respectively. The wireless sensors for occupancy measurements were deployed in a small office building environment at UTRC first to characterize the sensor performance in the built environment. This involved measurements of the occupancy levels under a variety of test conditions (e.g. with heavy occupant traffic and sparse occupancy) to establish statistical bounds on the sensor accuracy and performance over extended periods of time. Similar experiments and characterization were conducted at CERL involving larger scale deployment of the above-mentioned occupancy sensors at specified locations.

Pre-retrofit control strategy test period – The simplified control strategy mimicked the current pneumatic controls. The system was run as though it would operate twenty-four hours, seven days a week. The VFDs were set at 100%, the hot and cold deck temperatures at constant value of 120°F and 55°F respectively, and OA damper position was set at the current level (during the retrofit, this position was noted).

Post-retrofit control strategy test period – The post-retrofit control strategy consisted of operating the fan at variable speeds, resetting the cold and hot deck temperatures based on zonal calls for heating/cooling, OA control based on critical zone CO₂, and time based on/off schedule for operating the system based on typical occupancy patterns.

Optimal control strategy test period – Based on the predicted external and internal loads, the MPC algorithm generates optimal set-points for OA, supply hot deck and cold deck temperature, flows to each space, and fan speed. In this mode, the generated set-points over-ride the local controller set-points.

5.5 SAMPLING PROTOCOL

The three control modes (pre-retrofit, post-retrofit, and optimal) were run sequentially whenever possible to get performance data for different seasons and indoor usage (Figure 14). Each option spanned multiple days with warm-up scenarios, before switching to the next option. The data were collected at fifteen minute intervals, and spanned both energy consumption related data as well as zonal conditions (temperature, CO₂, and occupancy).

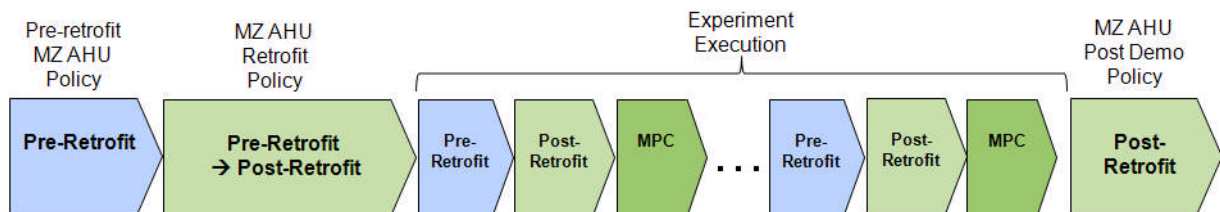


Figure 14. Operational testing sequence

5.6 SAMPLING RESULTS

Calibration of Reference Model for MPC: The thermal network model represents the performance of the building envelope, HVAC, and control systems. Metering data for fan electricity, chilled water usage, and hot water usage were used to calibrate and validate the model. Some monitored data such as real-time weather data were processed to provide inputs for the model. The internal loads including plug load and lighting load were assumed based on inputs from CERL team with respect to typical lighting wattages and internal equipment in each space, and applied as inputs to the reference model; limited measurements of plug loads were also carried out by deploying CT meters in the facility over an extended period of few weeks. The calibration aimed for $\pm 10\%$ NMBE (Normalized Mean Bias Error) and $\pm 30\%$ for CVRSME (Coefficient of variation of the root mean square error) as per ASHRAE guideline 14-2002 [12].

6.0 PERFORMANCE ASSESSMENT

The performance of the retrofitted system, as summarized in Table 1 was determined from recorded measurement data. A significant challenge in estimating the energy savings, as is the case for industrial applications, is the inconsistency in the weather and usage patterns. The energy savings, the approach and the pair-wise comparison between the three modes of operation is discussed in the following two sub-sections.

6.1 PERFORMANCE COMPARISON BETWEEN PRE- AND POST-RETROFIT MODES

To ensure consistent comparisons between the energy consumption levels for the two modes, they were implemented sequentially in July 2011 as follows: pre-retrofit mode during July 16th—July 31st, and post-retrofit mode during July 5th—July 13th. The similarity between the conditions corresponding to these two time interval is illustrated by plots of measured ambient temperature and the estimated zonal in Figure 15 and 16, respectively.

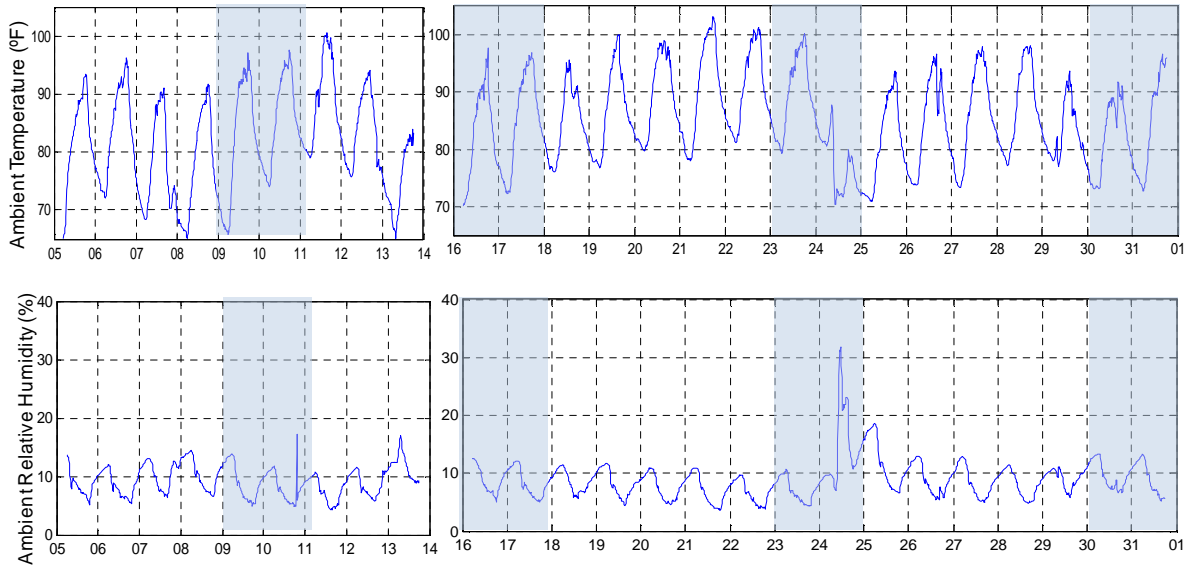


Figure 15. Ambient temperature (top) and relative humidity (bottom) during the pre- (left plots) and post-retrofit (right plots) modes; on x-axis: calendar days in July 2011 (shaded areas are weekends which are excluded from energy savings comparison)

The similarity between the ambient and usage conditions for the two modes makes possible a direct comparison of measured BTU and electrical meter energy consumption without additional normalization or averaging. Although this is possible, it may introduce sources of errors, as is the case with any model. Based on direct comparison of electrical and thermal energy consumption, as illustrated in Figure 18, one concludes that the relative energy consumption savings are nearly 30%. These are direct results of three improvements to the post-retrofitted system operation:

- **Schedule:** as opposed to the pre-retrofitted system that operates at constant volume and schedule at all times, the pre-retrofitted system has been scheduled to operate only during working hours with additional pre-cooling and heating. Outside the normal working hours, the occupants have the possibility to override the otherwise scheduled set points by selecting appropriate input of the thermostat.
- **Set point schedules:** as opposed to the pre-retrofit scheduled fixed set points for all weather and load conditions, the post-retrofit schedule uses heuristics to adapt these values. These differences are partly illustrated in Figure 18, where it can be observed that the pre-retrofit mode saves energy by using lower hot deck discharge air temperature and lower supply flow. Evidently, the pre-retrofit control mode conservatively utilized higher hot deck temperatures and lower cold deck temperatures, and much higher supply airflow rates.
- **Local control:** the local controllers are improved by using features beyond the capabilities of the original pneumatic-based controllers (such as the integral action of the DDC's PI control algorithm; economizer; temperature and pressure resets).

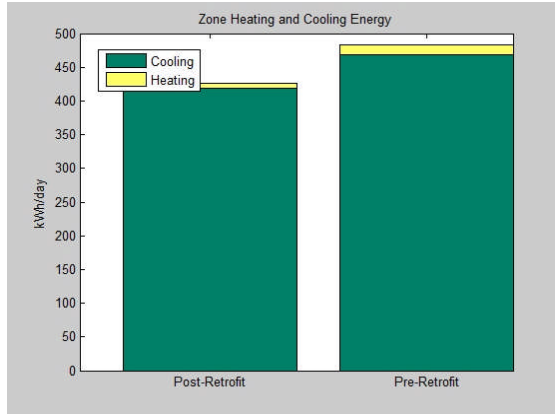


Figure 16. Average zonal load conditions during the pre- and post-retrofit modes

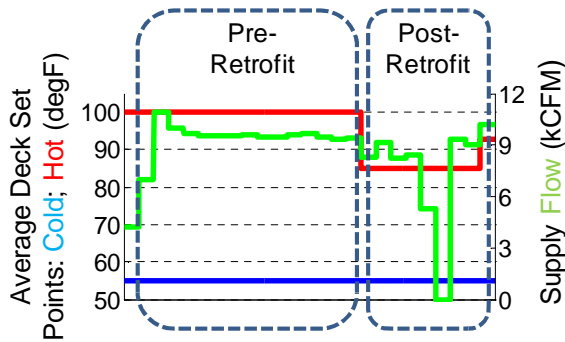


Figure 17. Average set points for cold and hot deck discharge air temperatures and supply flows

The noted savings are generated while improving the thermal comfort measured by the difference between the zone thermostat and actual space temperature values. As seen in Figure 19 the thermal comfort is significantly improved, a result of the control features of the DDC system. The post retrofit improvements were all achieved as part of the demonstration project.

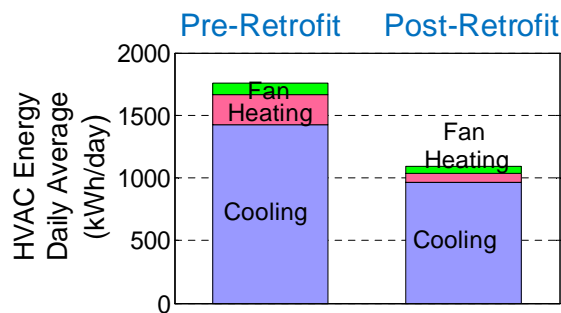


Figure 18. Illustration of HVAC energy consumption for the pre- and post-retrofit modes

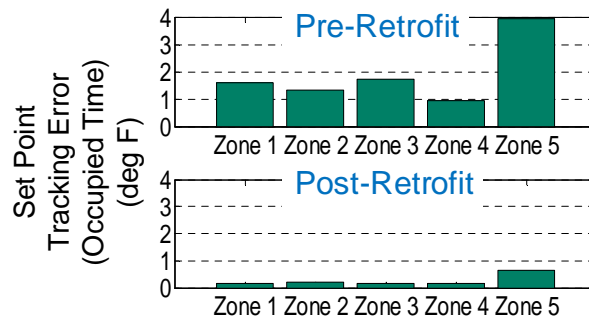


Figure 19. Average difference between set points and actual space temperature values for pre- and post-retrofit

6.2 PERFORMANCE COMPARISON BETWEEN POST-RETROFIT AND OPTIMIZATION MODES

This section summarizes the performance benefits of the optimized system controlled with set points generated by the developed model-based predictive algorithm. As mentioned the main challenge in estimating these benefits is the variations in ambient and usage conditions between these two modes. In order to use exclusively measurement data based calculations we have used data between days when the ambient conditions were similar. Therefore, for each day when the MPC algorithm was executed a set of days were identified when the post-retrofit mode was executed and when the ambient temperature has a similar pattern, as measured in terms of the profile and the average difference between the two temperature data sets. Such a comparison is illustrated in Figure 20 (showing similar outside air conditions for the entire post-retrofit baseline day and that for MPC), Figure 21 (showing energy savings achieved by MPC), Figures 22 and 23 (showing indoor zonal temperature tracking for both post-retrofit and MPC modes), Figures 24 and 25 (showing peak power consumption patterns and splits for the MPC and post-retrofit modes respectively); these were recorded for the MPC data, from Thursday, Oct 27th, 2011, and for post-retrofit data, from Monday, Oct 31st, 2011.

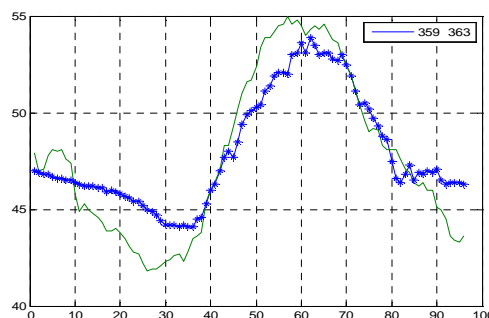


Figure 20. Ambient temperature for MPC (blue) and post-retrofit day (green)

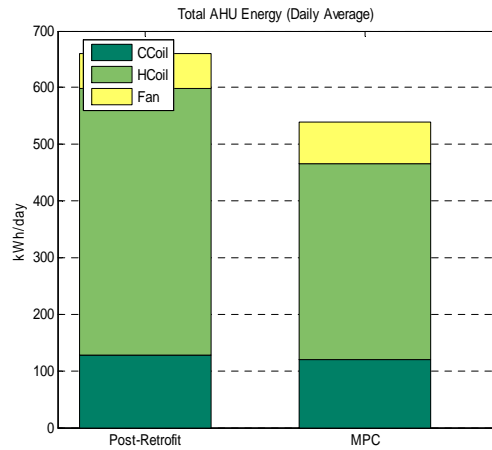


Figure 21. The total HVAC energy (electrical and thermal) consumption for the MPC day and post-retrofit days.

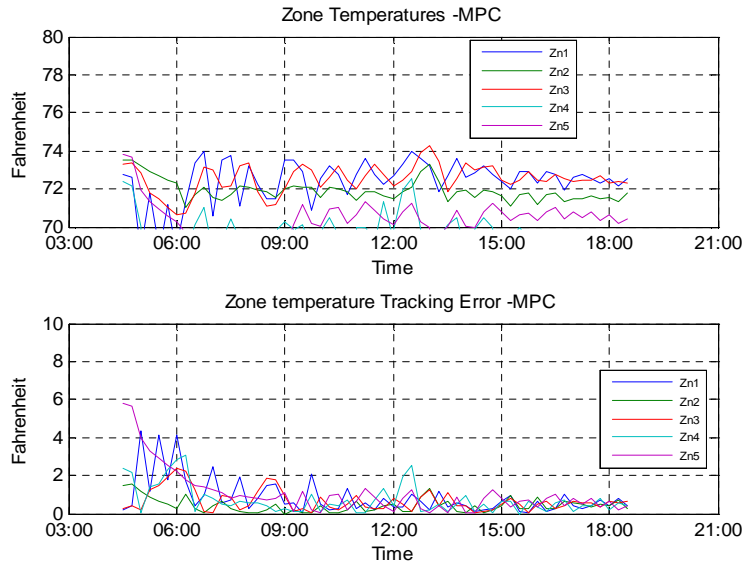


Figure 22. The zone temperatures and differences between thermostat and space temperatures for MPC data

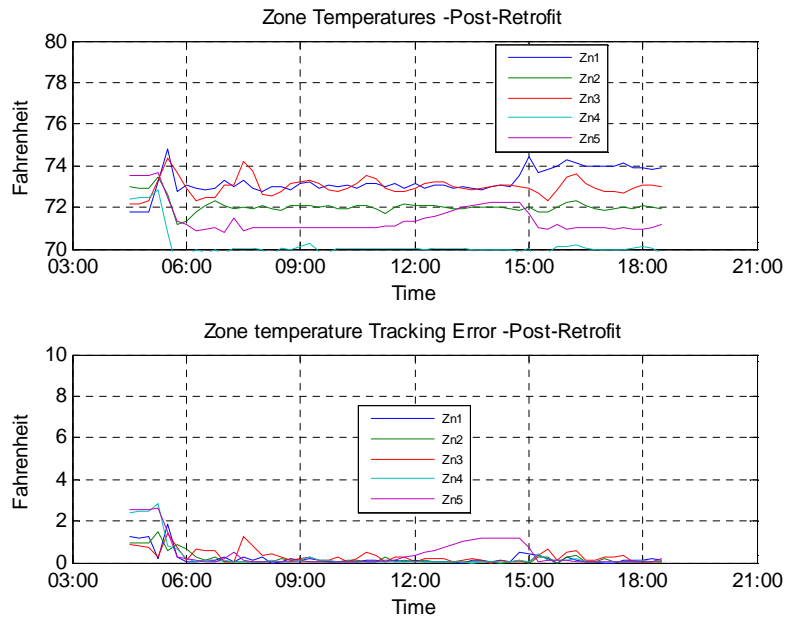


Figure 23. Illustration of zone temperatures and differences between thermostat and space temperatures for post-retrofit mode data

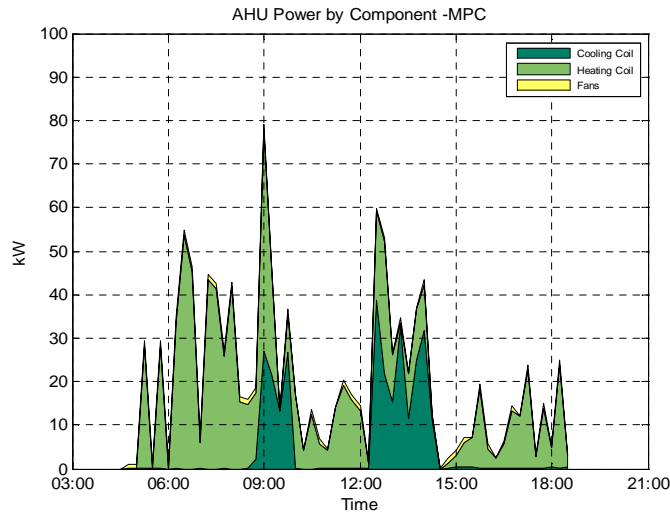


Figure 24. Illustration of the HVAC unit power consumption by component for the MPC data

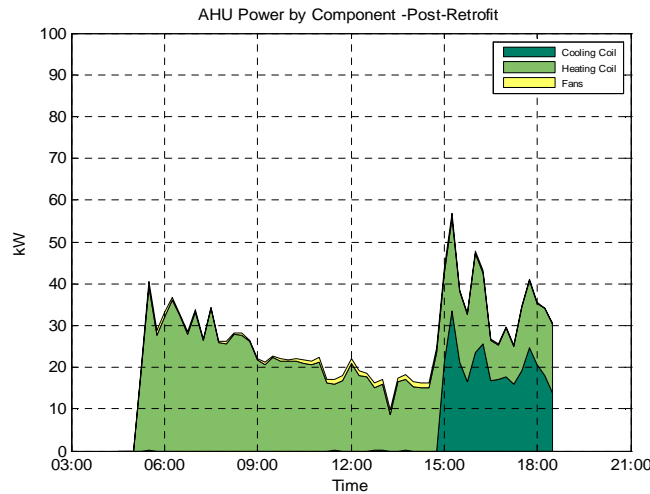


Figure 25. Illustration of HVAC unit power consumption by component for post-retrofit data

The data illustrated in these figures has been used to generate the overall estimates of Table 1. An analysis of these plots illustrates the following:

- The maximum thermostat set point tracking error is 1°F for the MPC mode and 0.5°F for the post-retrofit mode. This is a result of the flexibility of the MPC algorithm and its optimality. By flexibility it is meant that the designer can select the acceptable range of the thermal comfort and therefore define bounds around the thermostat set point within which it is acceptable to operate. By optimality is meant that in general MPC algorithm generates space temperature levels that are close to the acceptable bounds of the thermal comfort range. In this case the acceptable bounds was set at 0.5°F and the modeling error resulted in an additional 0.5°F totaling the average 1°F tracking error.
- Although energy is saved for the MPC mode, the peak power is increased. This increase can be explained as follows. The thermostat set point for the largest zone is changed around 9:00AM and this resulted in a higher than usual peak power value while the MPC algorithm tried to control the temperature within the new thermal comfort range. This is evidenced further in the energy performance measurement summary provided next.
- The space temperature for the MPC mode has higher frequency oscillations than for the post-retrofit mode. This could be explained by: (i) model errors: the MPC uses models for predictions that trigger the system to compensate, resulting in oscillations; (ii) the local control transient behavior which is not included in the supervisory controller. An assumption was made that the local controller responds consistently fast and accurately. After executing several sets of experiments it was observed that this was not the case.

To minimize the impact of the variations in ambient conditions on performance benefit estimation, the MPC data was compared against multiple post-retrofit datasets when ambient temperature patterns were similar. The data is summarized in Table 5 and detailed in Tables 6-10, providing details on the system, indoor and ambient conditions for the tests conducted in the post-retrofit and MPC modes of building operation. Positive entries in shaded columns titled “relative energy savings” and “relative peak power decrease” indicate reductions, whereas negative entries indicate increase for MPC mode.

Table 6. Experimental data and performance summary for MPC days in 2011, summarizing average energy and peak power consumption, indoor and ambient conditions (the relative peak power *decrease* is negative meaning that the peak power increased).

	Calendar Day	Average OA_T (degF)	Average OA_HR	Chiller Operation (Y/N)	Average SP (degF)	Average SP Tracking Error (degF)	STD of SP Tracking Error (degF)	Total Energy Consumption (Daily Average)	Relative Energy Savings	Coincident Peak Power (kW)	Relative Peak Power Decrease
MPC Day # 1	27-Oct-11	48.7	0.0014	Y	71.5	0.1	0.7	540		79	
Post-Retrofit Day	18-Feb-11	47.9	0.0013	N	70.9	-0.1	0.4	731	26%	60	-32%
Post-Retrofit Day	31-Oct-11	48.7	0.0014	Y	71.9	0	0.2	660	18%	57	-39%
Post-Retrofit Day	1-Apr-11	48.9	0.0013	N	73.2	0	0.2	578	7%	43	-84%
Average Post Retrofit Day								656.3333333	18%	53.33333333	-48%
MPC Day #2	1-Nov-11	60	0.0016	Y	72	0	0.5	676		68	
Post-Retrofit Day	13-Apr-11	63	0.0017	Y	72.4	-0.2	0.5	775	13%	56	-21%
Average Post Retrofit Day								775	13%	56	-21%
MPC Day #3	4-Nov-11	50.3	0.0014	Y	72	0	0.4	321		46	
Post-Retrofit Day	11-Mar-11	48.8	0.0013	N	72	0	0.3	602	47%	50	8%
Post-Retrofit Day	5-Apr-11	52.8	0.0014	Y	72.3	-0.2	0.4	887	64%	48	4%
Post-Retrofit Day	21-Oct-11	52.7	0.0015	N	71.2	-0.9	0.3	380	16%	21	-119%
Average Post Retrofit Day								623	48%	39.66666667	-16%
MPC Day #4	15-Nov-11	55.3	0.0016	Y	71.4	-0.1	0.8	755		85	
Post-Retrofit Day	8-Apr-11	56	0.0015	Y	72.6	0	0.4	870	13%	63	-35%
Post-Retrofit Day	18-Apr-11	54.5	0.0015	Y	71.9	-0.3	0.5	855	12%	61	-39%
Average Post Retrofit Day								862.5	12%	62	-37%

Despite best efforts to ensure consistency in indoor and ambient conditions, there is variability in the energy savings estimated. However, the average energy savings are evident in every case, providing consistent reductions in the range of 11-64% relative to the post-retrofit mode; the average savings were estimated by comparing the average baseline energy consumption with that for the MPC case in each case (also denoted as Test#). The causes of the variability in the baseline, despite careful choice of internal and ambient conditions (such as temperature set points and outside air temperatures) to be consistent between the post retrofit and the MPC modes, are still being investigated and will be further detailed in a second set of demonstration tests reported later in this section. Also, with two exceptions (see MPC day # 3 case), the peak power for the MPC mode is higher than for the post-retrofit mode. This was a direct consequence of the controlled system (oscillation) behavior discussed earlier and will be re-visited following control algorithm modifications later in this section. Figure 26 summarizes the average energy savings for the cases summarized in the table above, as well as the peak power usage average (which was generally affected adversely in the initial MPC implementation).

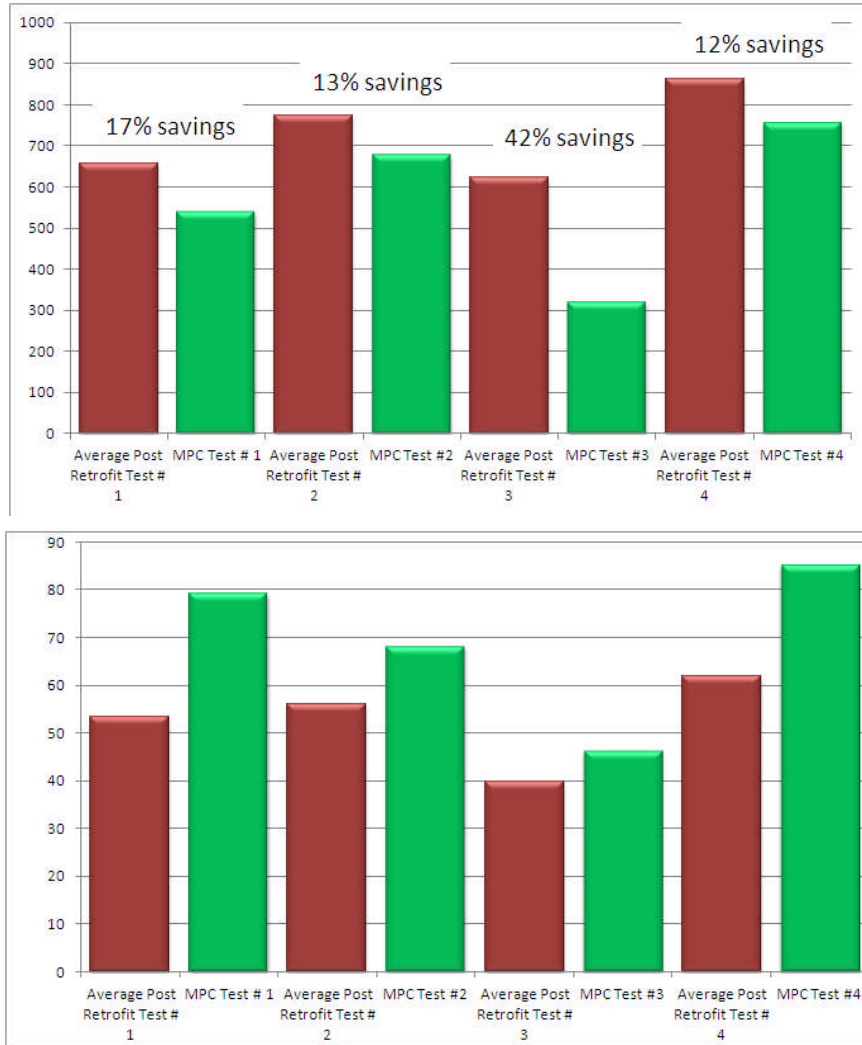


Figure 26. Summary of HVAC system energy use (top) and peak power consumption (bottom) for 2011 demonstration tests.

Using the insights gained after analyzing the 2011 demonstration experiment data summarized above, the MPC algorithm was revised and improved, including refined dynamical models for the mixing, hot deck and cold deck temperatures with the goal of improving the poor peak power usage performance for the MPC mode. Another set of demonstration experiments were proposed to CERL staff and, following their approval, were conducted during the week of Feb. 13-17, 2012. The results were processed following the same procedure as explained for the data generated in Despite best efforts to ensure consistency in indoor and ambient conditions, there is variability in the energy savings estimated. However, the average energy savings are evident in every case, providing consistent reductions in the range of 11-64% relative to the post-retrofit mode; the average savings were estimated by comparing the average baseline energy consumption with that for the MPC case in each case (also denoted as Test#). The causes of the variability in the baseline, despite careful choice of internal and ambient conditions (such as temperature set points and outside air temperatures) to be consistent between the post retrofit and the MPC modes, are still being investigated and will be further detailed in a second set of demonstration tests reported later in this section. Also, with two exceptions (see MPC day # 3

case), the peak power for the MPC mode is higher than for the post-retrofit mode. This was a direct consequence of the controlled system (oscillation) behavior discussed earlier and will be re-visited following control algorithm modifications later in this section. Figure 26 summarizes the average energy savings for the cases summarized in the table above, as well as the peak power usage average (which was generally affected adversely in the initial MPC implementation).

and they are discussed below for each of the experimental days when the refined MPC algorithm was implemented. For each MPC case (a day when the MPC algorithm was executed during the occupied hours), a number of similar ambient-temperature day were identified when the Post-Retrofit algorithm was implemented. The corresponding performance metrics (energy consumption and peak power) are summarized and overall performance metrics are illustrated in Tables 4.5-4.9. Positive entries in shaded columns for “relative energy savings” and “relative peak power decrease” indicate savings, whereas negative entries indicate adverse impact of MPC mode.

Table 7. Experimental data and performance calculations for MPC day Feb 13, 2012 (average values are calculated for occupied hours)

	Calendar Day	Average OA_T (degF)	Average OA_RH (%)	Mean OA_F (10 ³ cfm)	Mean MA_T (degF)	Mean CD_T (degF)	Mean HD_T (degF)	Average SP (degF)	Average SP Tracking Error (degF)	STD of SP Tracking Error (degF)	Total Energy Consumption (Daily Average)	Relative Energy Savings	Coincident Peak Power (kW)	Relative Peak Power Decrease	Max CO2 Level (ppm)	Zone Space Mean RH (%)
MPC Day #1	13-Feb-12	37.1	37.1	2.2	58.4	68.1	80.8	72.5	-0.08	0.4	186		70		590	12.5%
Post-Retrofit Day	2-Mar-11	38.9	38.9	2.9	62.1	63.5	87.5	71.2	-1.4	1.4	547	66%	64	-9%	593	19.4%
Post-Retrofit Day	10-Nov-11	39.5	39.5	7.7	39.4	56	96.8	71.4	-0.03	0.5	820	83%	71	0%	520	21.7%
Post-Retrofit Day	5-Nov-10	37.2	37.2	4.3	52.6	54.3	95	71.6	0.13	0.7	1427	87%	72	3%	530	18.1%
Average Post Retrofit											931	80%	69	-1%		

Table 8. Experimental data and performance calculations for MPC day Feb 14, 2012 (average values are calculated for occupied hours)

MPC Day #2	14-Feb-12	39	39	4	55	64.7	77.4	72.4	-0.04	0.6	315		46		970	20.4%
Post-Retrofit Day	15-Mar-11	40.3	40.3	6.7	51.1	55.7	93.8	72	-0.3	0.7	1070	71%	65	29%	550	25.1%
Pre-Retrofit Day	28-Nov-11	37.6	37.6	8.4	41.6	58.2	98.1	71.8	-0.44	0.2	1164	73%	67	32%	520	21.8%
Post-Retrofit Day	27-Jan-12	38.8	38.8	8.1	40.6	57.6	96.4	72	-0.07	0.4	777	60%	38	-20%	570	18.1%
Post-Retrofit Day	10-Nov-11	39	39	7.7	39.4	56	96.8	71.4	0.03	0.5	755	58%	71	0%	520	21.7%
Average Post Retrofit											942	67%	60	24%		

Table 9. Experimental data and performance calculations for MPC day Feb 15, 2012 (average values are calculated for occupied hours)

MPC Day #3	15-Feb-12	43.3	43.3	3.9	54.2	65.5	79.2	72.5	-0.05	0.5	301		48		620	23.9%
Post-Retrofit Day	14-Feb-11	42.4	42.4	7.4	41.3	61.3	94	71.8	-0.2	0.8	738	59%	49	0%	550	20.1%
Post-Retrofit Day	21-Dec-10	41.8	41.8	3.6	50.5	56.1	98.7	71.1	-0.1	0.5	655	54%	52	7%	590	21.3%
Post-Retrofit Day	23-Nov-11	44.1	44.1	9.4	38.3	58.8	97.9	71.7	-0.4	0.2	1112	73%	62	22%	500	27.3%
Average Post Retrofit											835	64%	54	11%		

Table 10. Experimental data and performance calculations for MPC day Feb 16, 2012 (average values are calculated for occupied hours)

MPC Day #4	16-Feb-12	43.7	43.7	4.3	51.5	65.6	77.2	72.6	-0.06	0.5	228		61		640	26.2%
Post-Retrofit Day	14-Feb-11	42.6	42.6	7.5	41.3	61.4	94	71.8	-0.2	0.8	747	69%	49	-26%	550	20.1%
Post-Retrofit Day	20-Apr-11	44	44	4.7	51.8	55.9	93.5	72.2	-0.02	0.2	532	57%	38	-48%	580	25.8%
Post-Retrofit Day	20-Oct-11	43.1	43.1	5.9	48.4	63	88.4	71.5	-1	1.2	600	62%	56	-9%	510	28.5%
Post-Retrofit Day	23-Nov-11	44.5	44.5	9.6	38.1	58.8	98.2	71.7	-0.4	0.2	1114	80%	62	2%	500	27.3%
Post-Retrofit Day	13-Dec-11	45.6	45.6	6.4	38.8	58.2	93	73.2	-0.03	0.4	579	61%	46	-34%	740	26.2%
Average Post Retrofit											714	68%	50	-22%		

Table 11. Experimental data and performance calculations for MPC day Feb 17, 2012 (average values are calculated for occupied hours)

MPC Day #5	17-Feb-12	44.2	44.2	3.5	50.1	67.1	74.5	72.6	-0.06	0.4	81		32		670	20.0%
Post-Retrofit Day	19-Nov-10	45.8	45.8	4.1	55.7	61.5	93.9	71.7	-0.7	1.3	445	82%	43	25%	500	22.1%
Post-Retrofit Day	30-Mar-11	44.3	44.3	5.7	52.3	56.1	92.8	73	-0.07	0.6	640	87%	52	37%	510	12.1%
Post-Retrofit Day	11-Nov-11	43.4	43.4	6.5	50.1	59	93.6	71.4	0	0.4	753	89%	51	36%	420	19.4%
Post-Retrofit Day	3-Feb-12	45.1	45.1	6.2	41.7	61	93.3	72.2	-0.08	0.4	382	79%	51	37%	620	24.8%
Average Post Retrofit											555	85%	49	35%		

From the above, the following conclusions can be drawn:

- Energy consumption for the HVAC system is reduced from 60-85%, relative to post-retrofit mode levels. These significantly exceed the 15% demonstration target metric.
- For three cases peak power usage was reduced from 10-35%. These values are also above the 10% target set for the technology demonstration.
- For two cases, the peak power usage was measured to increase by 1% and 22%. We analyze this data in more detail to explain the below target performance. For MPC Day Feb 13, 2012, when the peak power is increased by 1%, we observe in Figure 27 that the peak power of 70kW occurs early in the morning when the HVAC system is started. With this single exception all the power generated is below 50kW levels for the post retrofit mode. Upon post facto analysis, we conclude that this high initial peak could be decreased by adjusting the trade-offs between average energy use and peak power; for example the HVAC system could be started earlier. In this case the average energy consumption could be increased slightly

(still remaining above the 15% target). A similar pattern is observed on MPC Day Feb 16, 2012, see Figure 28 when the peak power increased to 61kW early in the morning while it remained below 38kW for the rest of the day. As explained above, this is due to an over-reaction of the MPC algorithm to the out-of-comfort-range temperature values reached while the HVAC system was shut down during night.

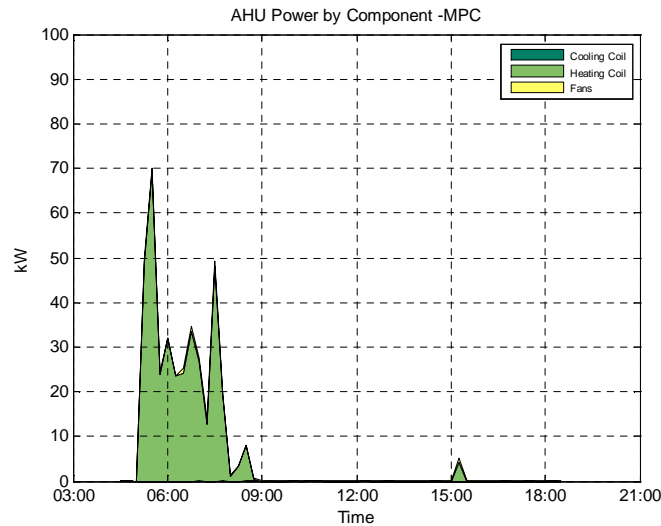


Figure 27. Total power for MPC Day Feb 13, 2012

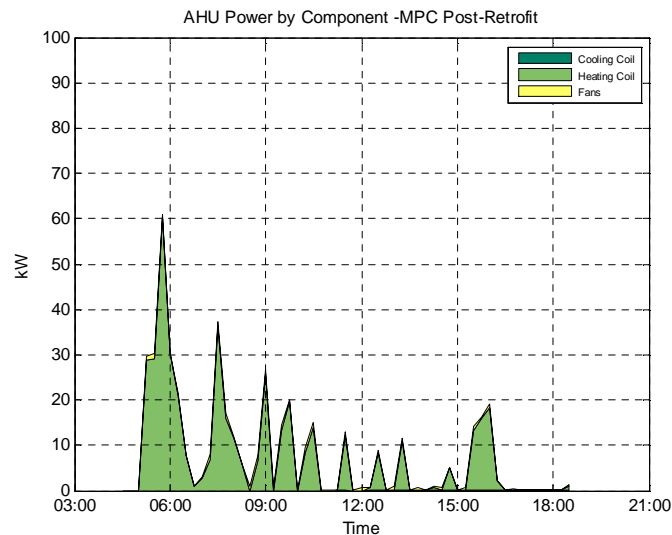


Figure 28. Total power for MPC Day Feb 16, 2012

Figure 29 summarizes the average energy savings for the cases summarized in the table above, as well as the peak power usage average (which was generally affected adversely in the initial MPC implementation).



Figure 29. Summary of HVAC system energy use (top) and peak power consumption (bottom) measurements from final demonstration tests in Feb. 2012.

The average HVAC system energy and peak power usage reductions accomplished above can be attributed to the following key factors:

- The MPC algorithm dynamically strives to decrease the multi-zone air handling unit hot deck temperatures when favorable (from system energy optimization perspective) compared to what was pre-programmed in the post retrofit mode.
- The MPC algorithm dynamically strives to increase the air handling unit cold deck temperatures when favorable compared to that for pre-programmed post retrofit mode.
- The MPC algorithm dynamically strives to decrease the amount of outside air admitted whenever favorable compared to what was pre-programmed in the post retrofit mode.

The above is accomplished by the MPC algorithm on a dynamic basis, i.e. via 15 minute updates as implemented currently. The daily average of the hot and cold deck temperatures resulting and system variables for the post-retrofit mode and for the MPC mode of operation for the 5 datasets that were summarized earlier (for 2012 demonstration experiments) are illustrated in Figure 30. It is evident that all (energy) relevant system variables were manipulated in a favorable direction, as argued above. This explains the substantial energy use reductions accomplished. The deck temperatures that were achieved for the pre-retrofit (pneumatic) controls are also illustrated for reference (see red and blue lines), supporting the large reductions in energy use accomplished when moving from pneumatic to DDC controls. It should also be noted that dual deck systems (prevalent in older buildings) are likely more prone to system duct losses and leakages driven energy waste, compared to single deck HVAC systems (which are deployed more commonly now). Thus, the impact of a higher difference between the heating and cooling deck temperature in driving energy use is likely more obvious for dual deck systems, such as in the present demonstration site. Finally, a more fine tuned DDC mode control strategy involving reset of the cooling and heating deck set points based on outside weather, rather than a seasonal setting (as currently employed in the demonstration site), would have captured some of the savings achieved by the MPC scheme. More detailed assessments and analysis for different variants of the central HVAC system and of baseline DDC mode control approaches are needed to ascertain the variability in the energy use and peak power reduction benefits across DoD stock.

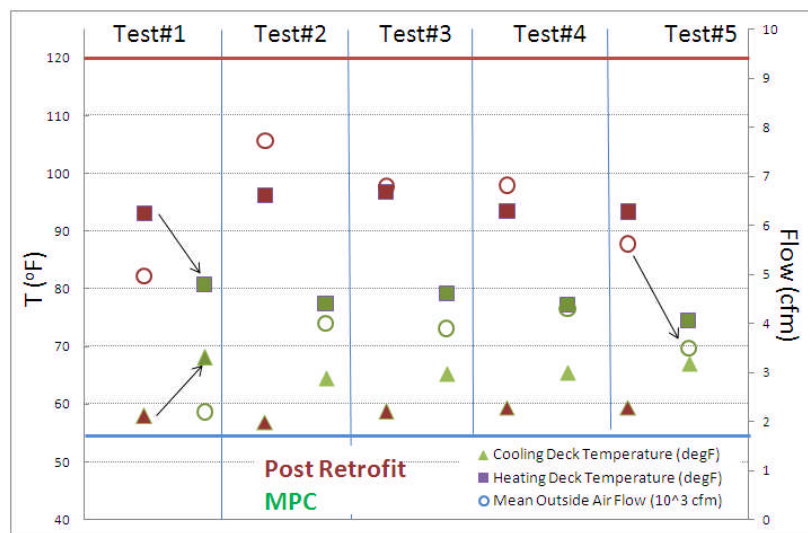


Figure 30. Summary for the post retrofit and MPC modes, from demonstration tests in Feb. 2012, illustrating the system operation changes accomplished by the optimization algorithm.

Also illustrated in Figure 31, are the indoor comfort metrics for zonal temperature tracking and CO₂ levels, showing that the controlled space temperatures never deviate beyond the constraints set, namely $\pm 1^\circ\text{F}$ of set point T_{SP} , and are within the CO₂ level limit (as derived from ASHRAE 62.1 standard) with the exception of one case where the constraint is violated.

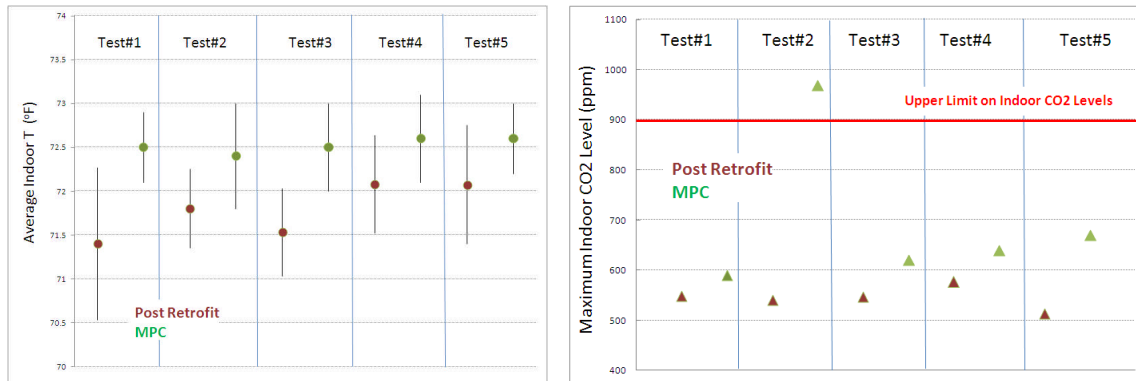


Figure 31. Summary for the post retrofit and MPC modes, from demonstration tests in Feb. 2012, illustrating the MPC performance in tracking occupant space temperature relative to zone set point T_{SP} during occupied hours (see left) and maintaining indoor CO_2 levels (see right).

7.0 COST ASSESSMENT

The demonstration was used to quantify both operational cost reduction due to energy efficiency gains, and installed (first) cost reductions and maintenance cost reduction or increase of using WSN and MPC for building HVAC control retrofits. Energy efficiency gains was quantified using the performance assessment described in Section 6. Average life of DDC before it is replaced is about twenty five years [15] so a twenty-five year time frame for the life-cycle cost estimate was used.

7.1 COST MODEL

Table 12. Cost Model for Wireless Sensor Network

Cost Element	Data Tracked During the Demonstration	Estimated Costs
Hardware and software capital costs	Estimates made based on component costs of Wireless sensors and related network infrastructure for demonstration and software for controls platform	\$53,895.00
Installation costs	Labor and material required to install sensors and controls platform	\$19,122
Consumables	Estimates based on rate of consumable use during the field demonstration including batteries, networking cables etc.	No consumables for the MPC installation
Facility operational costs	Reduction in energy consumption based on additional sensing relative to the baseline data	Pre-retrofit to Post-Retrofit: \$8,645 (57.7% savings) Pre-retrofit to MPC: \$9,640 (63.2% savings)

Maintenance	<ul style="list-style-type: none"> • Frequency of required maintenance for WSN and Controls platform • Labor and material per maintenance action 	<ul style="list-style-type: none"> • 2 hours average per month to attend to control configuration management and network diagnostics • Labor of the BAS technician/facility technician is \$2,225 per year and ideally no material cost involved in maintenance for this deployment
Hardware lifetime	Estimation of the life-cycle cost based on the equipment degradation, configuration management, and labor associated with the WSN hardware	The equipment used in this deployment does not have attributes that contribute to the life-cycle cost. The components used for the demo have a long lifetime up to twenty-five years with minimal degradation (wireless sensors, DDC boxes etc.).
Operator training	Estimate of training costs for facility personnel on usage of the equipment and operational adjustments to both WSN and controls algorithm	<ul style="list-style-type: none"> • The interface for the operator is similar to the existing interface and does not require special training for use. • Sequence of operations for post-retrofit controls is already documented and provided. Post-retrofit operator training has already happened. • Training for advanced algorithms was not provided since decision was made to discontinue the advanced control platform.

Each of the cost elements are described in more detail below:

- **Hardware capital costs:** This estimate is based on the component costs of the WSN system and compared with the hardware cost of a similar wired networking system. Cost of an additional sensor will be quantified to demonstrate the cost feasibility of scaling the network with additional sensors. Additional computer requirements, if any, for WSN and MPC compared to computer requirements for a BMS system, will also be included in the hardware capital costs.
- **Installation costs:** This estimate is based on the cost involved in installing and commissioning the WSN system. It will be compared with a quote for installation and commissioning of a similar functional system using wired sensors. Estimate of the installation cost of a wireless sensor and a wired sensor will be compared to demonstrate the long-term installation costs of the proposed technology. WSN uses a self-configuring routing protocol reducing the cost of the additional sensor installation as the number of sensors increases as opposed to a wired network.
- **Consumables:** This estimate is based on identifying the consumable equipment during the demonstration period and its impact on the operational efficiency of the system.

- Facility operational costs: This estimate is based on the measured electric energy consumption (KWh) and cooling/heating energy consumption (MMBtu/hr) after the installation of the technology (for optimal control strategy) and before the installation (baseline). Energy sub-metering will be done to obtain this measurement.
- Maintenance: This estimate will track the cost of each maintenance action including labor and hardware supplies over the period of demonstration. For the MPC, any actions needed for maintenance/tuning of the controls algorithm will be tracked.
- Hardware lifetime: a life-cycle cost of using WSN will be estimated based on the maintenance requirement mentioned above, equipment degradation, configuration management, and labor associated with the use of WSN for HVAC control.
- Operator training: This estimate includes the cost of the facility operation personnel training for using WSN and MPC.

7.2 COST DRIVERS

The project addresses three important aspects:

1. Regulatory Driver: Energy Policy Act (EPACT) of 1992, Energy Independence and Security Act (EISA) of 2007 (Title IV, Subtitle C) and Executive Order 13423 mandate DoD to improve facility energy efficiency by 30% beyond 2003 levels.
2. Technology Driver: Retro-commissioning advanced controls in existing old buildings to optimize the performance of the HVAC and building systems requires significant investments. Through this project we demonstrated the use of easy to retrofit wireless sensors to enable low footprint supervisory controllers based on existing systems and controls to improve energy efficiency. Recent advances in buildings automation and wireless technologies have fueled this deployment.
3. Economic Driver: Key to retro-commissioning in existing buildings it to understand the return-on-investment. This project potentially demonstrated a two-fold advantage 1) demonstration of significant energy savings using advanced sensing and control (60% or more energy demand reduction) 2) identification of the persistent unnoticed faults during retro-commissioning process (e.g., identification of stuck dampers)

The technology developed in this project is applicable to existing buildings with sub-optimal controls and particularly are not served by a building automation system. Particularly buildings that are not served by digital controls provide the best opportunity for deploying the technology developed. While climate zones with distinct four seasons will benefit from the technology other climate zones are also applicable. Buildings with existing building automation need careful interoperability considerations for deploying this technology. This technology can be applied to typical commercial buildings served by packaged roof top units or built-up systems.

7.3 COST ANALYSIS AND COMPARISON

DoD can realize the key to improved building automation in three phases:

1. Asset visibility: Advanced low-cost sensors improved the operational visibility of the assets with in energy related systems like dampers etc.

2. Process visibility: Retrofit energy management platforms provide improved operational envelope of the systems due to increased visibility in to the process like occupancy-based HVAC systems and demand-controlled ventilation
3. Enterprise visibility: This technology is repeatable across multiple DoD facilities (among other 300,000 DoD buildings) providing opportunities to integrate data and visualize energy usage across facilities in a unified fashion. Among the 250,000-300,000 DoD buildings, at least 32,000 are equipped with air handling unit, variable area volume unit systems for HVAC, for which this technology is readily applicable. The realizable energy savings would vary across different climates, and variants of central HVAC systems (single, dual deck systems, on-site chiller/boiler versus central cooling and heating plant etc). For the remainder, which are likely comprised of buildings served by unitary systems (e.g. packaged rooftop units) the technology demonstrated can also be extended, but the building served by packaged terminal units (e.g. standalone air conditioners) and variable refrigerant volume systems, the technology is not applicable in its current form.

Technology demonstrated in the project includes the following elements:

- Novel control methods for operating buildings based on occupancy patterns and buildings usage has significant potential for energy demand reduction
- Low-cost wireless sensors provide improved observability and controllability of existing buildings
- Improved human-machine interfaces (HMI) provides asset and process visibility reducing time to failure detection and in return reducing unattended energy losses.

A life-cycle cost (LCC) analysis is performed based on the data in Section 7.1 using National Institute of Standards and Technology (NIST) Building Life-Cycle Cost (BLCC) program. Three distinct scenarios are developed during this analysis:

Scenario 1: This includes the total investment in the MPC hardware and installation and demonstrated energy savings based on the current utility costs in the area.

Scenario 2: In this scenario the hardware cost is discounted to reflect the real installation in a typical facility – the cost of BTU meters is reduced from \$12,800 per unit to \$2,000 per unit since significant cost is in the installation specific to the facility. Discussions with the contractor suggested this improvement for typical installation where COTS devices can be used without sacrificing performance measurement fidelity required for implementation.

Scenario 3: In this scenario the BTU meters are eliminated assuming the algorithm can be run with existing meters or using the raw data from the balancer along with a software program to estimate energy.

Scenario 4: The electricity rates are doubled to reflect the electricity costs in other parts of the U.S (such as the Northeast and West) compared to the costs in Chicago, IL area. COTS devices as in Scenario 2 are used in this estimation.

The savings to investment ratio and payback are highly dependent on the hardware costs for installation. Cost effective BTU estimation using COTS hardware or advanced analytics based on the raw data from the balancer can significantly reduce the payback period.

Table 13. Post-retrofit to MPC comparison for four scenarios³

Attribute	Scenario 1	Scenario 2	Scenario 3	Scenario 4
Study Period	20 years	20 years	20 years	20 years
Capital – post-retrofit	\$0	\$0	\$0	\$0
Capital – MPC	\$52,856	\$31,256	\$27,256	\$31,256
Energy Cost – post-retrofit	\$95,043	\$95,043	\$95,043	\$190,085
Energy Cost – MPC	\$46,823	\$46,823	\$46,823	\$93,646
Energy Savings with MPC	\$48,220	\$48,220	\$48,220	\$96,440
Present Value LCC – post-retrofit	\$130,061	\$130,061	\$130,061	\$225,103
Present Value LCC – MPC	\$134,697	\$113,097	\$109,097	\$159,920
Net Savings	-\$4,636	\$16,964	\$20,964	\$65,184
Savings-to-Investment Ratio	0.91	1.54	1.77	3.09
Adjusted Internal Rate of Return	N/A	4.64%	5.36%	8.34%
Payback Period – Simple	18	11	10	6
Payback Period - Discounted	N/A	13	11	6

Ubiquitous sensing improves observability and controllability of building systems. This project demonstrated that standards-based sensing and control integration to existing buildings will drive down costs by inviting “non-traditional suppliers” into the market by increasing size of the market and potentially improving competition and rate of innovation. This requires end-users to support and early adoption of standards-based approaches. This project is intended to replace traditional wired communications and deploy advanced supervisory control. Table 14 shows the comparison between wired and wireless systems for the same site selection as detailed in Section 4. Wireless sensors used provided 11% saving in the procurement and installation.

Table 14. Wired versus Wireless comparison

Component	Wired (\$)	Wireless (\$)
Sensor & Materials*	20,951.65	\$10,062.50
Wiring	13,948.35	\$1414.50
Wireless Equipment	0	\$12,357
Labor [#]	126,189	119,445
Total	161,089	143,279

*Sensors that were replaced with wireless are counted toward this component. Cost of common components that would exist in both the installations is excluded.

[#]Labor costs reflect total project labor costs as integrated number of hours in various stages of labor changes based on the configuration.

The following considerations have to be made in interpreting Table 14:

- The comparison does not take into account the cost of the original LonWorks network installation. This assumes the exclusion of baseline infrastructure costs for the wired system.
- The installation of the wireless infrastructure is a one-time cost and incremental installation of the sensors has near zero labor & installation costs. Additional wireless point on the network (up to 150 points) is \$120 for this installation (excluding sensor). Additional wired point on the network would be in the range of \$400-\$900 depending on the installation location and labor involved. Figure 32 shows the growth of the network cost for comparable

³ The cost analysis does not include commissioning cost for Pre-Retrofit set point schedule and development cost for the MPC algorithm.

wireless and wireless systems. Figure 33 shows the cost savings of wireless compared to wired as the network size grows.

- The location of the wireless sensor is not constrained, as is the case of the wired installation, thereby providing optimal observable locations for energy-efficient control.

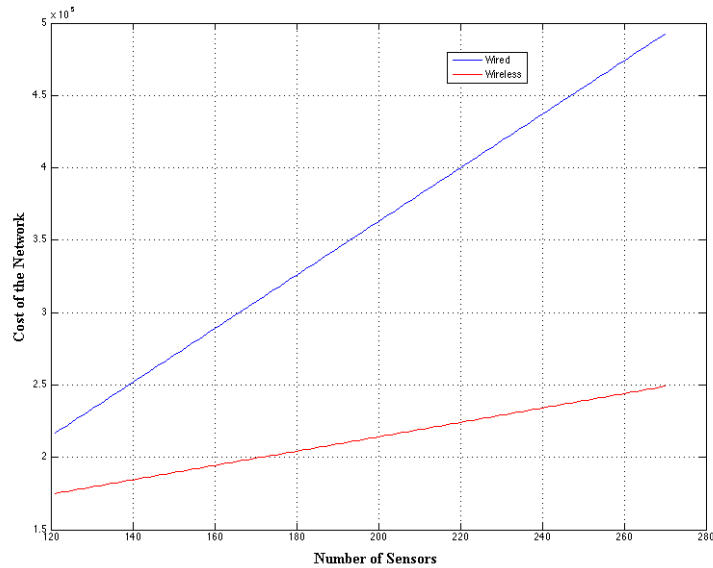


Figure 32. Comparison of Wired vs. Wireless as network size increases

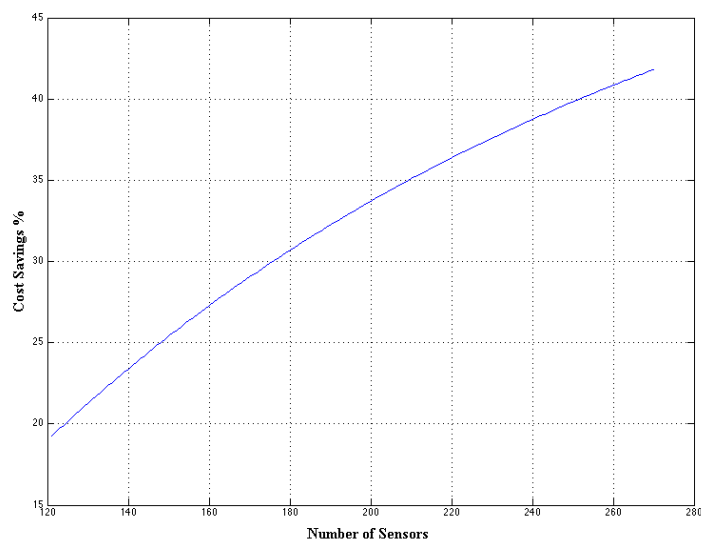


Figure 33. Cost Savings Using Wireless as network size increases

While this project is intended as a research demonstration we estimated the cost of repeating the functionality in an operational environment is 40-50% (as estimated by Alpha Controls LLC) lower than the current estimate as shown in Table 5 above. The primary driver is the integration expertise gained as part of the first deployment including developing data and control flow and

systems integration of non-traditional suppliers. Repeating similar installation in multiple DoD sites lowers the cost significantly benefiting from ease of placement for wireless sensors.

8.0 IMPLEMENTATION ISSUES

The project met significant implementation challenges that were resolved but resulted in delays and ultimately in a smaller data set than originally planned. These challenges range from sensor issues to network communication issues.

Related to the sensor issues, there are limited sets of data for which water-to-air enthalpy balance does not hold and an explanation could not be found. This is not resolved even after additional recalibration was made including sensor re-placement, and installation of averaging sensors. This calibration and validation issues are expected to occur for other systems, too. People counter sensors generated data that occasionally large accumulation errors that could only be explained by the well known sensor technology issues.

Network communication issues were relatively small. Twice there were issues with the on-board electronics of a wireless sensor that was replaced each time. In view of the large number of wireless sensor installed as part of the project, this was considered to be a minor malfunction. On a larger number of occasions the communication between the optimization platform and the BAS server was interrupted. Although this was improved by changing some of the communication protocol parameters (frequency of transmission, etc) these communication issues continued with a smaller frequency. As a result some of the experimental test data was compromised and was not included as part of the overall data processing effort.

An additional challenge was posed by the small set of options available for communication between an advanced optimization platform and a BAS. A significantly large effort, larger than original envisioned, was made to make possible communication between these platforms. The software toolchain for bi-directional communication and for overriding BAS set point in a consistent manner is relatively complex and not readily implemented at large-scale. The on-line data communicated between the two computers has been relatively small for this project, but it is expected to be significantly more challenging for a set of building HVAC units.

9.0 REFERENCES

1. <http://www.whitehouse.gov/news/releases/2007/01/20070124-2.html>
2. http://www.eia.doe.gov/emeu/cbecs/cbecs2003/detailed_tables_2003/detailed_tables_2003.html
3. *Energy Impact of Commercial Building Controls and Performance Diagnostics: Market Characterization, Energy Impact of Building Faults and the Energy Savings Potential*, TIAX Report D0180, for U.S. DOE Contract 030400101, Nov 2005.
4. <http://www.cecer.army.mil/>
5. A. Surana, S.P. Meyn, Y. Lin, S. Narayanan, "Anomaly detection in people traffic in buildings" submitted to Conference on Decision and Control Shanghai (China) 2009. Patent application pending at USPTO.

6. F. Borrelli 2003 in *Constrained Optimal Control of Linear and Hybrid Systems* 290; Constrained optimal control of linear and hybrid systems - Preface.
7. F. Borrelli, M. Baotic, A. Bemporad and M. Morari 2005 *Automatica* 41(10), 1709-1721. Dynamic programming for constrained optimal control of discrete-time linear hybrid systems.
8. F. Borrelli, T. Keviczky, G. J. Balas, G. Stewart, K. Fregene and D. Godbole 2005 in *Lecture Notes in Computer Science* 3414, 168-183. Heidelberg, Germany: Springer Verlag. Hybrid decentralized control of large scale systems
9. J. Nutaro, P. T. Kuruganti, R. Jammalamadaka, T. Tinoco, and V. Protopopescu, "An Event Driven TLM Method for Predicting Path-loss in Cluttered Environments," *IEEE Transactions on Antennas and Propagation*, Vol. 56, No. 1, pp. 189-198, January 2008.
10. www.energyplus.gov
11. Elmahdy, A. H.; Beattie, D. G.; *Direct Digital Control of Small and Medium-Size Buildings*; Division of Building Research, National Research Council of Canada, 1981
12. ASHRAE Guideline 14-2002, Measurement of energy and demand savings.
13. CO₂ emissions for natural gas; <http://www.eia.doe.gov/oiaf/1605/coefficients.html>
14. CO₂ emissions for electricity; <http://www.eia.doe.gov/oiaf/1605/ee-factors.html>
15. ASHRAE: Service Life and Maintenance Cost Database; <http://xp20.ashrae.org/publicdatabase/default.asp>
16. Meyn, S., Surana, A., Lin, Y., Oggianu, S., Narayanan, S. and Frewen, T., *A Sensor-Utility-Network Method for Estimation of Occupancy Distribution in Building*, 48th IEEE Conference on Decision and Control, 2009.
17. Henze, G., Dodier, R., Krarti, M., *Development of a Predictive Optimal Controller for Thermal Energy Storage Systems*, International Journal of Heating, Ventilating, Air-Conditioning and Refrigerating Research, 1996.

APPENDICES

Appendix A: Points of Contact

Table A.1 Point of Contact Information

POINT OF CONTACT Name	ORGANIZATION Name Address	Phone Fax E-mail	Role in Project
Satish Narayanan	United Technologies Research Center 411 Silver Lane, MS 129-13 East Hartford, CT 06118	Ph: (860)-610-7412 Fax: (860)-660-1291 Email: narayas@utrc.utc.com	Principal Investigator (PI)
Teja Kuruganti	Oak Ridge National Laboratory, Extreme Measurement Communications Center (EMC2) 1 Bethel Valley Road, MS-6085, Oak Ridge, TN 37831	Ph: (865) 241-2874 Fax: (865)-576-0003 Email: kurugantipv@ornl.gov	Co-PI
Francesco Borrelli	University of California at Berkeley Department of Mechanical Engineering 5132 Etcheverry Hall, Mailstop 1740 Berkeley, CA 94720-1740	Ph: (510) 643-3871 Fax: (510)-643-5599 Email: fborrelli@me.berkeley.edu	Co-PI
David M. Schwenk	U.S. Army Corps of Engineers ERDC-CERL 2902 Newmark Dr. Champaign, IL 61822	Phone: (217)-373-7241 Fax: (217)-373-6740 Email: David.M.Schwenk@usace.army.mil	DoD liaison at the demo site

Appendix B: Health and Safety Plan (HASP)

The demonstration was conducted in accordance with the health & safety requirements applicable to CERL facility HVAC retrofits, local and/or DoD regulations. In addition, the team members complied with the applicable health & safety policies for their organization whether work was performed locally or remotely. CERL R&D staff adhered to Research Safety Evaluation Checklist items in accordance with CERL Form (CF) 176. UTRC staff complied with the UTRC Environmental Health & Safety (EH&S) policies and the five UTC cardinal rules of safety covering confined spaces, control of hazardous energy (lockout/tagout procedures), electrical safety, fall protection and machine guarding. ORNL & UCB shall similarly comply with their respective organizational health & safety policies.

The National Fire Protection Agency (NFPA) requirements for smoke detector placement applied to this retrofit demonstration where smoke detectors do not already exist in the supply air ducts. The retrofits conformed to the code requirements for the controls stated in NFPA para 1.4: 1.4 Retroactivity. The provisions of this standard shall not be intended to be applied retroactively. Where a system is being altered, extended, or renovated, the requirements of this standard applied only to the work being undertaken.

The potential for worker exposure to hazardous environment is expected to be low in this demonstration. The HVAC equipment retrofits were conducted by a trained & licensed contractor Alpha Controls. The work performed by project staff from UTRC, ORNL, UCB and CERL was involved predominantly data collection & analysis from a computer. The installation & maintenance of wireless sensors was estimated to be low risk. The technology demonstrated involves automatic control of HVAC equipment. The system was configured and monitored from one or more computers allowing both local & remote access. Thus, the need for project personnel to be physically present to operate the system was low. Fail-safe operational modes were programmed into the DDC controllers so that any failures in the un-proven elements of the technology such as the wireless sensors or the model predictive control cause no major inconvenience to the building occupants.

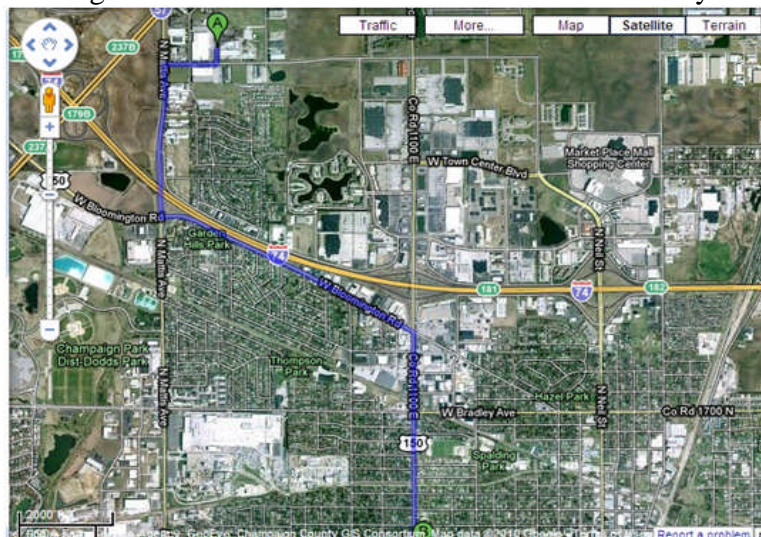
Closest Medical Facility

In the event of a medical need, whether an emergency or not, the nearest medical facility is located at:

Pavilion, 809 West Church Street,
Champaign, IL
(217) 373-1700

The directions to the above facility from CERL (2902 Newmark Dr) are shown in Figure .

Figure B.1 Directions to the nearest medical facility



Appendix C: EMC² Report Concerning ISM Band Electromagnetic Site Survey and Characterization Interference Tests Conducted at the Construction Engineering Research Laboratories Champaign, IL

The purpose of this task was to evaluate the U.S. Army Corp. of Engineers, Construction Engineering Research Laboratory (CERL) office building for potential radio frequency (RF) interference that may be detrimental to use of wireless sensors for building automation, and to determine propagation characteristics of wireless sensors within the building.

Wireless technology is fueling new paradigms in personal, commercial, and industrial communications systems throughout the marketplace. The Extreme Measurement Communications Center (EMC²) at Oak Ridge National Laboratory is chartered to facilitate the deployment of wireless technology in the harsh environments common to industrial applications. This facility, jointly funded by DOE's Energy Efficiency/Renewable Energy Program and the Nuclear Energy Commission, is being made available to other government agencies and any private sector companies interested in pursuing wireless technologies for harsh environments. The Construction Engineering Research Laboratory was surveyed for RF signals detrimental to the use of wireless sensors within the building and to determine propagation and wireless range for sensor use within the building. The ambient RF signals are recorded and later analyzed to draw conclusions which help deploying wireless sensors in these environments. Six sites within the building were selected for recording RF signals.

The Construction Engineering Research Laboratory has Wi-Fi based wireless Internet system installed, plus there are several small laboratory rooms that may employ RF generating equipment, such as microwave ovens, power electronics, X-ray equipment, and chemical analysis equipment. Two calibrated test antennas, an Electro-Metrics rod/discone antenna for frequencies below 1 GHz and a calibrated Discone antenna for signals between 800 Mhz and 6 GHz are used for recording the signals. These antennas, along with monitoring equipment, were mounted on a wheeled cart and moved to the six sites located as described in Figure 1. The antennas were swapped as needed between the Aeroflex CS65040 Broadband Signal Recorder and Generator (hereafter referred to as the CS65040) and a Rohde & Schwarz FSH3 spectrum analyzer (hereafter referred to as the spectrum analyzer) that was controlled with FSH3 software. While reviewing these results, it is important to keep the ISM frequency bands in mind, they are

- 902–928 MHz
- 2400–2485 MHz
- 5725–5875 MHz

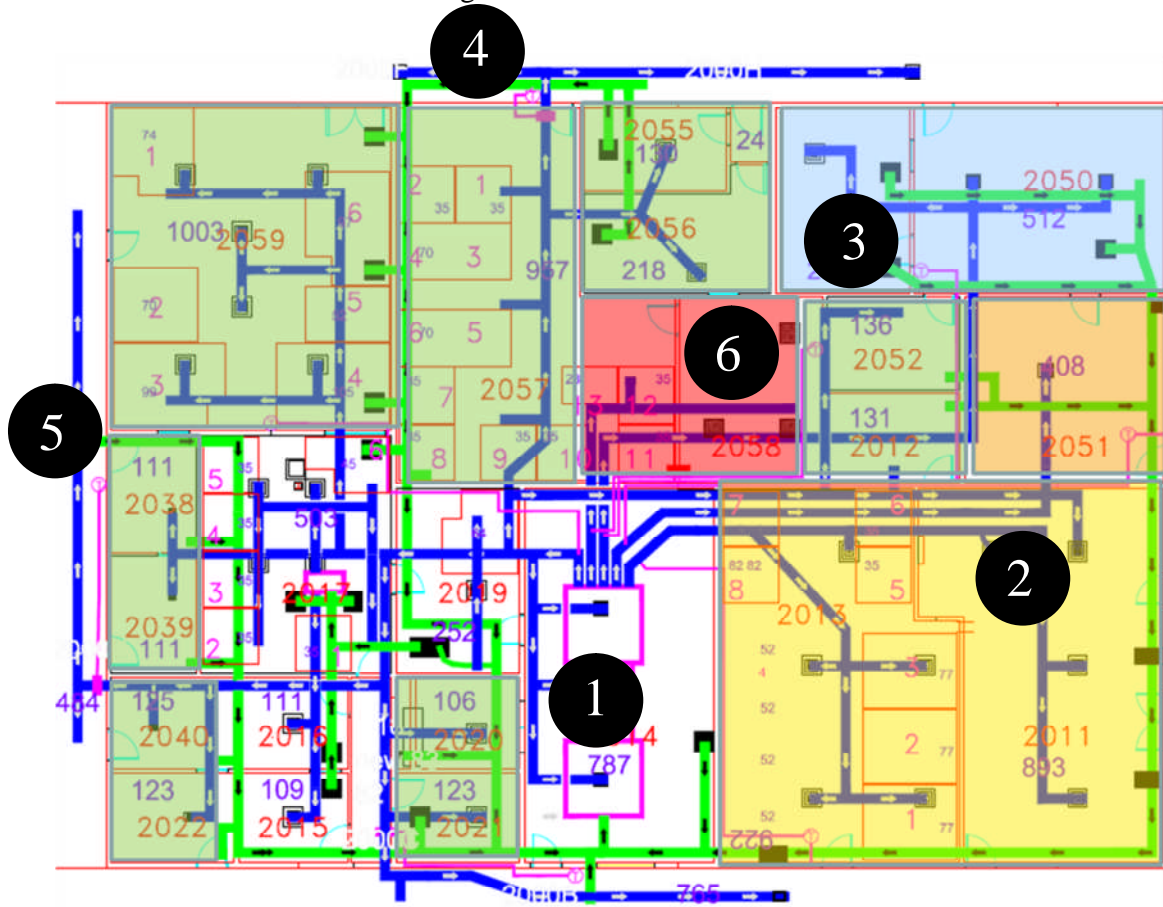
EQUIPMENT USED

Rohde & Schwarz Spectrum analyzer Model FSH3
Aeroflex CS65040 Broadband Signal Recorder and Generator
Dell Laptop Computer Model D600 Serial Number 3BV6V31
Electro-Metrics Wideband Discone Antenna Model EM-6106 SN 464 10 kHz – 2 GHz
Electro-Metrics Power Supply Module Model DCA-30 SN 460
Calibrated Wideband Microwave Discone antenna Model DA-1 800MHz – 6GHz

Test Locations illustrated on campus map and denoted include:

1. Computer Network room
2. Cafeteria
3. Power Electronics Lab
4. North Hallway
5. West Hallway
6. Conference room

Figure C.1 Test locations



NOTE ABOUT THE PLOTS

The CS65040 plots provided are the result of replaying the signals that were recorded during the test. During the replay, interesting segments were captured for the report with a screen capture and inserted here as graphics. The plots provided show the spectrum along with a display of time recent to that spectrum. The spectrum is 130 MHz wide in all cases unless noted otherwise. This span, along with the center frequency and Resolution Bandwidth (RBW) is noted at the bottom of each plot.

The CS65040 analyzer has an anomaly that can be seen as four CW signals, one at -15 MHz from center, second at -10 MHz from center, third at +5 MHz from center, and fourth

at +30MHz. The signal at -15 MHz pulses; other are constant. They are present at these frequency offsets in all plots, in all frequency bands. These signals should be ignored.

The CS65040 spectrum plots provided show the instantaneous signal (in yellow) along with the result of a maximum hold (in green). Each sample taken with the CS65040 analyzer was the result of 400 million samples per second and was recorded for the duration of the memory limit of the analyzer which is 2.56 s. The instrument can observe and record 130MHz wide band with the center frequency changed to observe 900MHz, 2.4GHz, 5.8GHz ISM bands. The time window shown in these plots extends for 366 samples (chosen arbitrarily to provide a good screen balance between the spectrum and the time windows). The current sample is displayed at the bottom of the time window. As a result, even though the time window does not provide a scale, it can be shown that it is the result of the current sample and includes samples for the previous 163 μ s.

The Rhode & Schwartz FSH3 spectrum analyzer is controlled by a laptop running FSH3 software. Six frequency bands were individually monitored at each location until no new peaks appeared. The bands are 1MHz to 30 MHz, 1 MHz to 470 MHz, 500MHz to 1 GHz, 1 GHz to 2 GHz, and 2 GHz to 3 GHz. The laptop records the frequency and power level at designated increments and records the maximum signal presented during the total scan. The resolution bandwidth is 300 KHz for the 1 to 30 MHz measurements and 1 MHz for the others.

For ease of reading the normal looking plots, for more than one location, are omitted. Sweep frequency measurements are shown to show the RF activity (radio, PCS, cell phone, etc). Typical 802.15.4 nodes transmit at 0dBm. At 2.4GHz typical 1st meter loss is 40dBm and further loss is dependent on the physical properties of the channel.

The plot images show three plots each top part is the time domain plot with time on x-axis and magnitude on y-axis, middle plot is a spectrogram (waterfall graph) with frequency on x-axis and time on y-axis, the bottom plot is a frequency domain plot with frequency on x-axis and magnitude (dBm) on y-axis.

Overall the plots show the CERL building to be a relatively benign operating environment for wireless communication. Background noise and interference levels were relatively low. This is to be expected in that the CERL building consists primarily of offices, however there were several lab rooms that had high power electronic equipment and chemical analysis instruments. Our observations were that most of this equipment was not being used at the time of our test. We also specifically requested a survey in the computer network server room since computers can emit Electro-Magnetic Interference (EMI). The server network was fully operational at the time. Interestingly, some of our strongest received signals were in the cell phone frequencies, most likely from the phones we were wearing while conducting the test.

Because much of our test results were the same for the various locations, only the plots that have the most activity are presented here. All plots in their entirety are listed at the end of the report.

RESULTS OF WIRELESS TRANSMISSION AND RECEPTION TESTS

The receive-only study identifies the ambient RF signals within the building and helps identify existing wireless networks within the building and also any spurious signals in the building. The ambient RF signals are recorded and later analyzed to draw conclusions, which help deploying wireless sensors in these environments. Six sites within the building were selected for recording RF signals. Appendix C details the measurement procedure, data collected and analysis. The two primary bands of interest are 2.4GHz and 900MHz bands. No spurious transmissions are identified during the test period and the average maximum noise floor is -80dBm which is typical for such facilities.

The transmit-receive study helps understand the attenuation characteristics within the building. The wireless sensors in this project used 900MHz and 2.4GHz ISM bands. The RF propagation study is performed in both the bands. Digi-MaxStream transmitter and receiver pair is used to record the path loss data in 900 MHz. The transmitter is set to +30dBm frequency hopping spread spectrum signal and moved across the facility to correlate with the people counter location, the received signal strength is recorded at the central computer location. The path attenuation varied from 88-70 dBm. The 2.4GHz Ubiquity transmitters are used for studying the propagation in 2.4GHz band used by all of the Spinwave wireless sensors. The transmitter is set to +29dBm 5Mh/Hz wide direct sequence spread spectrum signal and located in the central computer room, the receiver is moved across the sensor locations to record the received signal strength. The path loss attenuation varied from 99 – 49 dBm. The test is conducted in a star topology to understand the worst-case propagation loss to the central computer. However, the Spinwave wireless sensors will be configured as a mesh network, which provides the sensors with shorter links and multiple hops before the sensor data reaches the destination. This provides enhanced radio coverage. Figures 2.3 and 2.4 show the wireless coverage map in 900MHz and 2.4Ghz respectively. Each node location depicts the received signal strength.

Figure 2.3 Received Signal Strength at Various Locations in 900MHz

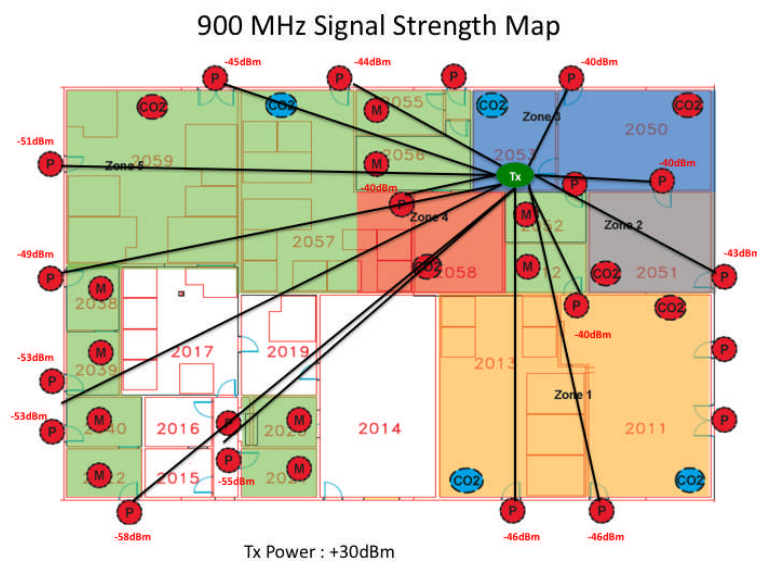


Figure 2.4 Received Signal Strength at Various Locations in 2.4GHz

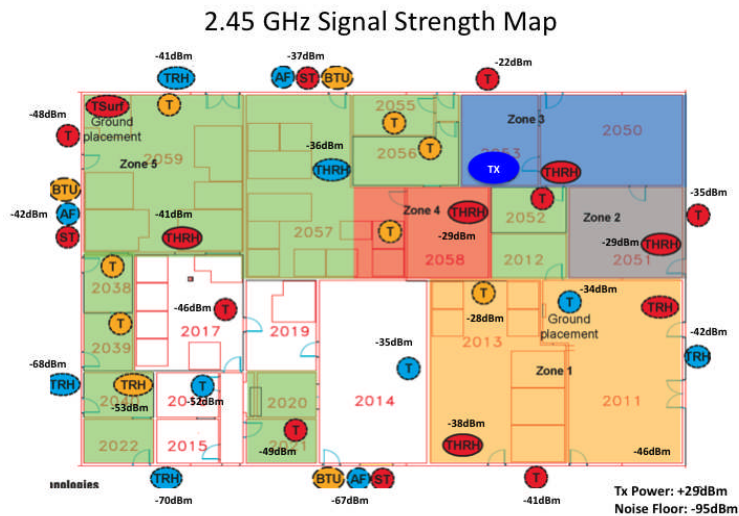


Figure 2.5 Signal-to-Noise Link Margin in 2.4GHz bandwidth

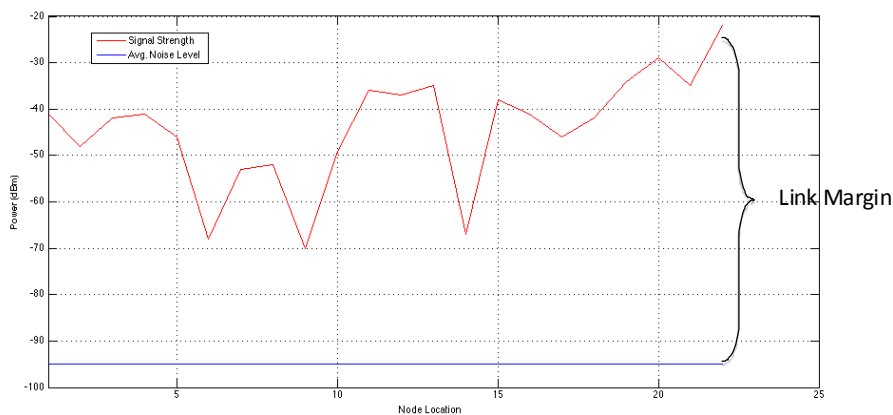
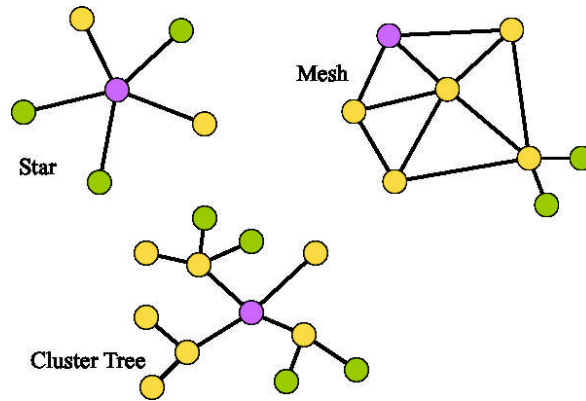


Figure 2.6 Received Signal Strength at Various Locations in 2.4GHz bandwidth

Figure 2.6 shows the summary of the propagation tests. The red line represents the received signal strength across 22 locations within the buildings and the blue line represents the average noise level in the building as seen by the receiver's RF front-end. This demonstrates excellent signal to noise ratio with promise for strong link quality. As mentioned before these are worst-case propagation links. Figure 2.3 displays the received signal strengths at the various demonstration site locations, indicating sufficiently strong signals.

Three different topologies exist for laying out the wireless networks. The topology of the network dictates the connectivity and routing of packets across the network. The shorter the propagation distance lower the RF power required to transmit. RF power required to transmit is inversely proportional to the squared of the distance required for the signal to propagate. Lower RF power improves the battery life. Figure 2.7Error! Reference source not found. depicts the three different common topologies.

Figure 2.7 Various network topologies



In star topology all nodes (sensor nodes) are connected to a central node and communicate the measurements. The longer the distances of the end nodes the higher the RF transmission power required. The mesh topology uses a network of nodes and each node hops its messages across the network through other nodes. Each node acts a repeater and helps in routing packets across the network. The advantage of mesh network is the low RF transmission power required since the maximum distance a node has to communicate is the nearest node. The network has to be designed with a tradeoff between the spatial density of the network and RF transmission power. Mesh networks have proven to extend node battery life times to 2-3 years. The third interesting topology is a cluster tree which is a combination of mesh and star topologies with the some nodes acting as repeaters (may be plug powered) but still providing the deployment flexibility of the end nodes. The repeater nodes are networked in a mesh fashion to relay messages to the central node (gateway node). The two networks deployed at CERL are 1) as shown in Figure 2.3 the 900MHz network is set up as a star network, and 2) The 2.4GHz network is setup as a cluster tree mesh network connected by three repeaters. Figure 2.7 shows the topology.

20696	103.89	109.96
20723	170.21	113.86
20730	20.44	30.8
20733	78.84	35.75
35104	17.82	10
35105	32.62	33.93
35106	58.61	54.5
35109	116.54	132.25
35110	78.52	82.16
35113	97.77	52.65
35115	143.06	152.07
35127	131.49	162.18
35129	30.07	44.99
35130	56.26	57.89
35131	88.11	39.6
36000	97.6	93.02
36001	251.41	210.44
36002	189	137.64
36004	126.62	101.27

Figures 7 and 8 represent the link quality of nodes 17341 and 35104, chosen at random, over four hour time period; note the variance in link quality over time. While node 17341 performs at a higher link quality over time, node 35104 has significant variance in link quality. This can be due to interfering sources like Wi-Fi. Increased variance can introduce packet retries there by increasing the latency for the node.

Figure 2.9 Link Quality Over Time for Node ID 17341

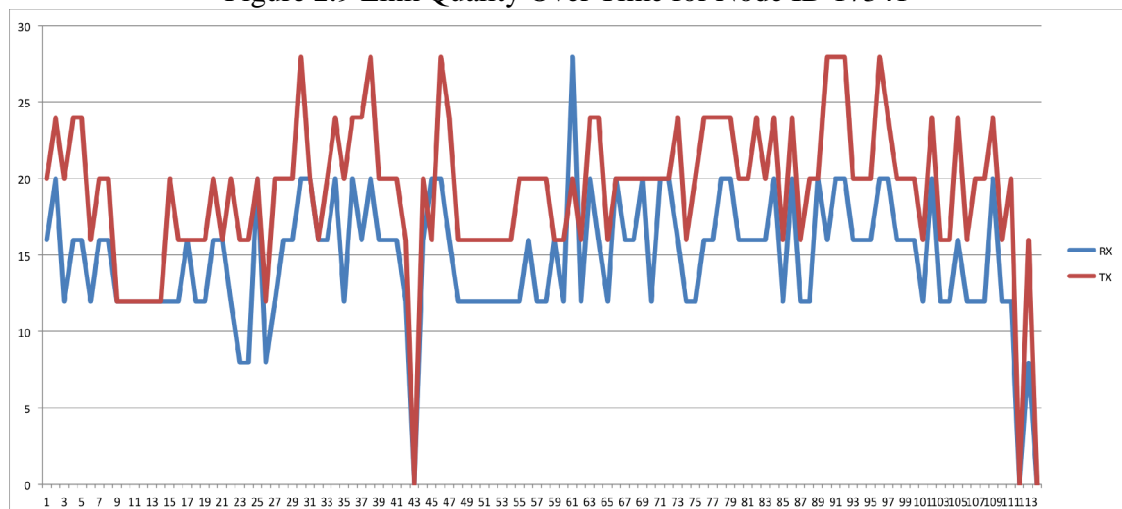
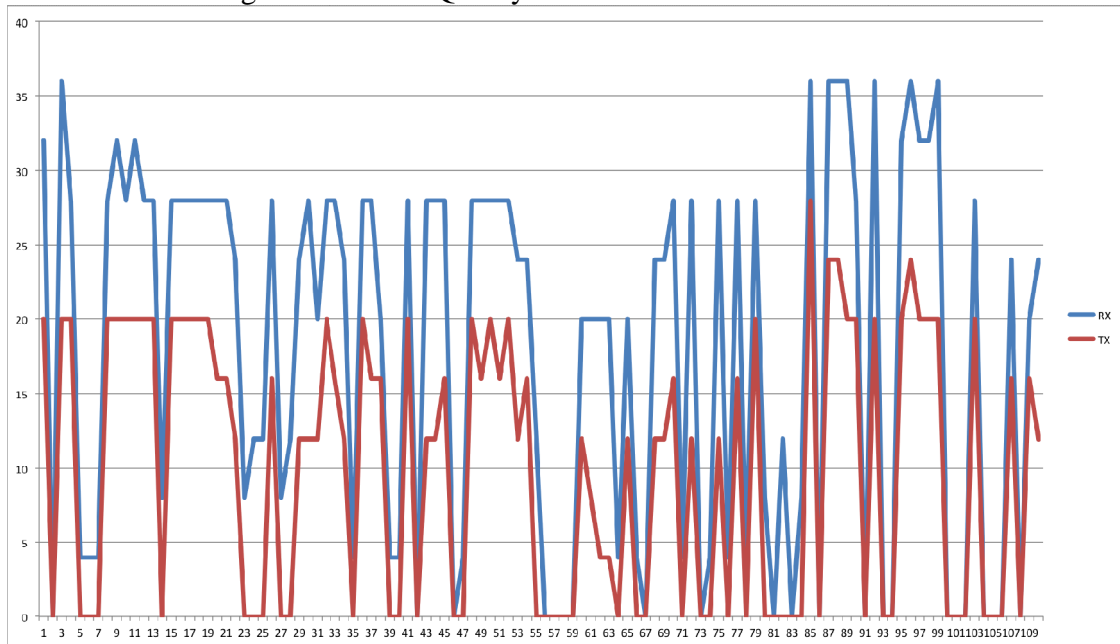
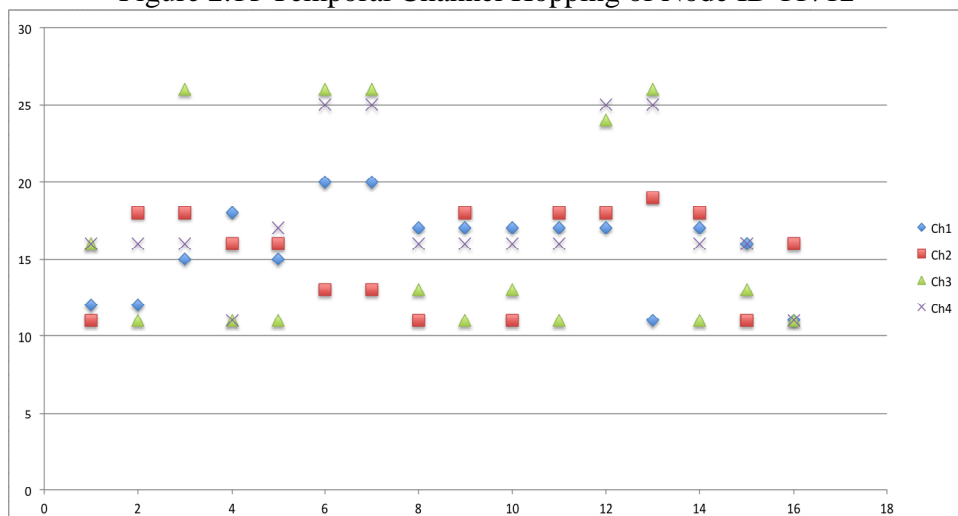


Figure 2.10 Link Quality Over Time for Node ID 35104



To survive long-term in harsh radio frequency environments the nodes used for demonstration dynamically hop across various frequency channels providing immunity against interference sources like existing networks in 2.4GHz band. The 802.15.4 networks have 16 channels in 2.4GHz band and numbered from 10 to 26. Figure 2.11 shows an example of temporal channel hopping pattern on one node. The network dynamically determines the 4 best IEEE 802.15.4 channels at any given time and performs channel hopping among those 4 channels to further avoid interference. Figure 9 shows an example of temporal channel hopping pattern on one node. The network dynamically determines the four best IEEE 802.15.4 channels at any given time and hops among those four channels to avoid interference. The channels are selected based on ambient RF conditions and to avoid any mutual interference among various nodes in the network.

Figure 2.11 Temporal Channel Hopping of Node ID 11712



PLOTS FROM THE TIME-DOMAIN BROADBAND RF RECORDER

Figures C.2 – C.5 shows a 2.6 second snapshot of the environment in various ISM frequency bands. There are no persistent signals with the average noise floor around -80dBm.

Figure C.2: Average noise floor centered at 500MHz at Location 1. There are no noticeable transmitters.

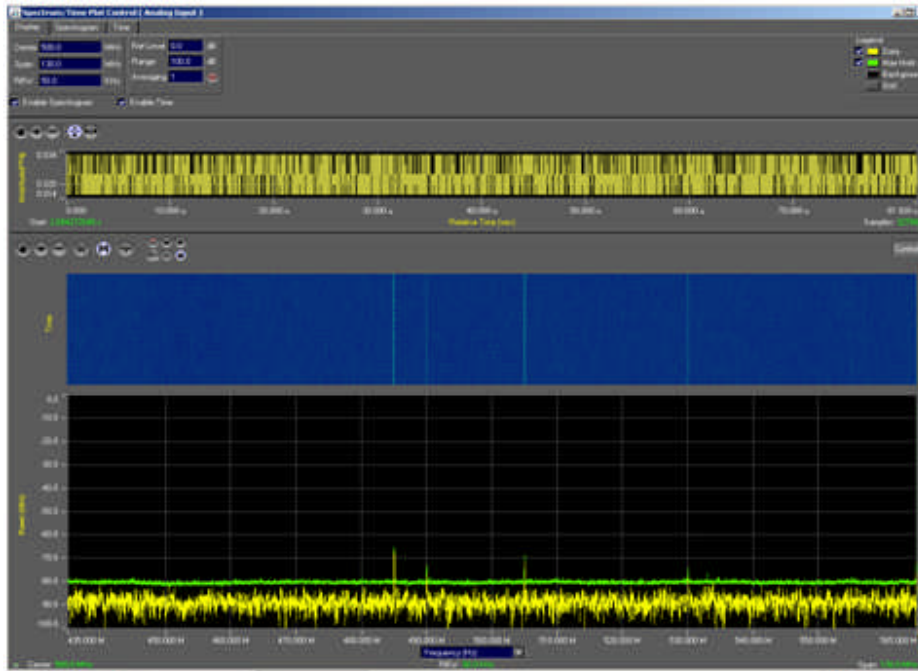


Figure C.3: The average noise floor centered at 900MHz at Location 2.

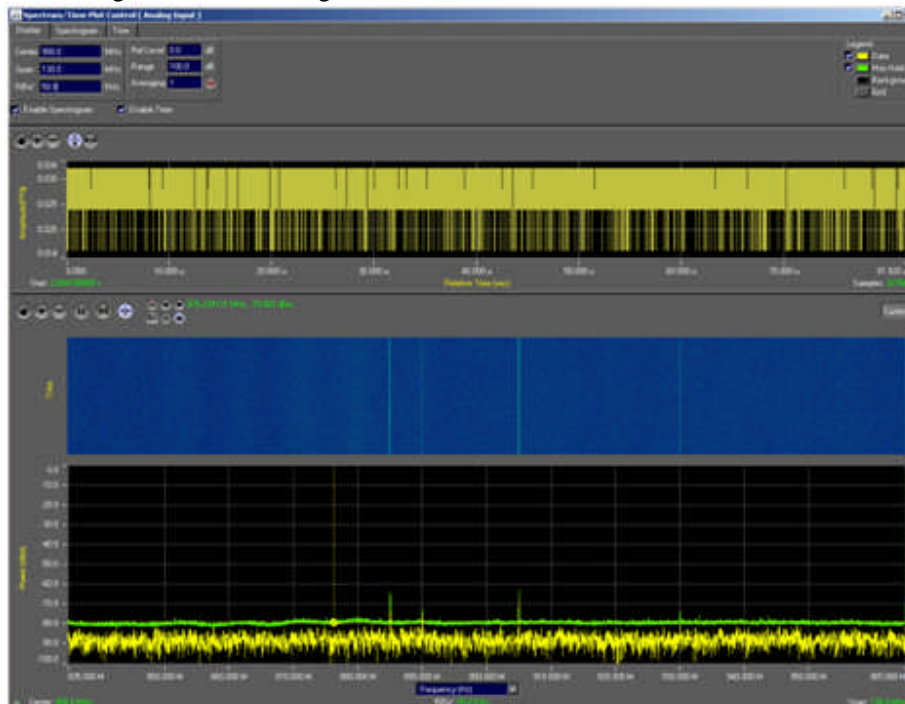


Figure C.4: The average noise floor centered at 2450MHz at Location 3.

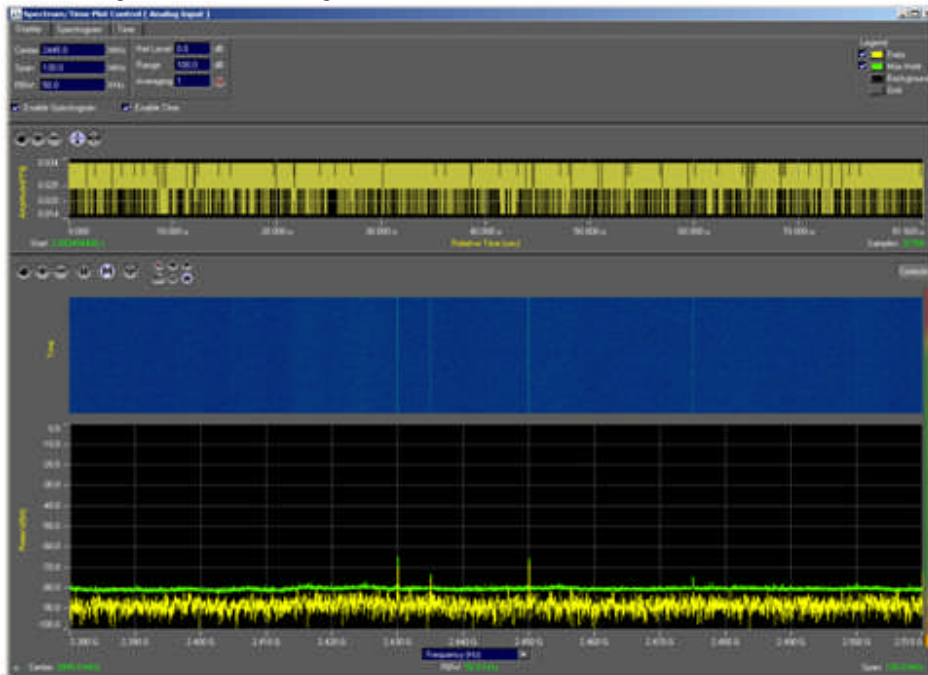
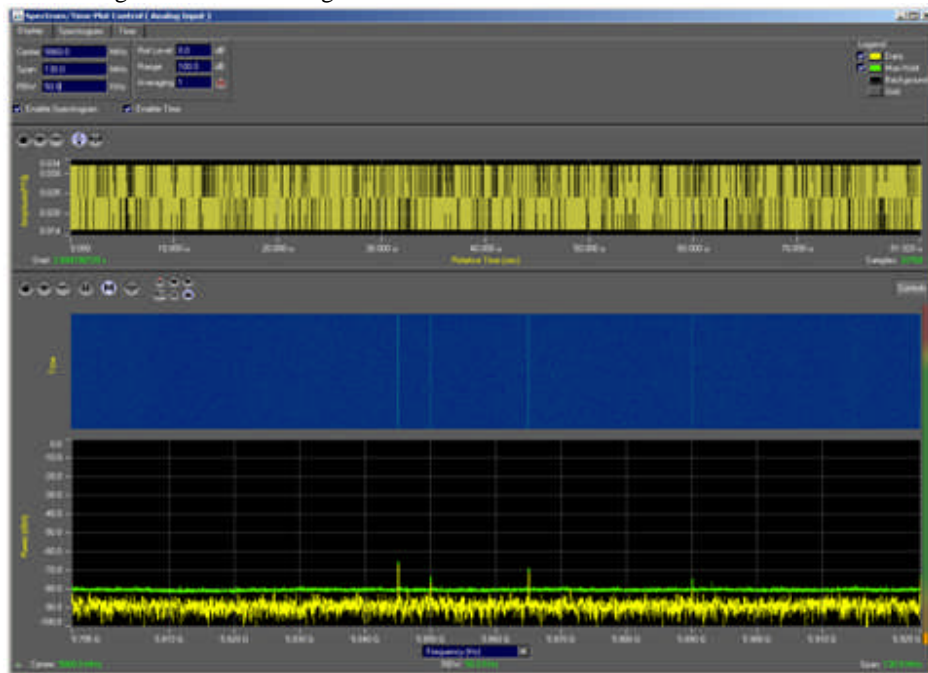


Figure C.5: The average noise floor centered at 5860MHz at Location 5.



PLOTS FROM THE SPECTRUM ANALYZER

The following plots are the frequency domain snapshots of the RF activity in various frequency bands over 3 minute time period.

The 1 to 30 MHz Band: This band is not under consideration for our wireless sensors, however measurements were performed here to identify potential interference. The band is traditionally known as the “High Frequency” or HF band and is the band for early generation radios. In this band are AM radios (0.55 to 1.6 MHz), Amateur Radios (3.5, 7, 14, and 28 MHz), international broadcasts (7.5 MHz), Citizens Band Radios (27 MHz), Industrial Scientific and Microwave (ISM) (13.8 MHz), and numerous others. Most of the occupants for this band are here for historic reasons, such as AM, or for the peculiar propagation characteristics of these frequencies, such as Amateur Radio. It is not in favor for new designs because of the large physical size of the transmitter antennas. This band is also susceptible to atmospheric interference from lightning storms and EMI interference from computers and switching power supplies. A future potential interference in this band is the Broadband Over Power Line system for delivering Internet access since it uses these frequencies on unshielded power lines.

Figure C.6: 1 MHz to 30 MHz at location 1, computer server room. The signals at 2.5 MHz are likely the computer power supplies and the 13.8 MHz is likely from an industrial heating experiment in the building.

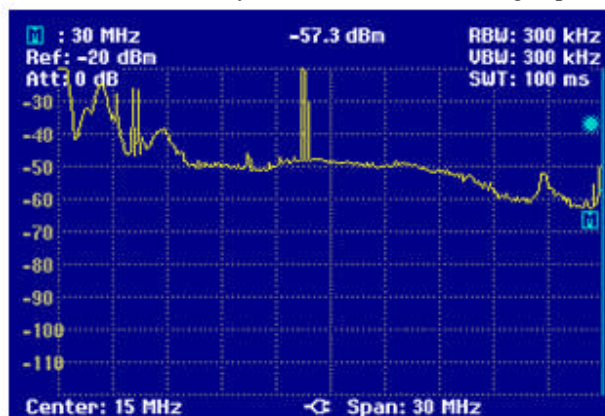
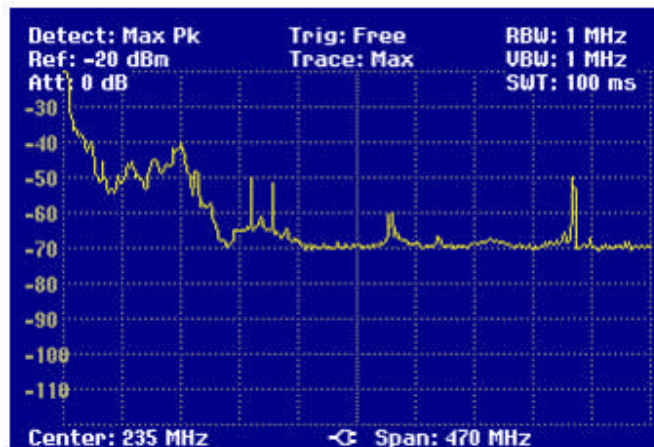


Figure C.7: 1 MHz to 30 MHz at location 6, the conference room. Background noise is unusually high, probably from computer and projector systems in the conference room.



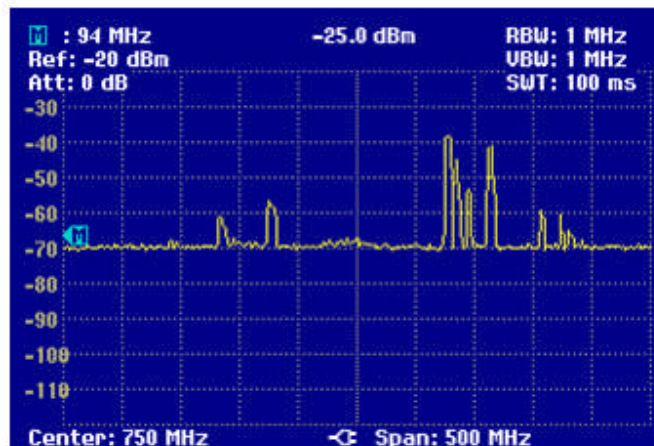
The 1 to 470 MHz Band: This band is of interest because it includes the 433 MHz ISM frequency, used for RFID tags, key fobs and wireless sensors. It includes numerous high powered sources, such as television stations and FM broadcast. Other strong sources are walkie talkies in the 150-174 MHz, 406-420 MHz, and 450-470 MHz bands. These walkie talkies are not necessarily high power but they can be transmitting very close to our equipment. Since CERL is a federal institution, its protective force should be using the 406-420 government band.

Figure C.8. 1 MHz to 470 MHz, location 4, north hallway. The peak near 100 MHz is the FM broadcast stations and the 410 MHz is local land-mobile use.



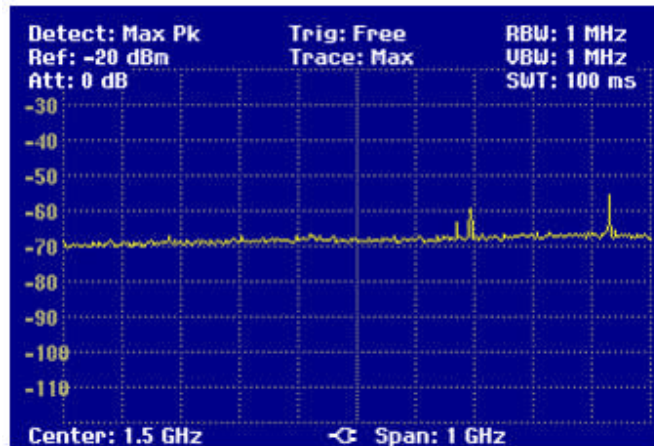
The 500 to 1000 MHz band: This band is of interest because a major wireless networking band is at 902-928 MHz. The majority of cell phones also operate in the 800 MHz range, plus high powered UHF televisions are in this band. At all sites we observed cell phone activity, and at most sites we observed 902-928 MHz activity. We also observed what appeared to be broadcast television signals in the 600 MHz range.

Figure C.9: 500 to 1000 MHz, location 5, west office hallway. This area is closest to a window which would enable broadcast reception. Note 902-928 activity.



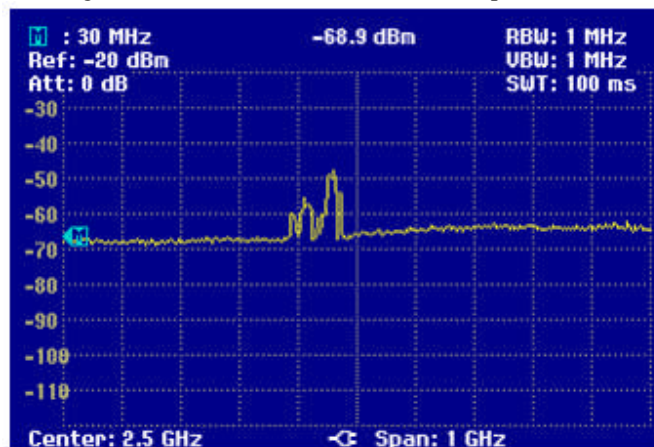
The 1 to 2 GHz band: This band is primarily used for satellite communications and radar, although there is a Personal Communication System (PCS) band at 1.8-2.0 GHz, which effectively is another cell phone band. We found this band to be relatively quiet except for the PCS frequency.

Figure C.10: 1 to 2 GHz, location 2, cafeteria.



The 2 to 3 GHz Band: This band contains a key ISM band at 2400 to 2480 MHz that is used by microwave ovens, Wi-Fi (IEEE 802.11), Bluetooth, and Zigbee. It is of interest to us because most of the available wireless sensors are operated in this band. As expected, we saw significant activity in this band from the CERL Wi-Fi system. Fortunately, facility Wi-Fi systems can be adjusted to accommodate additional systems such as the wireless sensors we propose to install. All locations displayed a similar amount of Wi-Fi traffic, and location #1 is merely representative.

Figure C.11: 2 to 3 MHz, location 1, computer room.



Antenna Calibration measurements

ELECTRO-METRICS DISCONE ANTENNA CALIBRATION

ElectroMetrics broadband antenna. To calculate the actual power spectral density values at the antenna location, the antenna factor (in units of dB m^{-1}) is added to the voltage (units of dB re

1 V) at the input of the measuring instrument. The R&S and CS65040 analyzers display amplitude as dB re 1 mW (dBm) referenced to their 50-Ω inputs, so an additional factor of – 13 dB must be included in to complete the field strength calculation.

$$E \text{ (dBV/m)} = \text{Reading (dBm)} + \text{AF (dB}\cdot\text{m}^{-1}) - 13 \text{ dB(V/mW)}$$

The antenna factor as a function of frequency for the ElectroMetrics broadband antenna is shown in Fig. 12.

Figure. C.12. Antenna factor as a function of frequency.

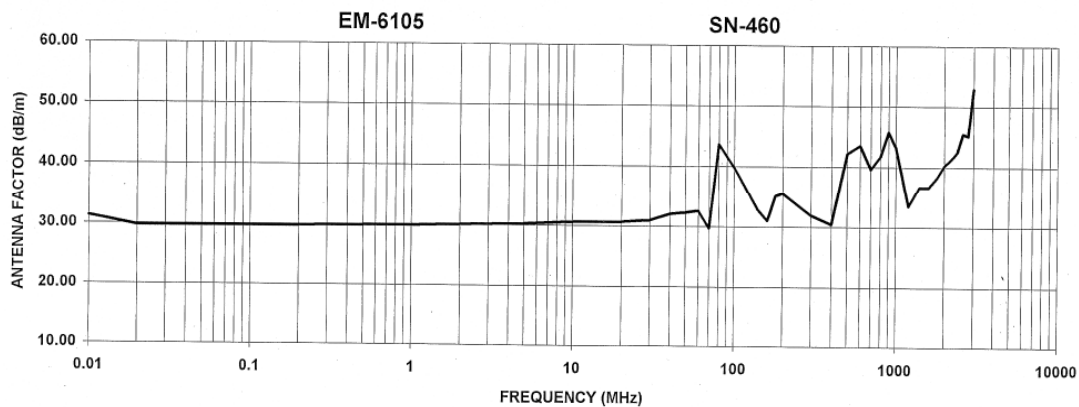
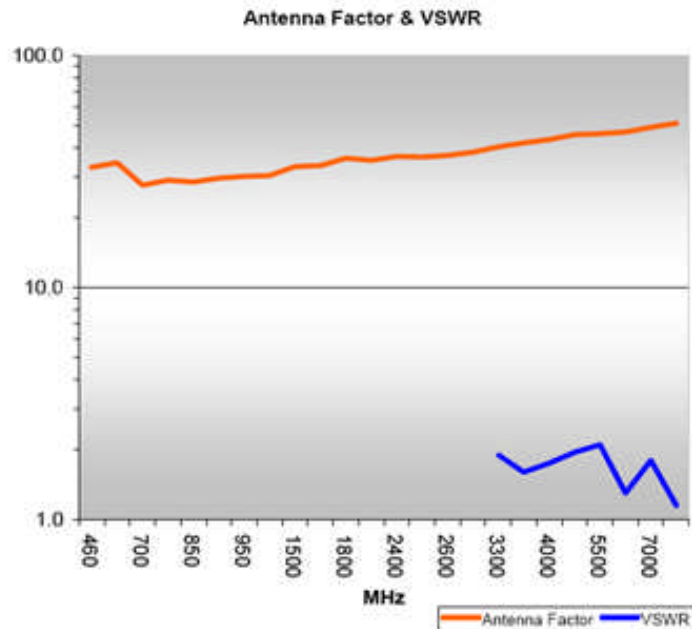


Figure C.13: Antenna Factor and SWR Plot for Microwave Discs.



LABORATORY MICROWAVE DISCONE ANTENNA CALIBRATION
Spectrum Analyzer Data

Figure C.14: Location 1, 1 to 30 MHz

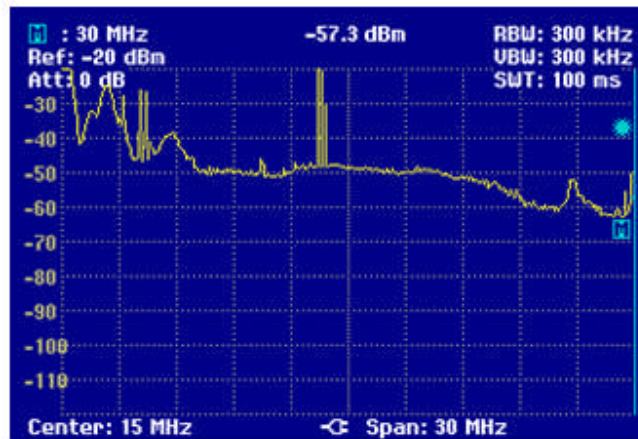


Figure C.15: Location 1, 1 to 470 MHz

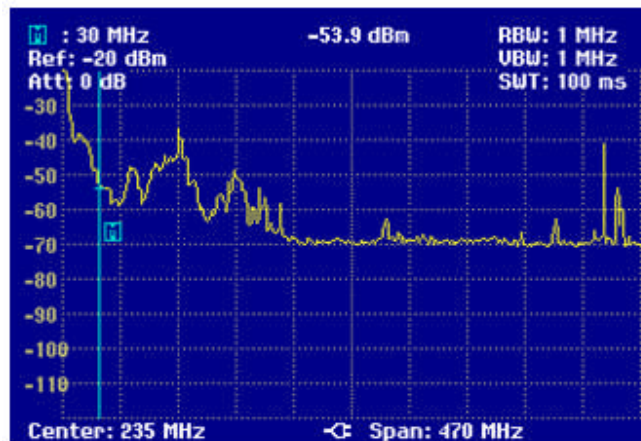


Figure 16: Location 1, 500 to 1000 MHz

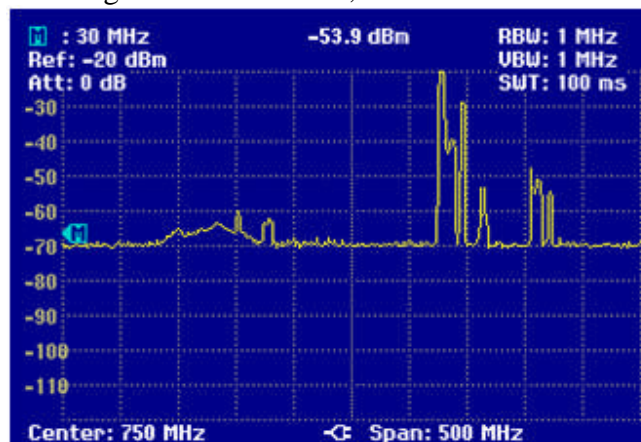


Figure C.17: Location 1, 1 to 2 GHz

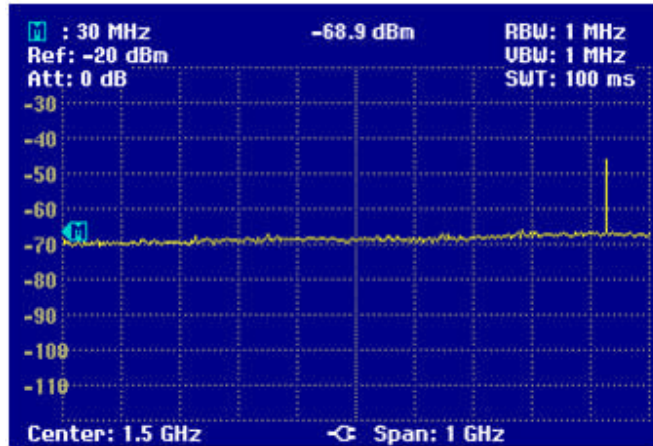


Figure C.18: Location 1, 2 to 3 GHz

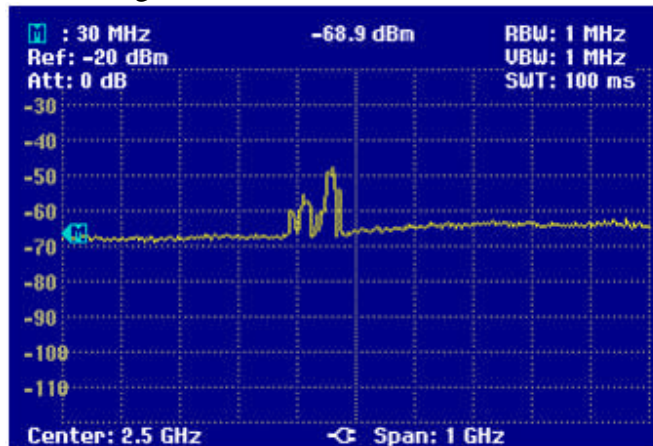


Figure C.19: Location 2, 1 to 30 MHz

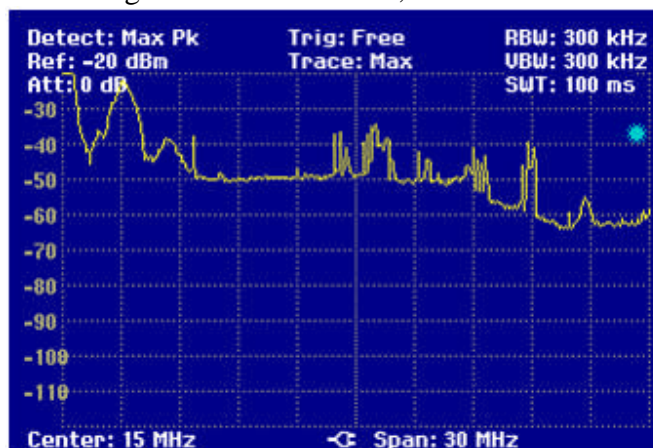


Figure C.20: Location 2, 1 to 470 MHz

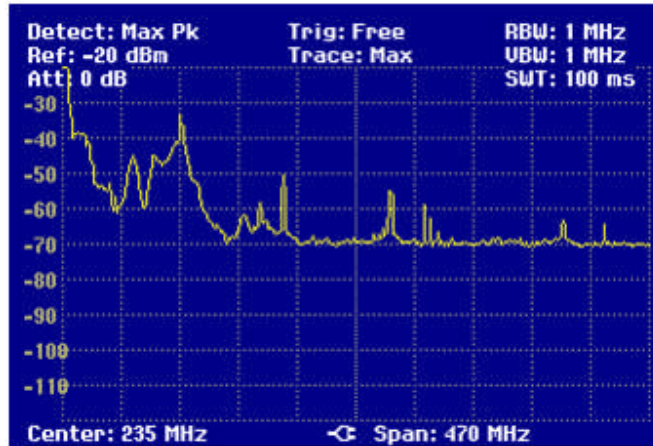


Figure C.21: Location 2, 500 to 1000 MHz

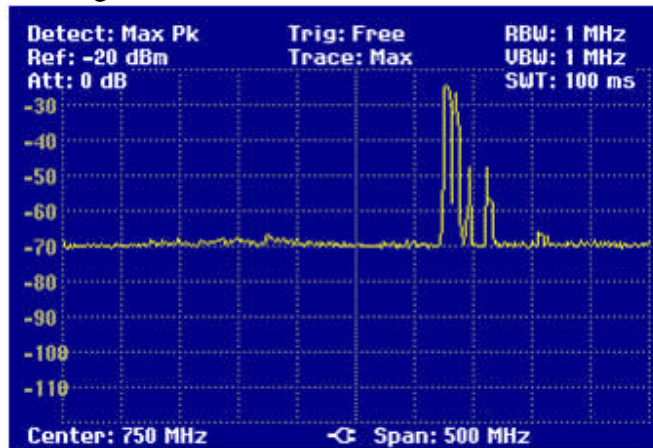


Figure C.22: Location 2, 1 to 2 GHz

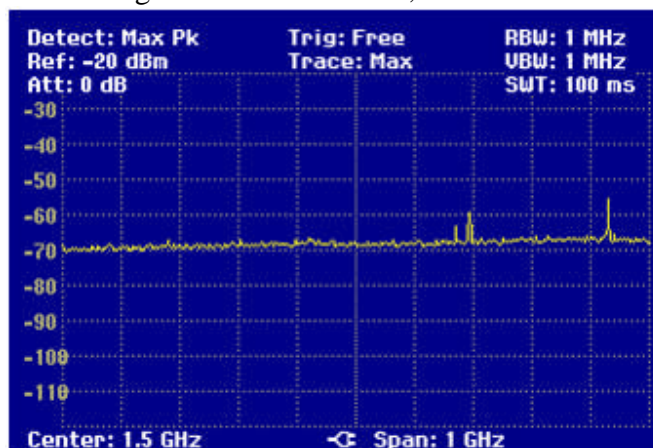


Figure C.23: Location 2, 2 to 3 GHz

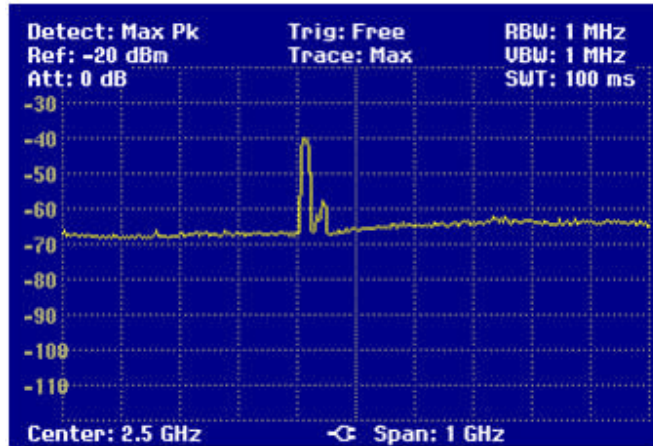


Figure C.24: Location 3, 1 to 30 MHz



Figure C.25: Location 3, 1 to 470 MHz

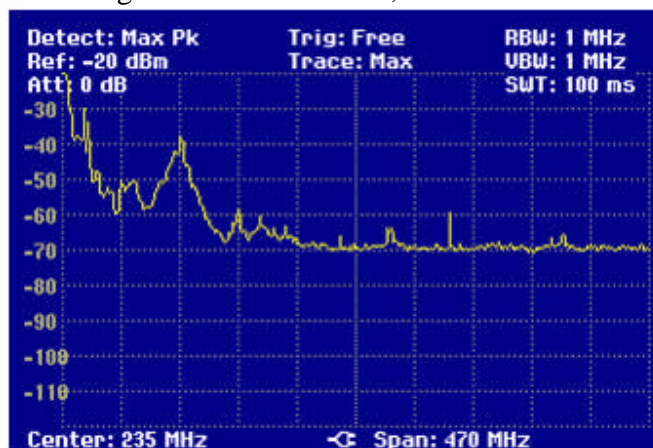


Figure C.26: Location 3, 500 to 1000 MHz

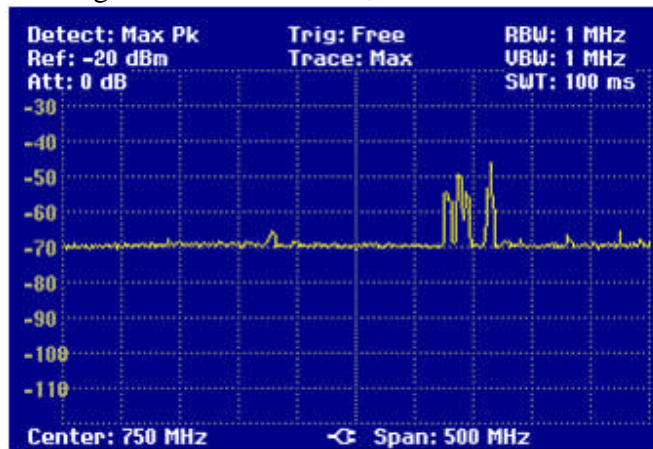


Figure C.27: Location 3, 1 to 2 GHz

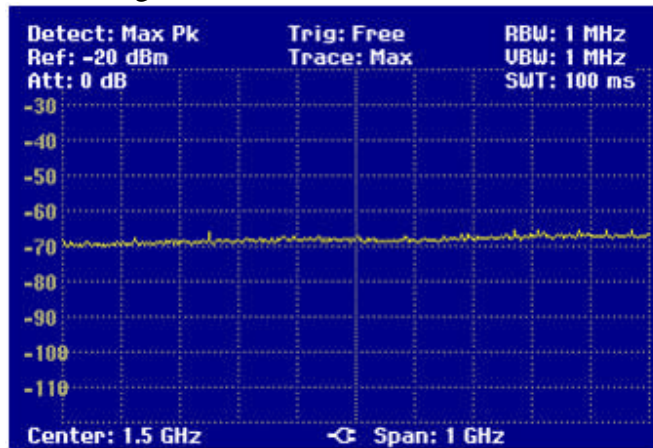


Figure C.28: Location 3, 2 to 3 GHz

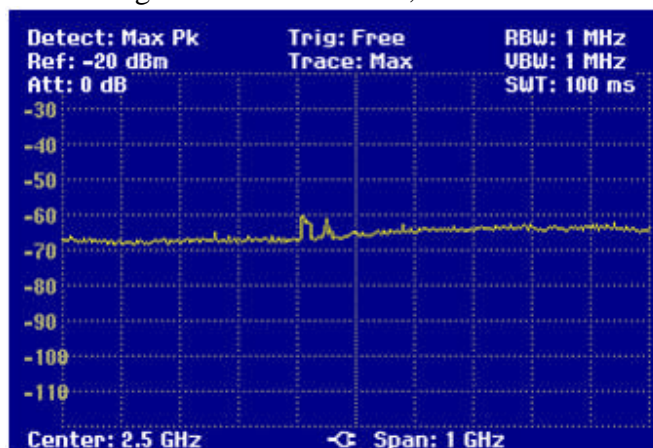


Figure C.29: Location 4, 1 to 30 MHz

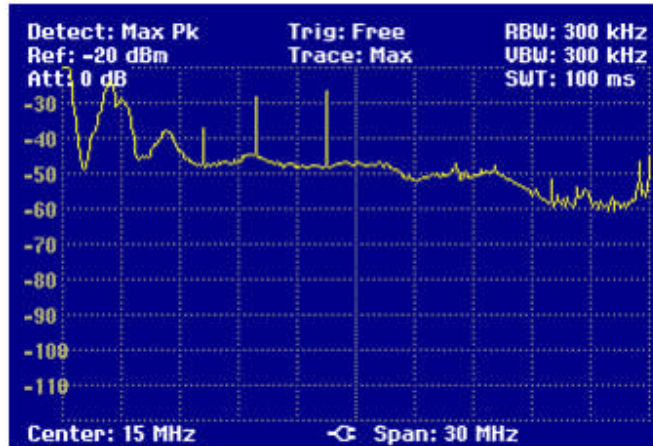


Figure C.30: Location 4, 1 to 470 MHz

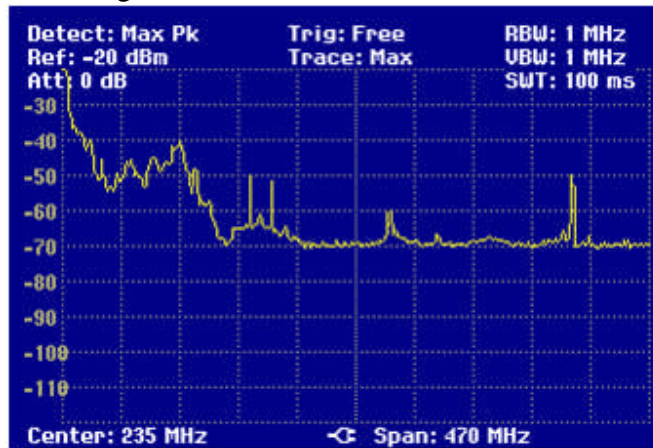


Figure C.31: Location 4, 500 to 1000 MHz

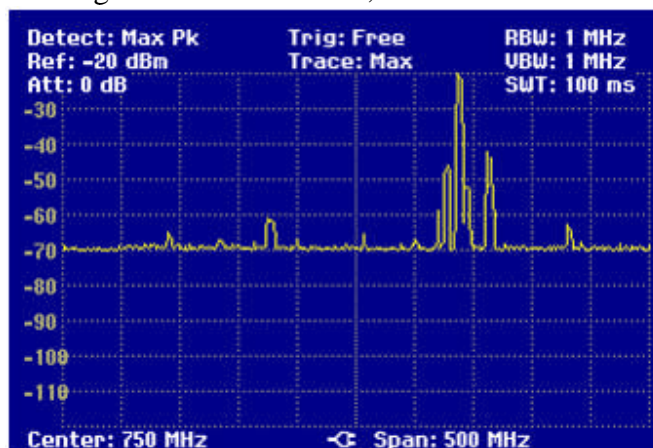


Figure C.32: Location 4, 1 to 2 GHz

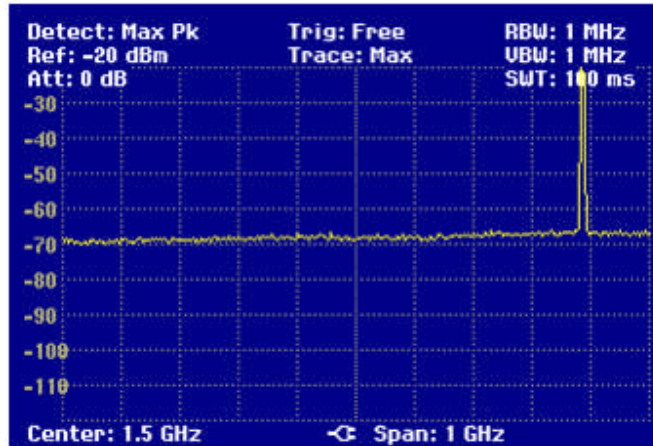


Figure C.33: Location 4, 2 to 3 GHz

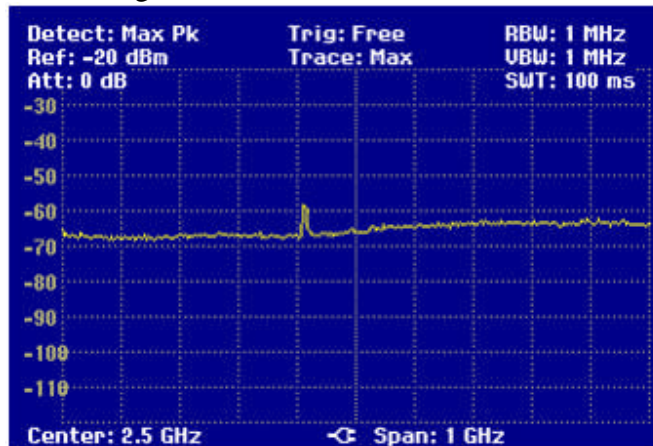


Figure C.34: Location 5, 1 to 30 MHz



Figure C.35: Location 5, 1 to 470 MHz

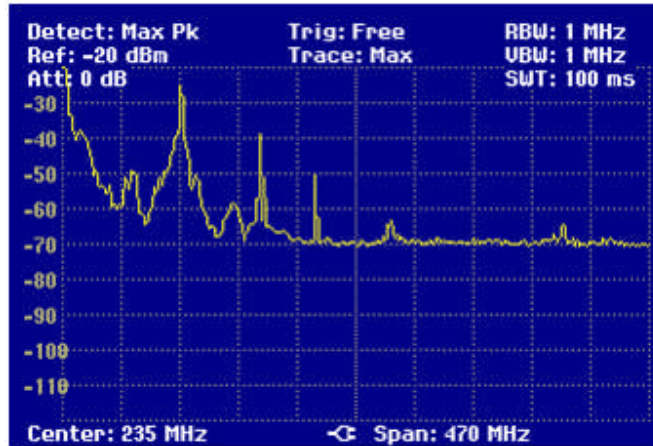


Figure C.36: Location 5, 500 to 1000 MHz

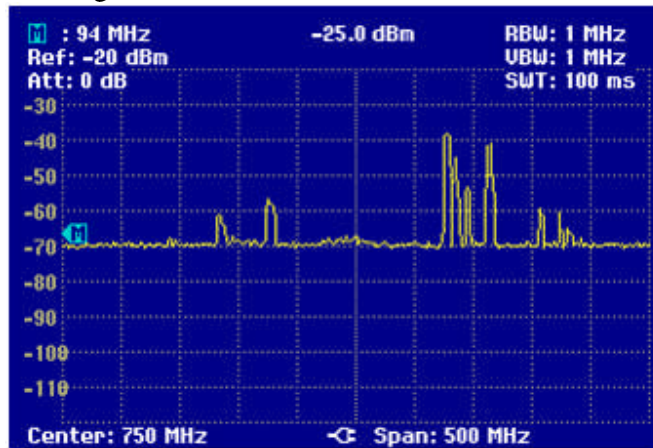


Figure C.37: Location 5, 1 to 2 GHz

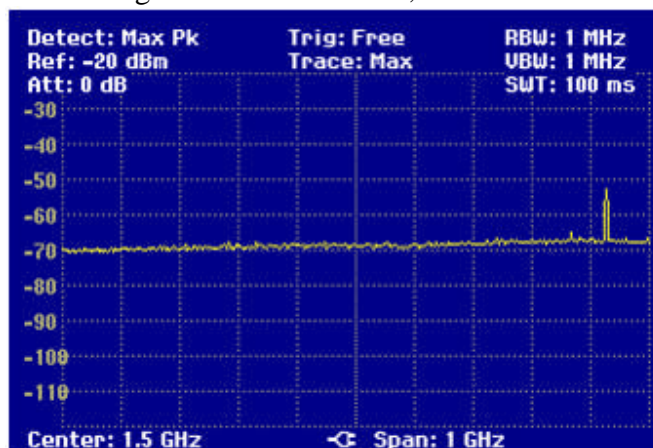


Figure C.38: Location 5, 2 to 3 GHz

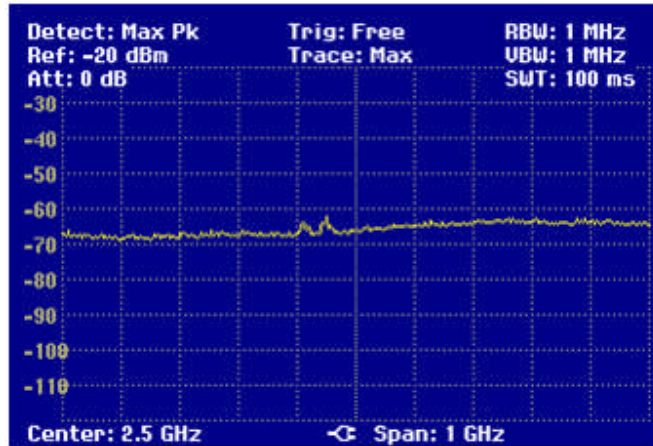


Figure C.39: Location 6, 1 to 30 MHz



Figure C.40: Location 6, 1 to 470 MHz



Figure C.41: Location 6, 500 to 1000 MHz

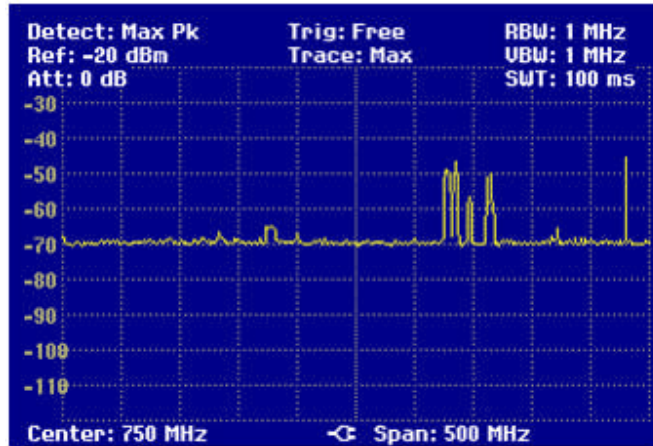


Figure C.42: Location 6, 1 to 2 GHz

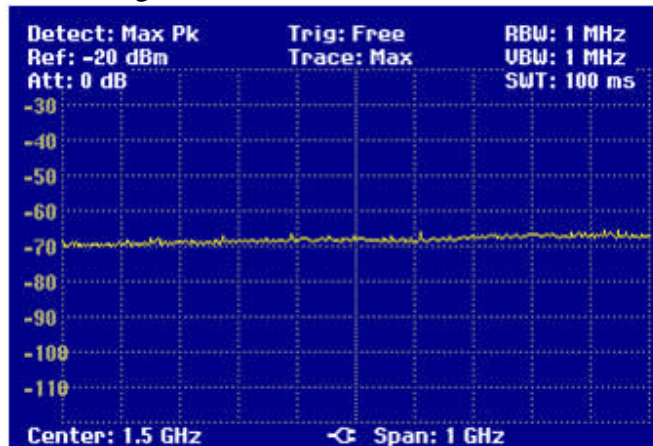
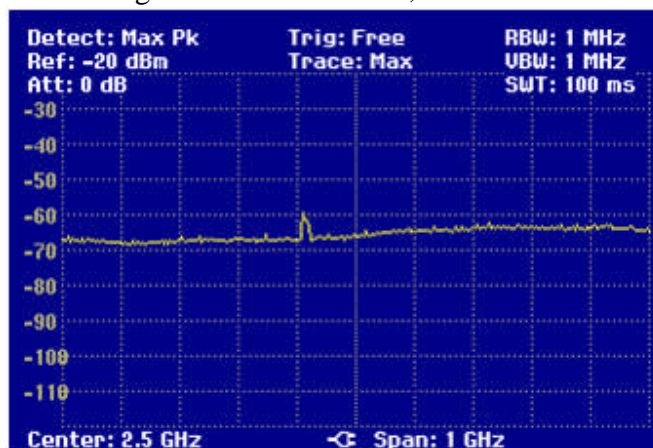


Figure C.43: Location 6, 2 to 3 GHz



Time-domain Recorder Data

Figure C.44: Location 1, 435 to 565 MHz

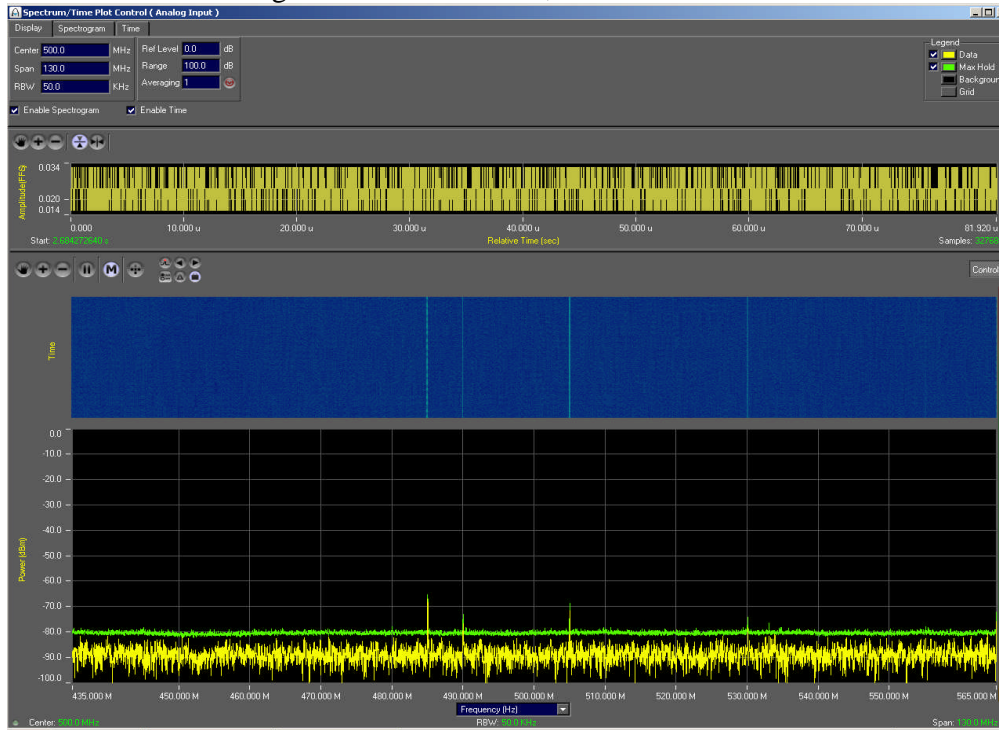


Figure C.45: Location 1, 835 to 965 MHz

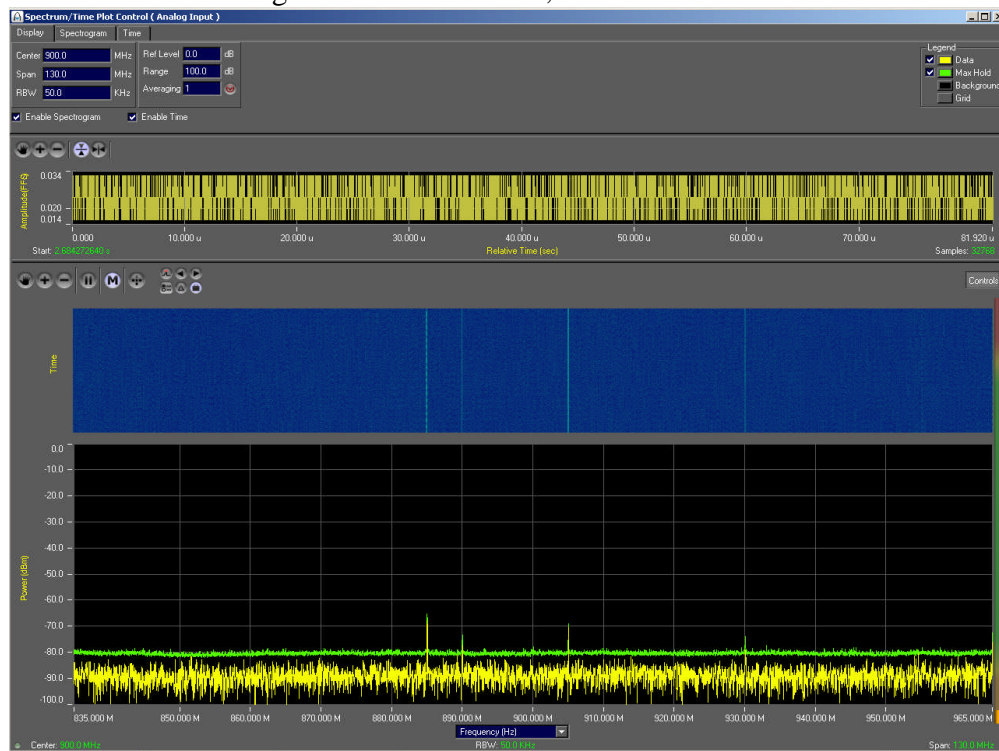


Figure C.46: Location 1, 2.38 to 2.51 GHz

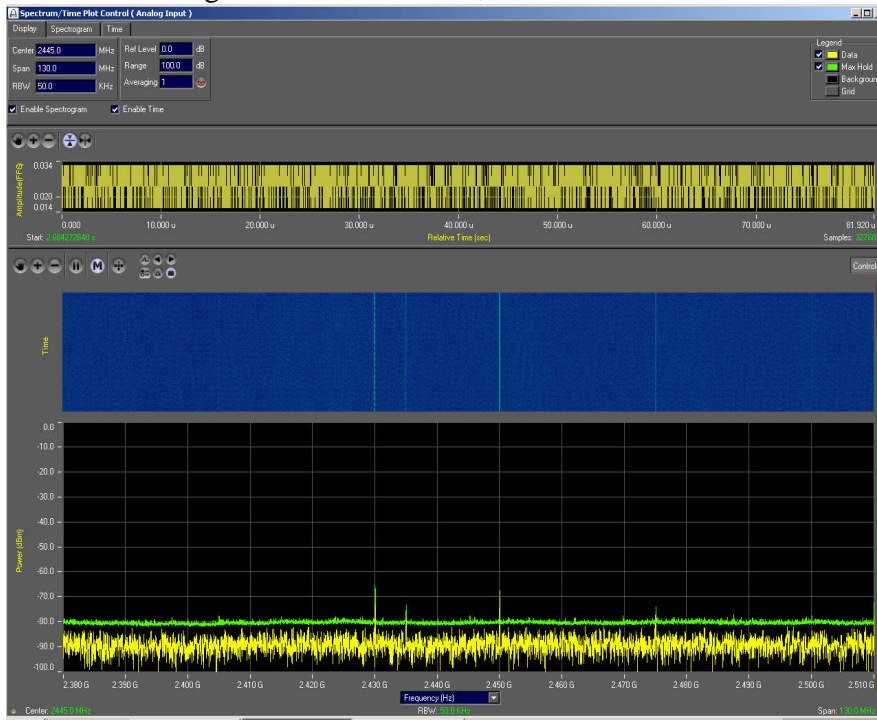


Figure C.47: Location 1, 5.795 to 5.925 GHz

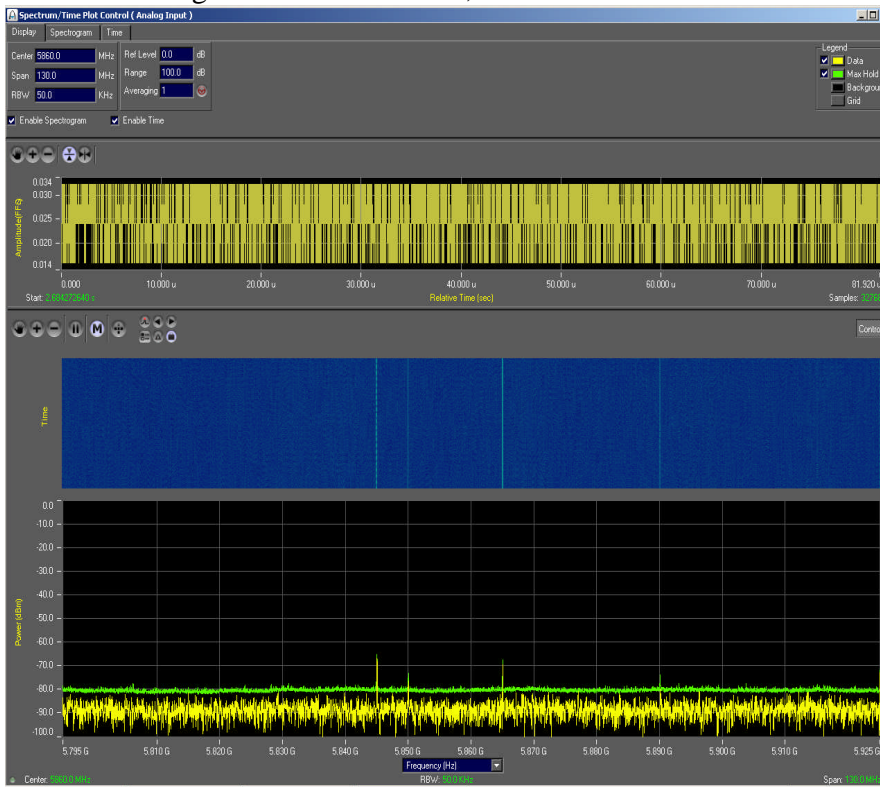


Figure C.48: Location 2, 435 to 565 MHz

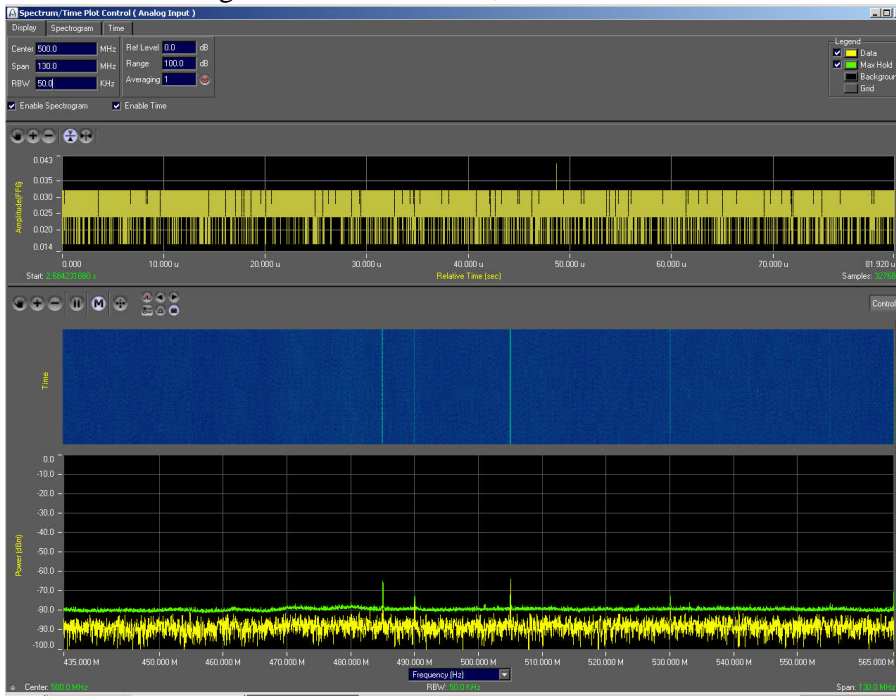


Figure C.49: Location 2, 835 to 965 MHz

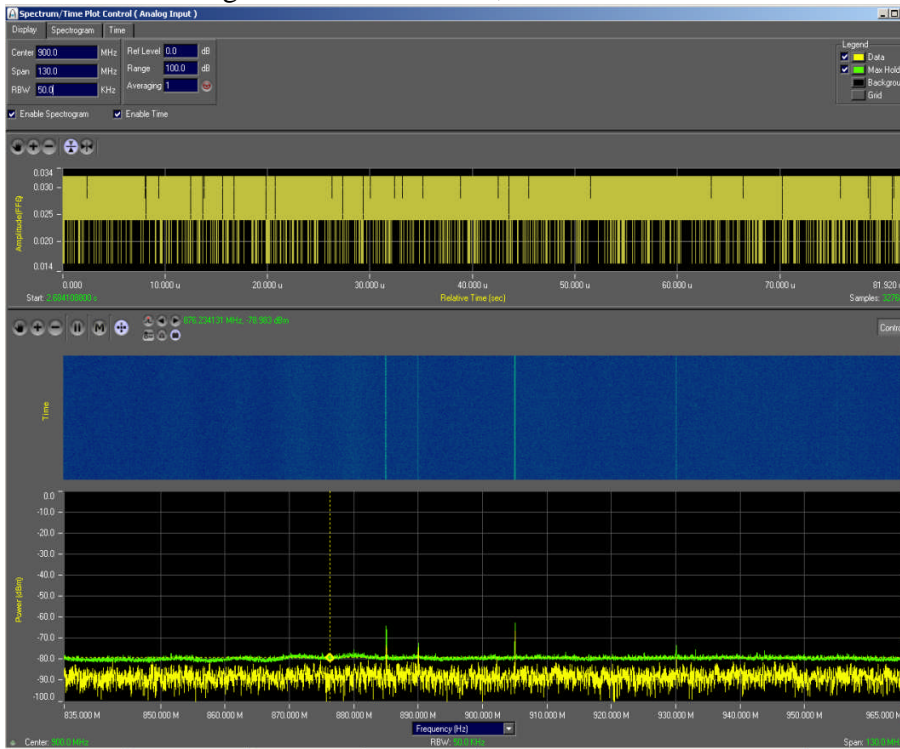


Figure C.50: Location 2, 2.38 to 2.51 GHz

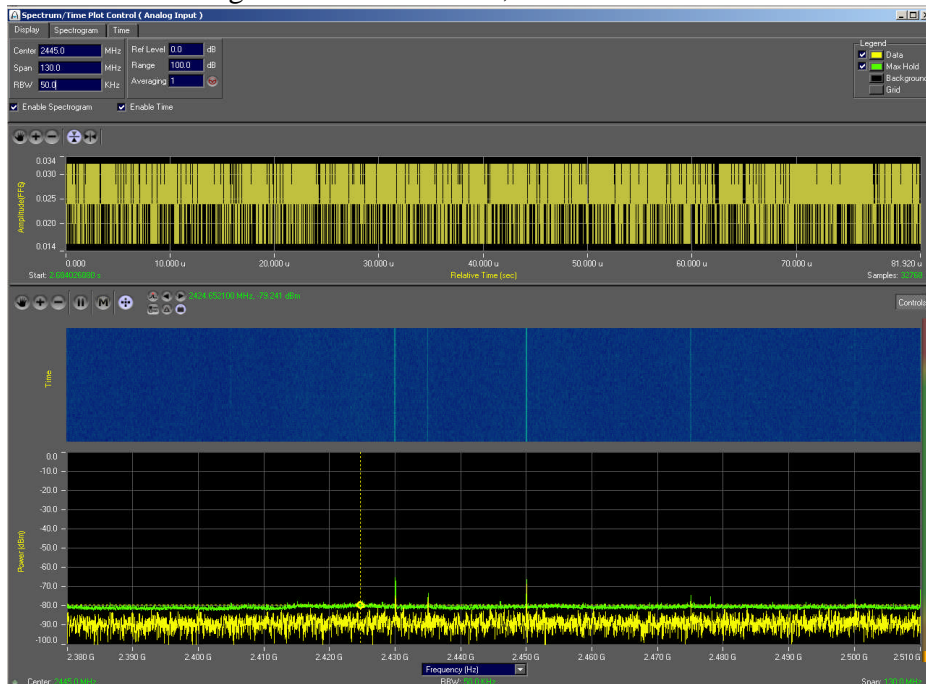


Figure C.51: Location 2, 5.795 to 5.925 GHz

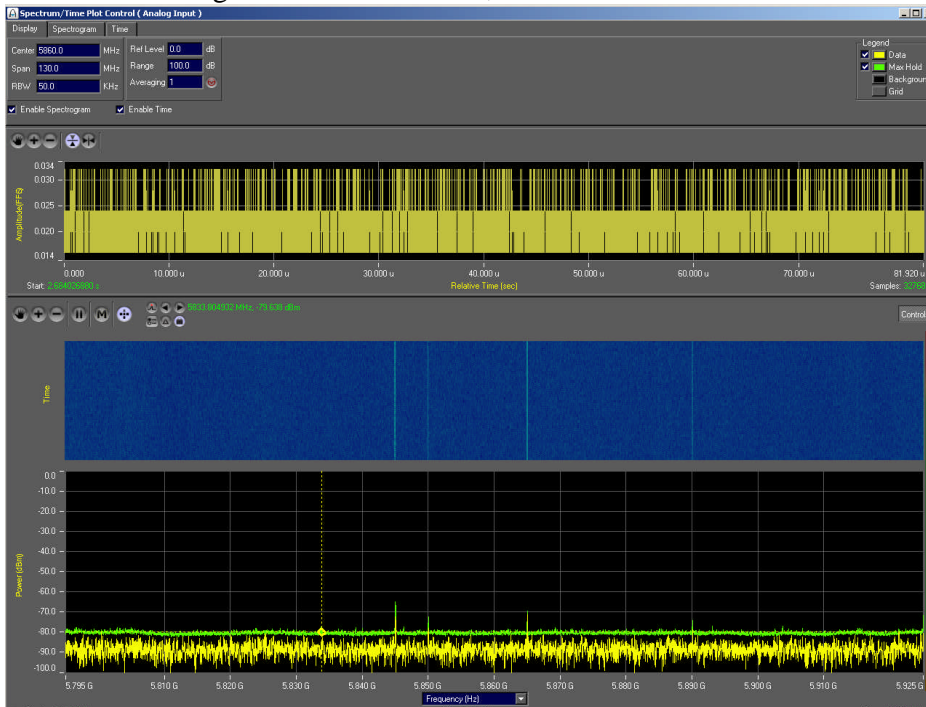


Figure C.52: Location 3, 435 to 565 MHz

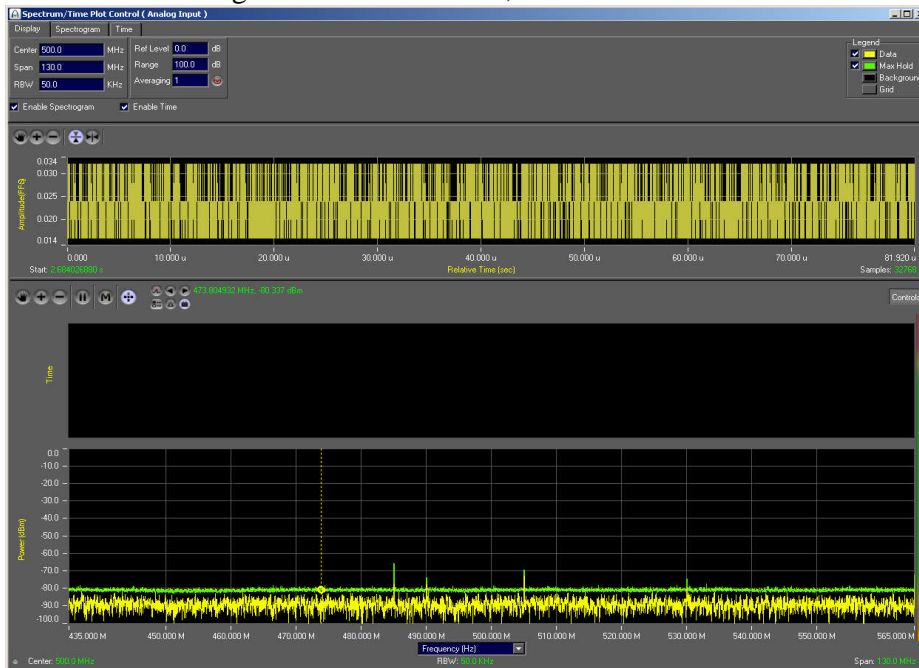


Figure C.53: Location 3, 835 to 965 MHz

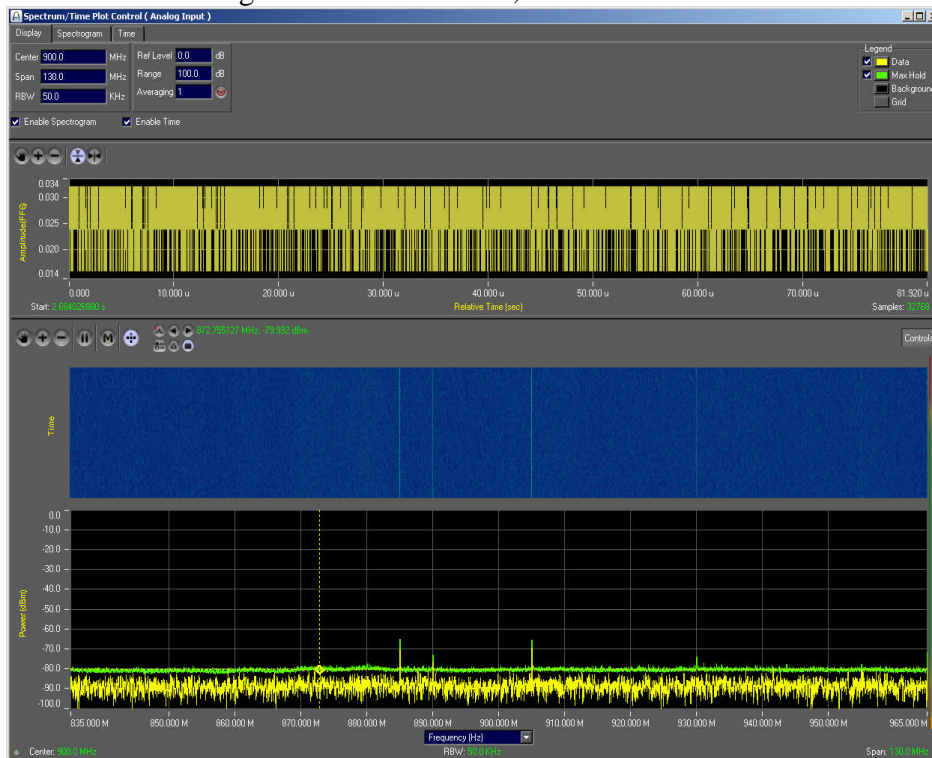


Figure C.54: Location 3, 2.38 to 2.51 GHz

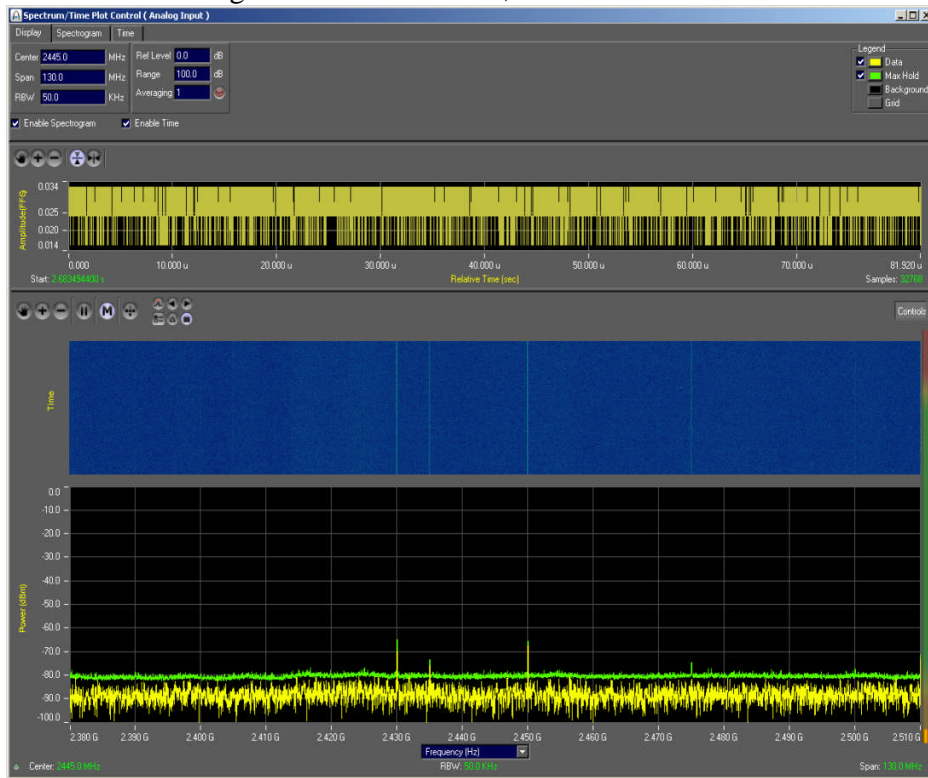


Figure C.55: Location 3, 5.795 to 5.925 GHz

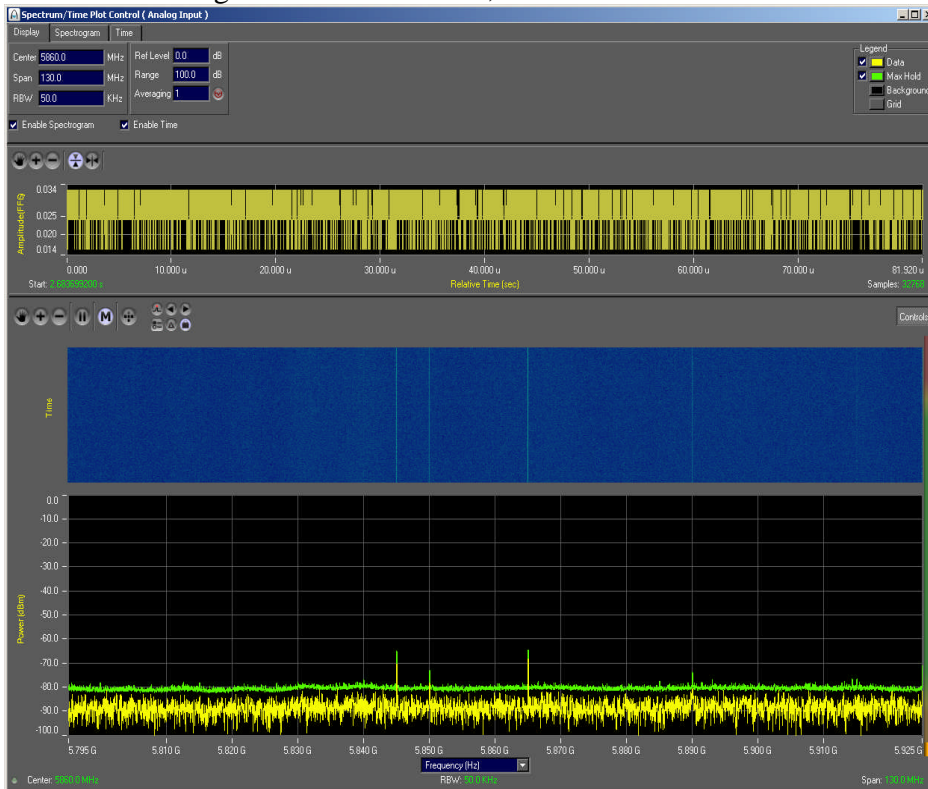


Figure C.56: Location 4, 435 to 565 MHz

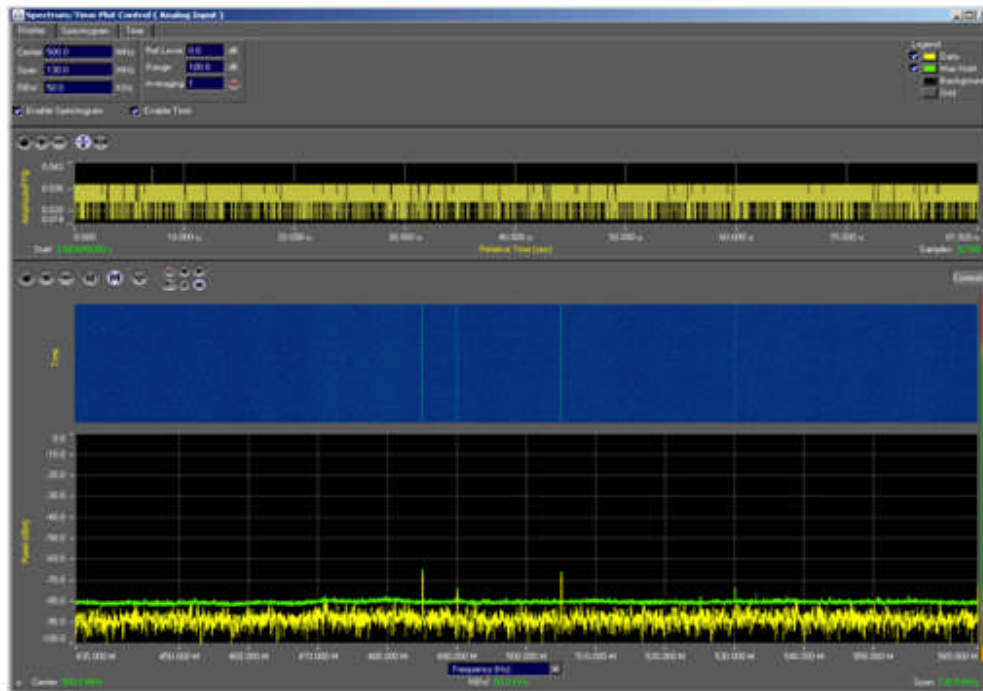


Figure C57: Location 4, 835 to 965 MHz

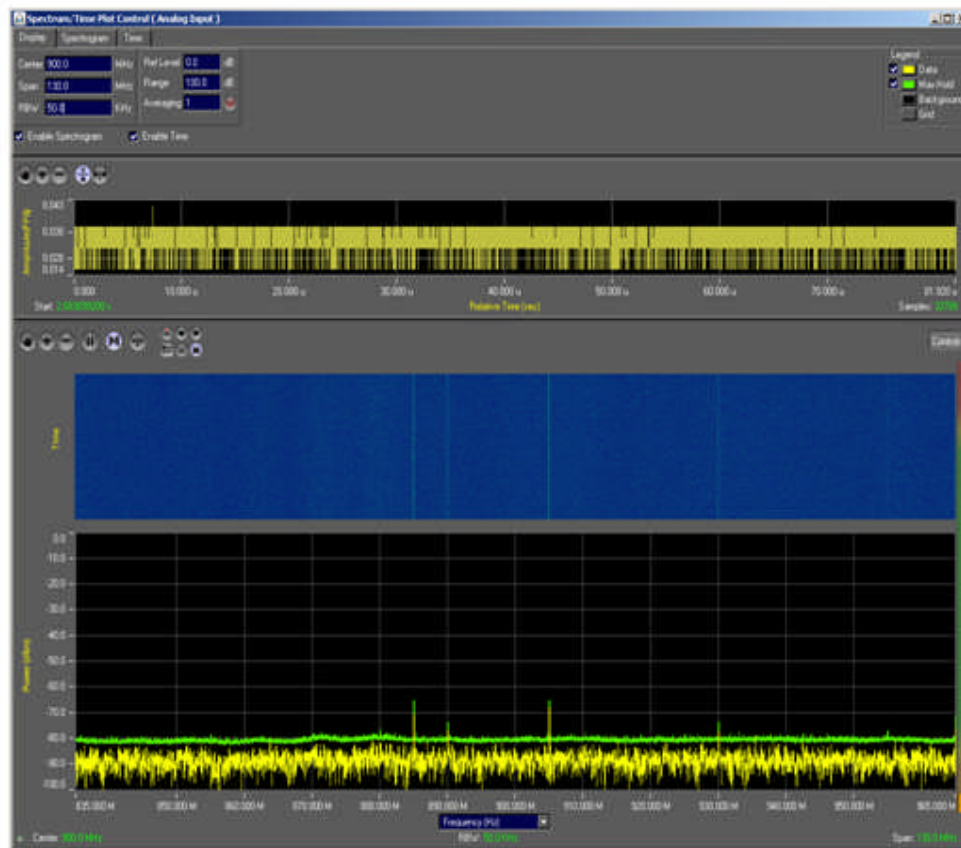


Figure C.58: Location 4, 2.380 to 2.51 GHz

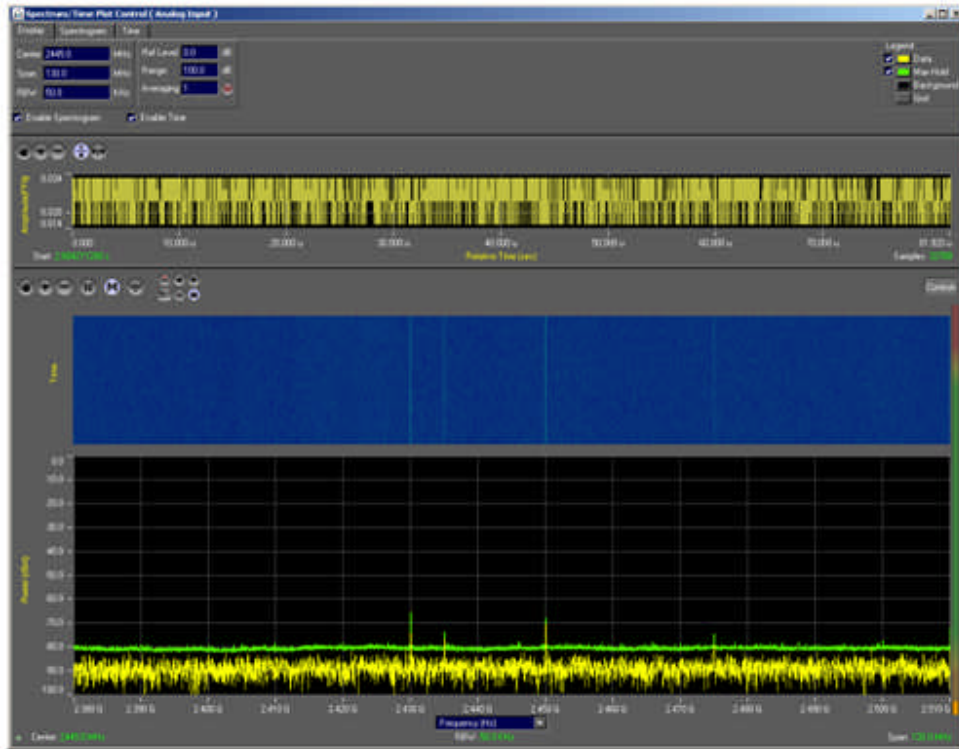


Figure C.59: Location 4, 5.795 to 5.925 GHz

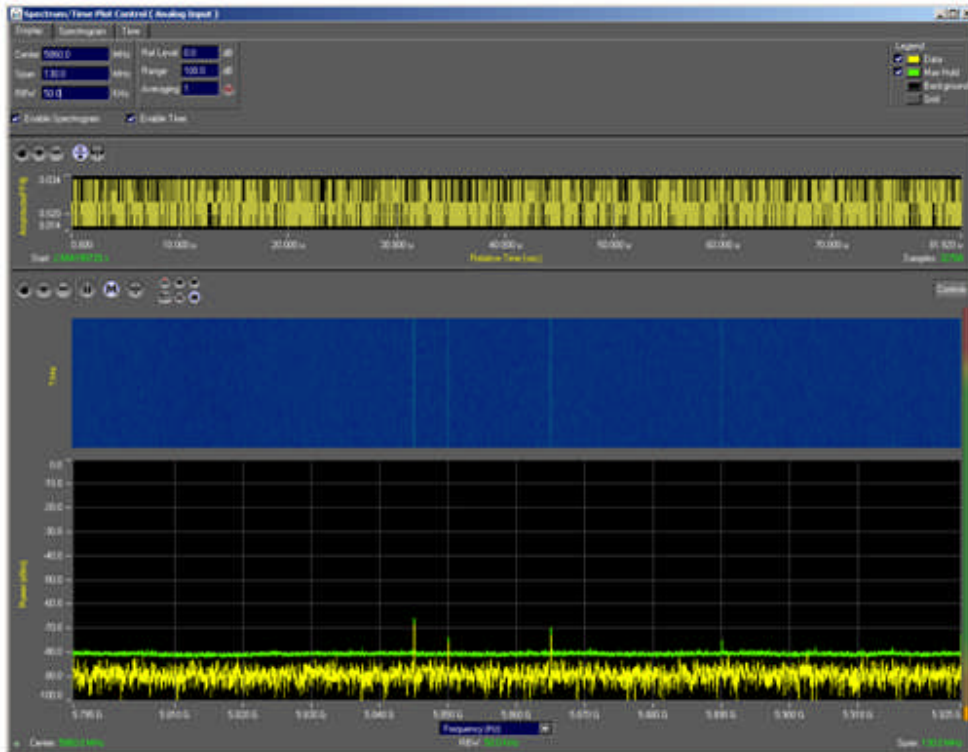


Figure C.60: Location 5, 435 to 565 MHz

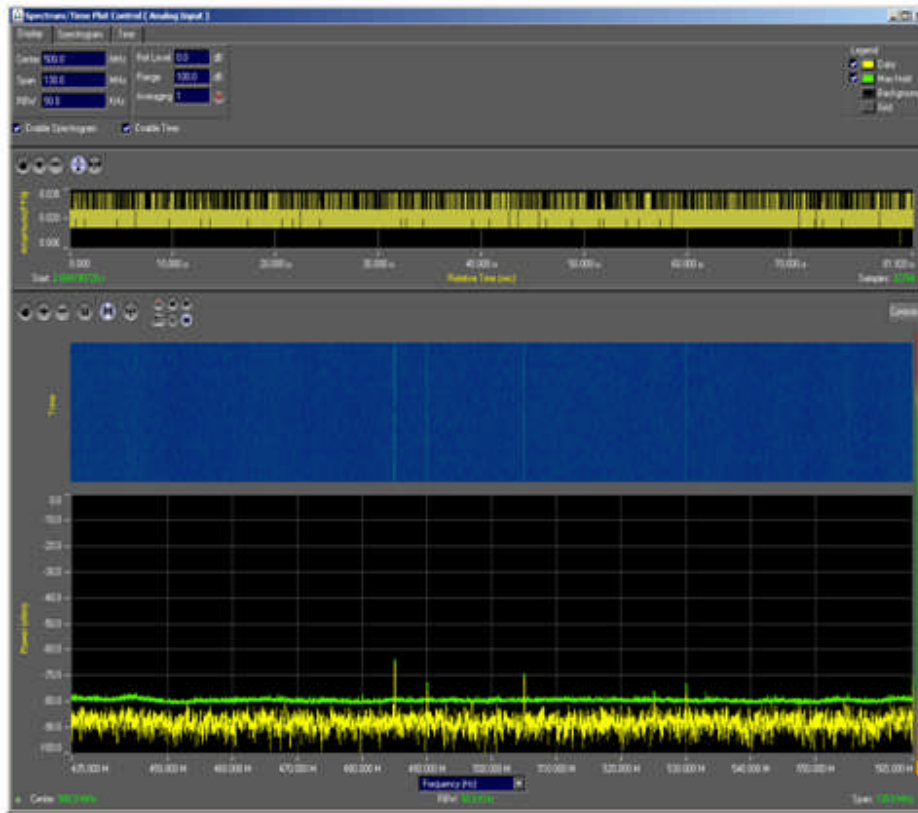


Figure C.61: Location 5, 835 to 965 MHz

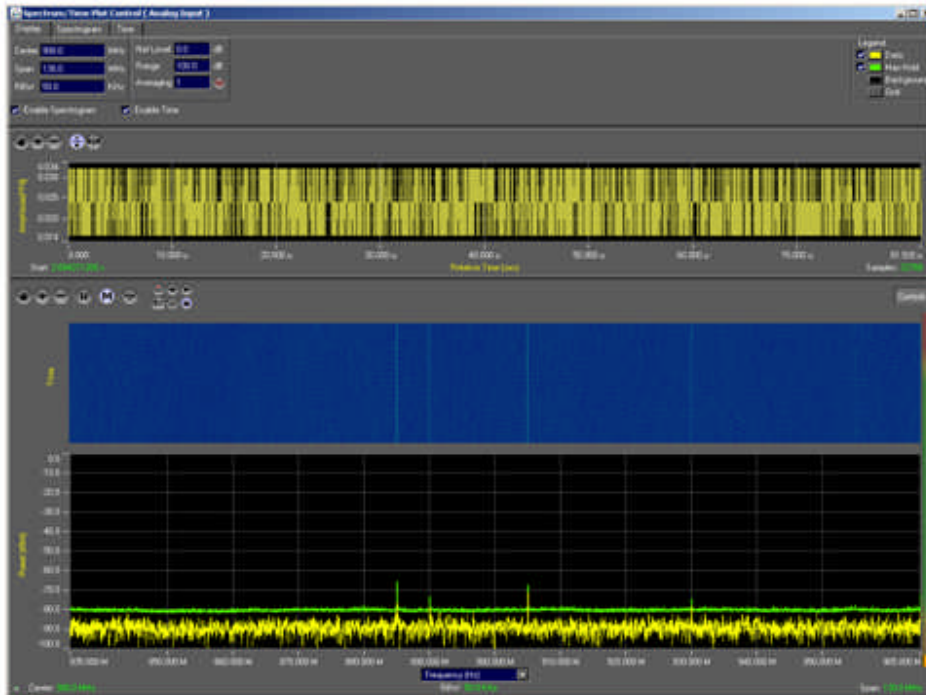


Figure C.62: Location 5, 2.38 to 2.51 GHz

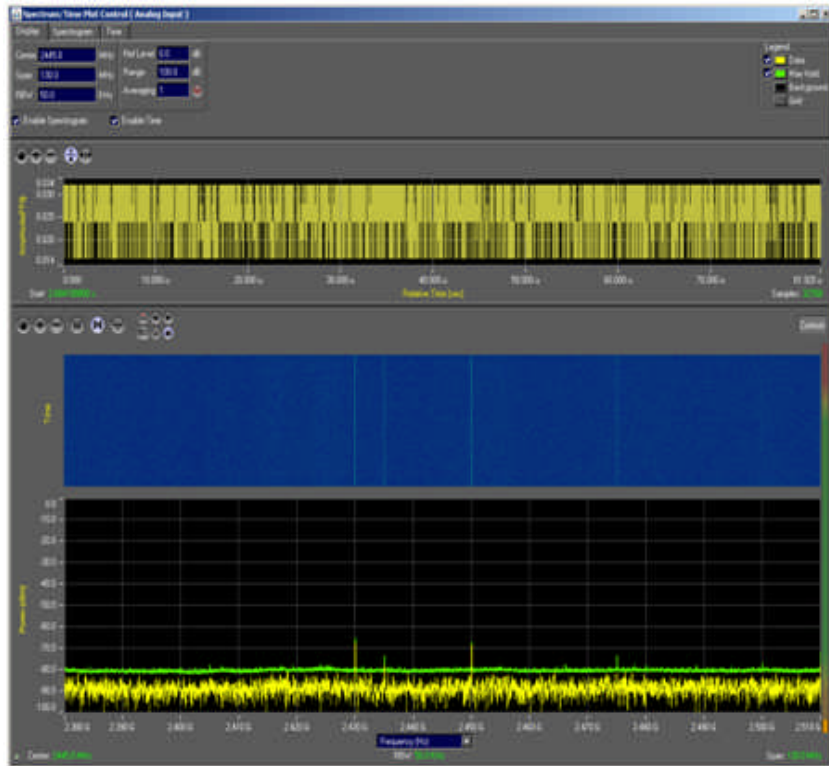


Figure C.63: Location 5, 5.795 to 5.925 GHz

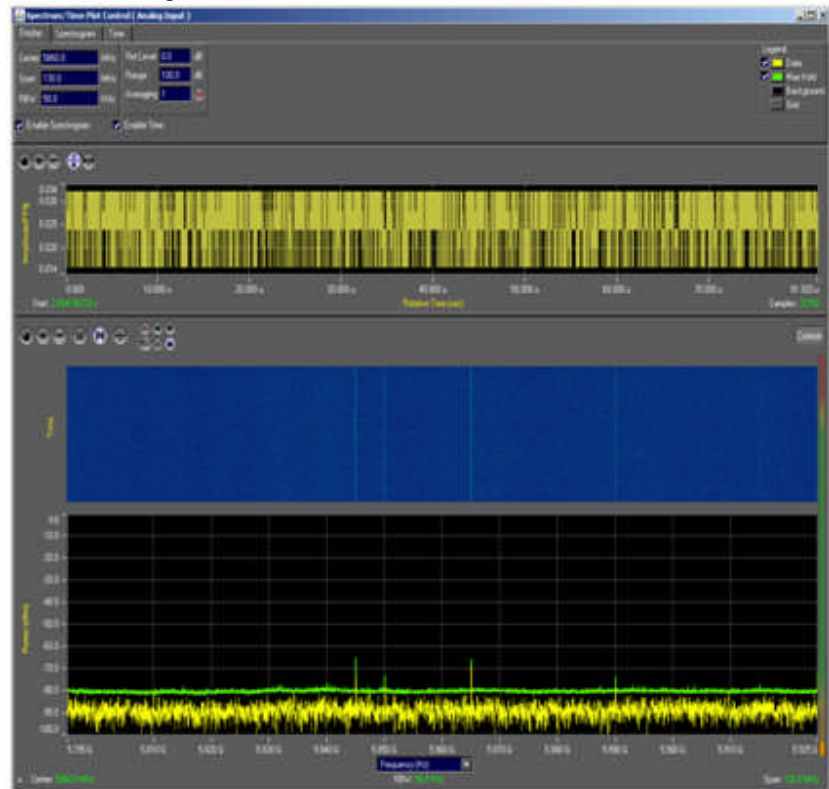


Figure C.64: Location 6, 435 to 565 MHz

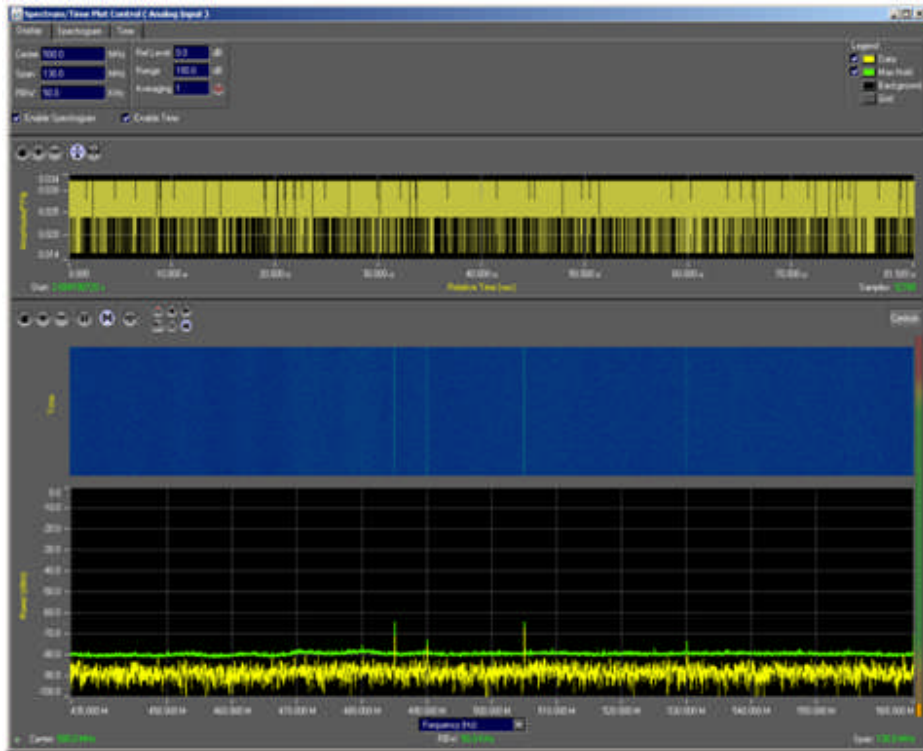


Figure C.65: Location 6, 835 to 865 MHz

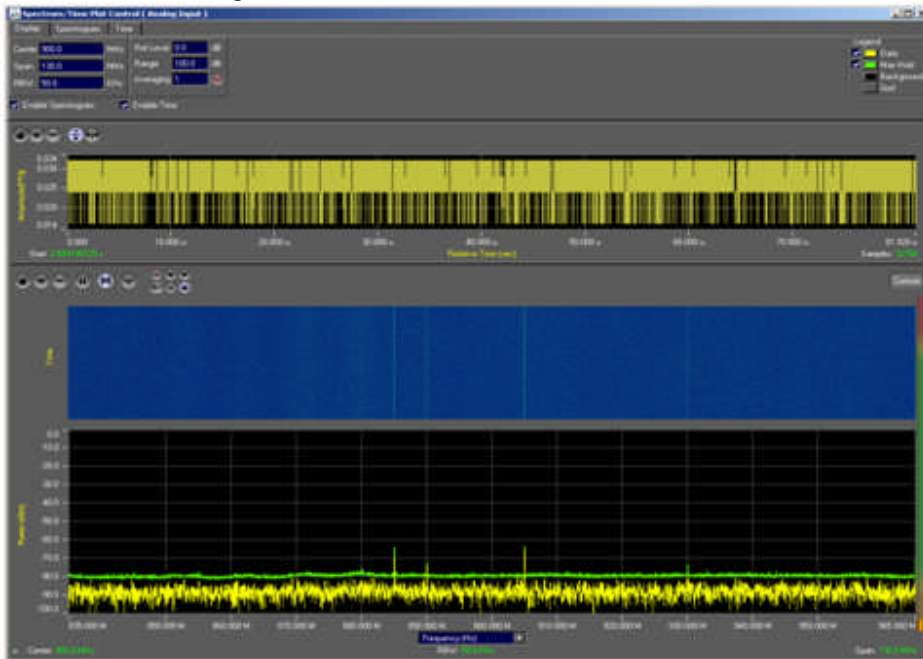


Figure C.65: Location 6, 2.38 to 2.51 GHz

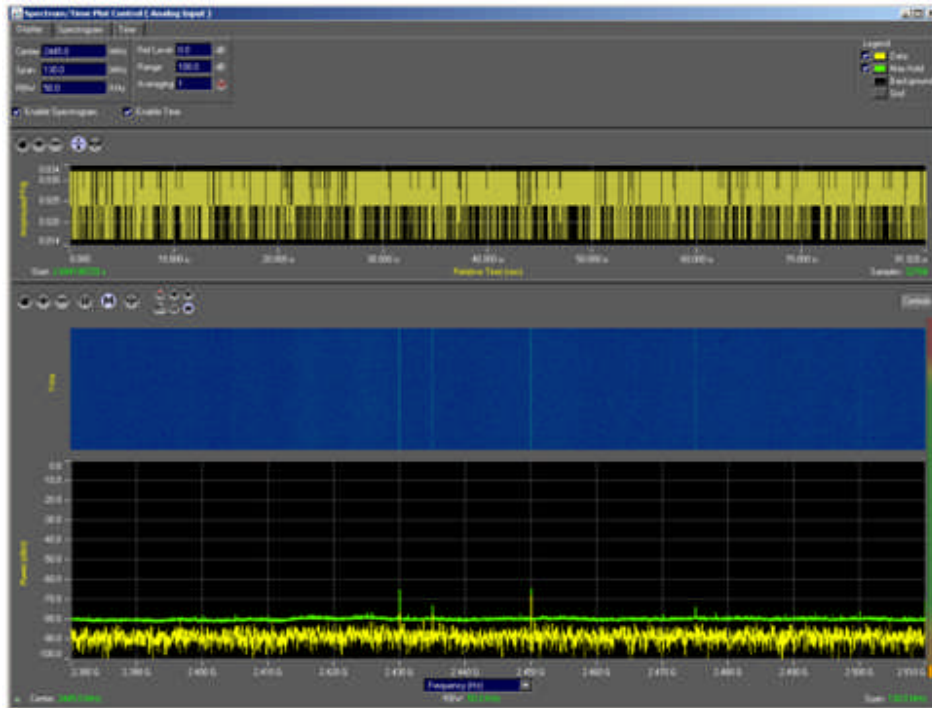
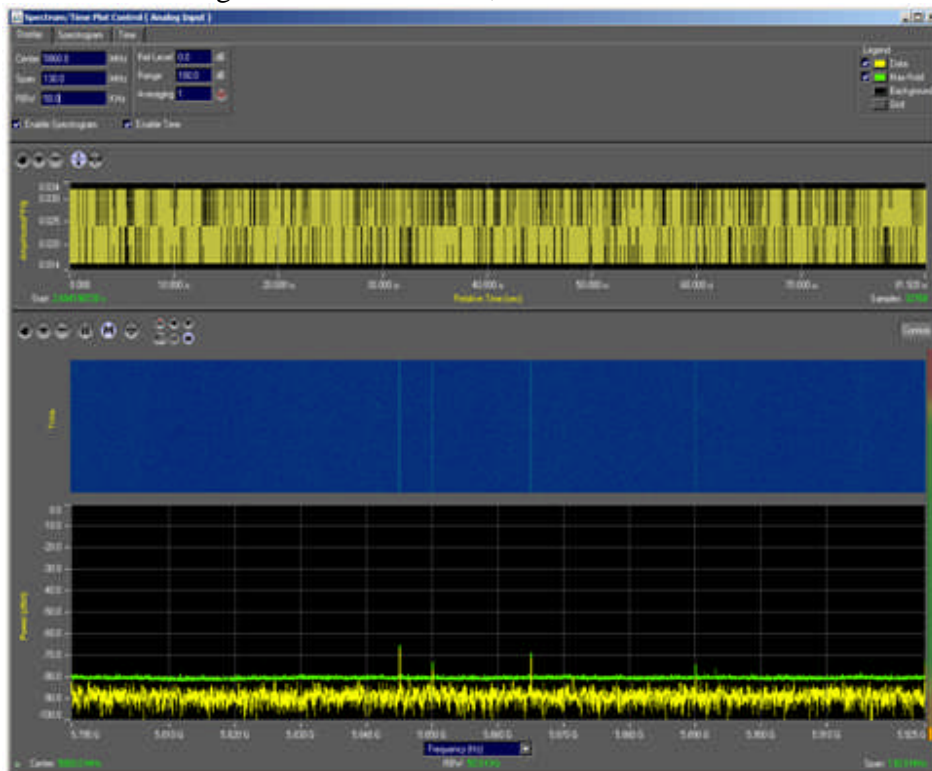


Figure C.66: Location 6, 5.795 to 5.925 GHz



Appendix D: Development of Occupancy Estimation and Forecast Algorithms

This section details the development of occupancy estimator mode which is implemented as an optimization problem as described below.

$$\begin{aligned} \min \quad & \|X(0) - \tilde{X}(0)\|_{W_{X_0}}^2 + \|Z^f(0) - \tilde{Z}^f(0)\|_{W_{Z_0}}^2 + \sum_{t=1}^T \|Z(t) - Y(t)\|_{W_Y}^2 + \\ & \sum_{t=0}^{T-1} \|X(t+1) - R(t)X(t)\|_{W_X}^2 + \sum_{t=0}^T \|X(t) - M(t)\|_{W_M}^2 + \\ & \sum_{t=1}^{T-1} \|Y^c(t+1) - (a \cdot Y^c(t) + (1-a)Y^{SA}(t+1)) - b_1 \cdot X(t) - b_2 \cdot X(t+1) - c\|_{W_C}^2 \end{aligned}$$

Such that

$$\begin{aligned} X(t+1) &= X(t) + B \cdot Z^f(t+1), t = 0, \dots, T-1 \\ \underline{X}(t) &\leq X(t) \leq \overline{X}(t), t = 0, \dots, T \\ \underline{Z}(t) &\leq Z(t) \leq \overline{Z}(t), t = 1, \dots, T \\ Z^m(t) &\leq X(t) \leq C \cdot Z^m(t), t = 1, \dots, T \end{aligned}$$

Input Data :

$\tilde{X}(0)$: input on initial occupancy level

$\tilde{Z}^f(0)$: input on initial people counter measurements

$Y(t)$: input sensor measurements at time t for people counter, CO2 and motion sensors

$Y^c(t)$: CO2 sensor measurements at time t

$Y^{SA}(t)$: CO2 measurements at supply air at time t

$R(t)$: prior knowledge on occupancy rate change from time t to time t + 1

$M(t)$: prior knowledge on mean occupancy level at time t

B : people counter sensor - zone adjacency matrix

$\underline{X}(t), \overline{X}(t)$: lower and upper bounds on occupancy level at time t

$\underline{Z}(t), \overline{Z}(t)$: lower and upper bounds on estimated sensor measurements at time t

C : vector of zone occupancy level capacity

Model parameters :

a, b_1, b_2, c : zone - dependent CO2 model parameters

$W_{X_0}, W_{Z_0}, W_Y, W_X, W_M, W_C$: weights for each term in the objective function with $\|X\|_W^2 = X^T \cdot W \cdot X$

Output estimation :

$X(t)$: zone occupancy level at time t

$Z(t) = \begin{pmatrix} Z^f(t) \\ Z^c(t) \\ Z^m(t) \end{pmatrix}$: estimated sensor measurements at time t with

$Z^f(t)$: estimated people counter sensor measurement

$Z^c(t)$: estimated CO2 sensor measurement

$Z^m(t)$: estimated motion sensor measurement

The objective function minimizes the difference between the model estimates and the input data on sensor measurements and prior knowledge on building occupancy patterns. Each term has a different weight factor representing the confidence in the input data. The more accurate the input data is, the greater the weight factor should be, so that the data will have a higher influence on the model estimates. The last term in the objective function represents a soft constraint on the CO2 model developed in the project, and will be described in details later.

The set of constraints in the formulation specifies the lower and upper bounds on the number of occupants in each zone and the number of occupants moving between zones at each time step. In addition, it ensures that the number of occupants in each zone is consistent with the number of occupants entering and leaving at any given time. The last constraint models the correlation between motion sensor and occupancy level. If the estimated motion sensor output is 0, then the room should be unoccupied with occupancy level 0. If the motion sensor output is a positive number, then occupancy level should be a positive number as well.

CO₂ model

It has been found in practice that there is a strong correlation between CO₂ level and number of occupants in a room. Such correlation is quantified and modeled in the occupancy estimator. The general CO₂ – occupancy level model is assumed to be as follows:

$$Y^c(t+1) = a \cdot Y^c(t) + (1-a)Y^{SA}(t+1) + b_1 \cdot X(t) + b_2 \cdot X(t+1) + c$$

This model assumes that the CO₂ level at time t+1 is a linear combination of the CO₂ level at the previous time step t, the CO₂ level of the supply air at t, and the numbers of occupants in the room from the current and previous time steps. As the time step considered in this model is 15 minutes, this model takes into account the delay of the impact of occupancy level change on CO₂ level change, which has been observed as 10-20 minutes.

Model parameters a, b1 and b2 depend on factors such as the location of the CO₂ sensor, and whether the door of the room is closed or open. Therefore, the parameters are tuned for each room. Specifically, CO₂ measurements and the corresponding ground truth occupancy data were collected for the working hours of a day, and then linear regression was run to find the optimal set of parameters that minimizes the difference between actual CO₂ levels and the predicted CO₂ levels by the model.

The plots in Figure 2.12 show the actual and model predicted CO₂ levels for selected rooms. Model parameters are listed in the table.

Figure 2.12 Comparison between measured and model predicted CO₂ levels.

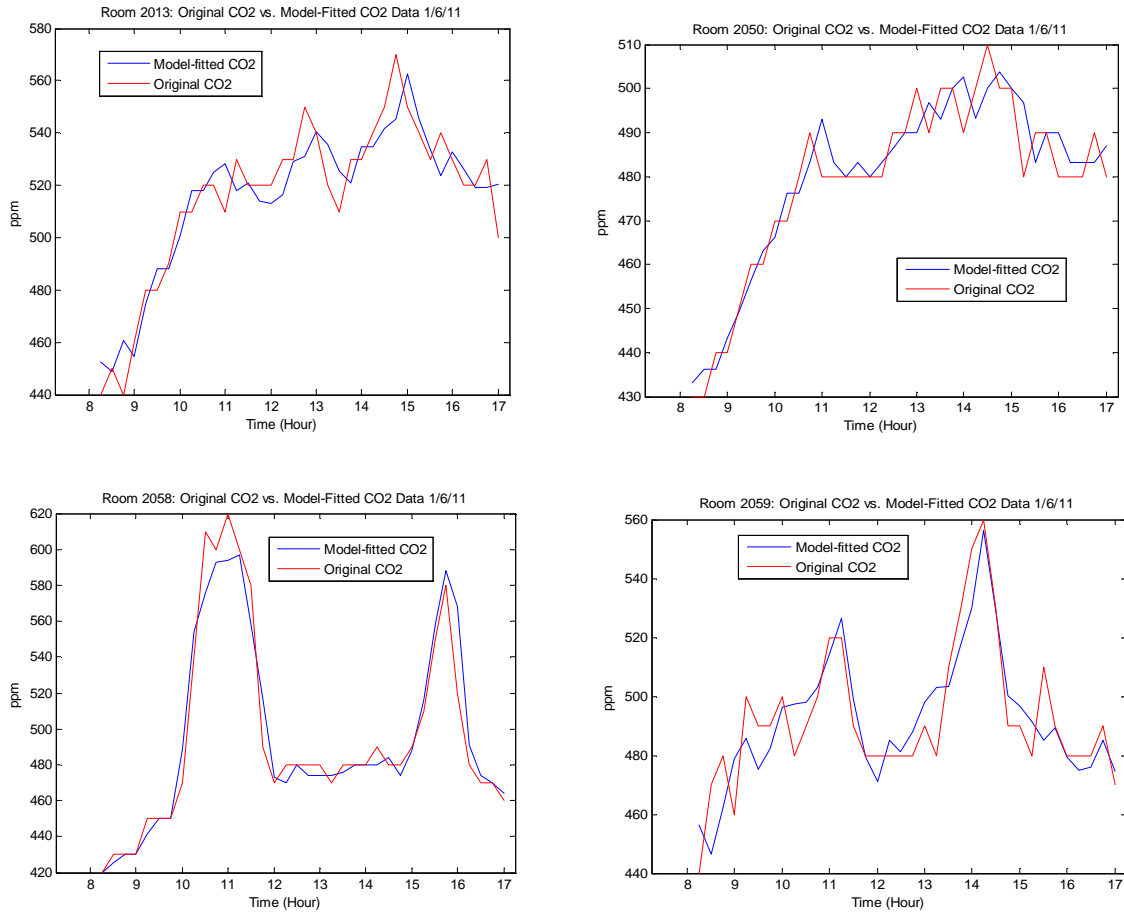


Table 2.2 CO₂ Model Parameters for Selected Rooms

	a	b1	b2	c
Room 2013	0.69	0.27	2.58	10
Room 2050	0.61	6.14	0	10
Room 2058	0.43	12.8	8.2	-10
Room 2059	0.48	10.4	1.3	-10

It can be seen from the plots and Table 2.2 that although all the plots show reasonable match between actual and predicted CO₂ levels, model parameters differ significantly. For most cases, b₁ is larger than b₂, which means that the CO₂ level at the current time step is affected more by the occupancy level at the previous time step than the current time step, which reflects the delayed impact of occupancy level change on CO₂ levels. Parameter c reflects the difference in base level CO₂ level when there is no occupancy, and for all rooms, they are insignificant. The summation of b₁ and b₂ shows the total impact of occupancy level on CO₂ level. If it is a relative

large number, then it means that the correlation between CO₂ and occupancy is strong; otherwise, the correlation is weak.

The correlation could be weak because the CO₂ sensor is installed close to the door, and the door is open most of the time. So, CO₂ measurements are influenced more by the CO₂ level in the corridor, and less by the room occupants. The other reason is due to the occupancy patterns. If occupants remain in a room for a short time period, then their impact on CO₂ level is low, compared with when the occupants tend to dwell for a while. For the rooms considered in this project, the strongest correlation between CO₂ level and occupants is observed in room 2058, which is a conference room. When people are in a meeting, they tend to remain in the room for a while, and have the door closed. Therefore, the impact of occupancy on CO₂ level is high.

In the current model, if the summation of b1 and b2 is greater than 10, then it is assumed that there is a significant correlation between CO₂ and occupancy level, and the CO₂ model is used in the occupancy estimator. On the other hand, if the summation is less than 10, then it is assumed that the correlation is insignificant, and the CO₂ model is turned off in the occupancy estimator by setting the weight of the corresponding term in the objective function to 0.

For rooms with low correlation, an alternative CO₂ model is used. In this case, as the CO₂ level cannot be correlated well with number of occupants, a weaker correlation is sought on whether or not there is occupancy. For rooms without motion sensors, this information derived from CO₂ sensor is valuable to reduce the possible accumulated estimation errors from people counter sensors. Specifically, it is assumed that the relative of CO₂ level for a room, defined as the difference between the room CO₂ level and the supply air CO₂ level, is higher during occupied time period than during unoccupied time period. This assumption still assumes correlation between occupancy and CO₂ levels, but not as quantitative as the CO₂ model described above.

The alternative CO₂ model first sorts the relative CO₂ data, and then for the portion of the time period when the occupancy level should be zero, set the portion of the occupancy level to 0 based on the CO₂ level ranking. For example, if it is assumed that 8 out of 24 hours of a day an office is empty, then after the relative CO₂ level for a day is sorted, the occupancy level is set to 0 for the time instances when the relative CO₂ level is among the lowest one third. Through experiment, it was found that the portion needs to be set to be a very conservative number so that no time intervals will be mistakenly set with an occupancy level 0. This alternative CO₂ model is mainly used in the occupancy estimator when historical occupancy pattern is estimated.

Occupancy forecast

Based on the occupancy level estimates for the current time step, occupancy forecasting for a given time horizon into the future is required for internal load estimation. Building load forecast approaches vary from simple bin predictor model to more sophisticated autoregressive predictor models [Ref. Henze]. The uniqueness in occupancy pattern is that it is highly non-stationary and does not have strong correlation with any external factors such as weather data. From our analysis on historical occupancy data for several office buildings, it has been found that the occupancy level during working hours usually follows the pattern of two peaks during mid-

morning and mid-afternoon hours, and a decrease during lunch hours. Therefore, time of the day information is critical to an accurate forecasting model.

For this project, an empirical Markov model is developed for the occupancy forecast. The underlying assumption is that the future occupancy level only depends on the level of current step and is independent of the levels of the previous steps. This assumption is valid as the rooms under consideration are multiple-person offices. While the occupancy pattern for each individual may not satisfy the Markovian assumption, the summation of the occupancy patterns from multiple people does. From historical occupancy data, the following probabilities are calculated:

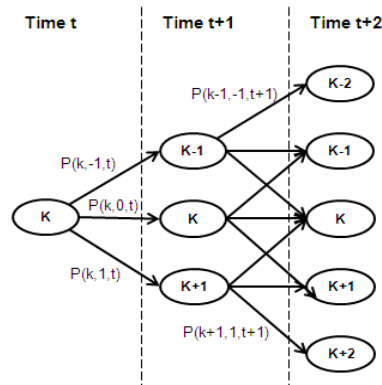
$$\hat{P}(k, \Delta, t) = \frac{\sum I(O(t) = k) \cdot I(O(t+1) = k + \Delta)}{\sum I(O(t) = k)}$$

where

- $O(t)$: Occupancy level at time k
- $\hat{P}(k, \Delta, t)$: Probability of $O(t) = k$ and $O(t+1) = k + \Delta$
- $I(O(t) = k)$: Indicator function in historical data on $O(t) = k$

This probability counts the proportion of the instances when the occupancy level changes from k at time t to $k+\Delta$ at time $t+1$. From the probabilities, a time-dependent Markov model is defined for the occupancy patterns over time. A subset of the states is shown in the figure below, where the number in each node shows the occupancy level.

Figure 2.13 Time-dependent Markov model for occupancy forecast



Once the Markov model is ready, during real-time occupancy forecasting, multiple Monte Carlo simulation runs will be carried out using the model probabilities to generate multiple sample paths of future occupancy levels. The average of the sample paths will be the output occupancy forecast.

Model validation

Occupancy estimation model is validated by comparing the ground truth data collected and the model output. The accuracy of the occupancy estimator depends on the accuracy of the input sensor measurements as well as the estimator model.

The accuracy of the people counter sensors have been evaluated at the UTRC site before shipping to CERL. The evaluation is performed by comparing the ground truth data collected from the surveillance video and the measurements from the sensors. People counter sensors were installed in a single person office, a conference room and a low traffic corridor entrance. Based on a one-day comparison, it was found that the overall detection rate is 96% and the false alarm rate is 1.5%. Specifically, the people counter sensor is 100% accurate in the single-person office, while in the conference room, the detection rate is 91.5% and the false alarm rate is 2.3%. Most missed detections and false alarms occur when a meeting ends and multiple people leave the room almost simultaneously.

The accuracy of motion sensors is usually very well, therefore, no evaluation was performed on the specific motion sensors used in this project. However, during the experiment period, several issues were identified and corrected, such as high false alarm rates due to the location of the sensor. In addition, several malfunctioning sensors were identified and replaced.

To evaluate the accuracy of the occupancy estimator, ground truth data on occupancy level was collected. Ideally, the ground truth data should be collected continuously so that occupancy level at each time instance is known. However, such data was not able to be collected as surveillance video was not allowed on site. Therefore, the data was collected by a person touring the site every 15 minutes, and counting the number of people in each room at the time instance. Such ground truth data give a series of snapshots of the occupancy levels at difference time periods of a day.

Although such ground truth data is very useful, it has two limitations. First, it is expensive to collect, as it requires someone to go around the building every 15 minutes. Secondly, it only gives snapshots of occupancy patterns. As the sensor data were collected on a different interval, there may be a mismatch between the ground truth and occupancy estimation, not due to any model error, but due to the fact that they reflect different time instances of a day. The ground truth data were manually collected twice during the project. Each time some sensor performance issues were identified, therefore another round of ground truth data collection would be required after the issues were solved. As such a procedure is expensive and impractical to be carried out whenever needed, to facilitate the model validation, an alternative type of ground truth is used for those rooms that sensor problems were identified during the second time ground truth data were manually collected.

The alternative type of ground truth data is defined based on people counter sensors. The people counter measurements are considered to be 100% accurate and can be used as ground truth data, if by simply adding up the net number of people in the room using sensor data, the net number of people at the end of the day is 0. In addition, the occupancy level during the day is always non-negative. The rationale is that the probability that the people counter miscounts people yet satisfying these two conditions is extremely low. It is more likely that the sensor gives accurate measurements during these instances. Therefore, they can be used as ground truth data.

By analyzing one month people counter data for each room without actual ground truth data, there are a few days that such conditions are satisfied. Such data were then used as the alternative

ground truth data for those rooms, and were excluded from model calibration, as people counters were part of the sensors used in the occupancy model.

The metrics used to measure model accuracy is normalized root-mean-square error (NRMSE),

which is

$$NRMSE = \frac{\sqrt{\sum_i (g_i - o_i)^2 / n}}{g_{\max} - g_{\min}}$$

where

g_i : ground truth occupancy level at time i

o_i : estimated occupancy level at time i

n : number of samples

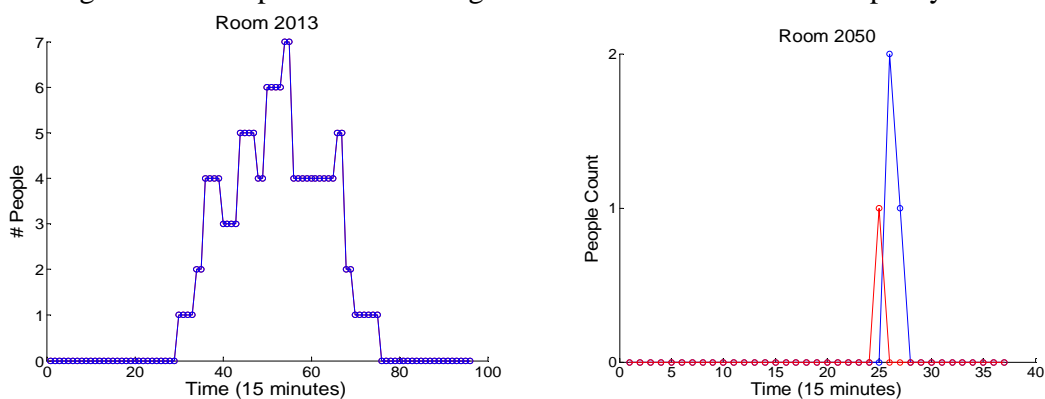
g_{\max} / g_{\min} : maximum/minimum of ground truth level

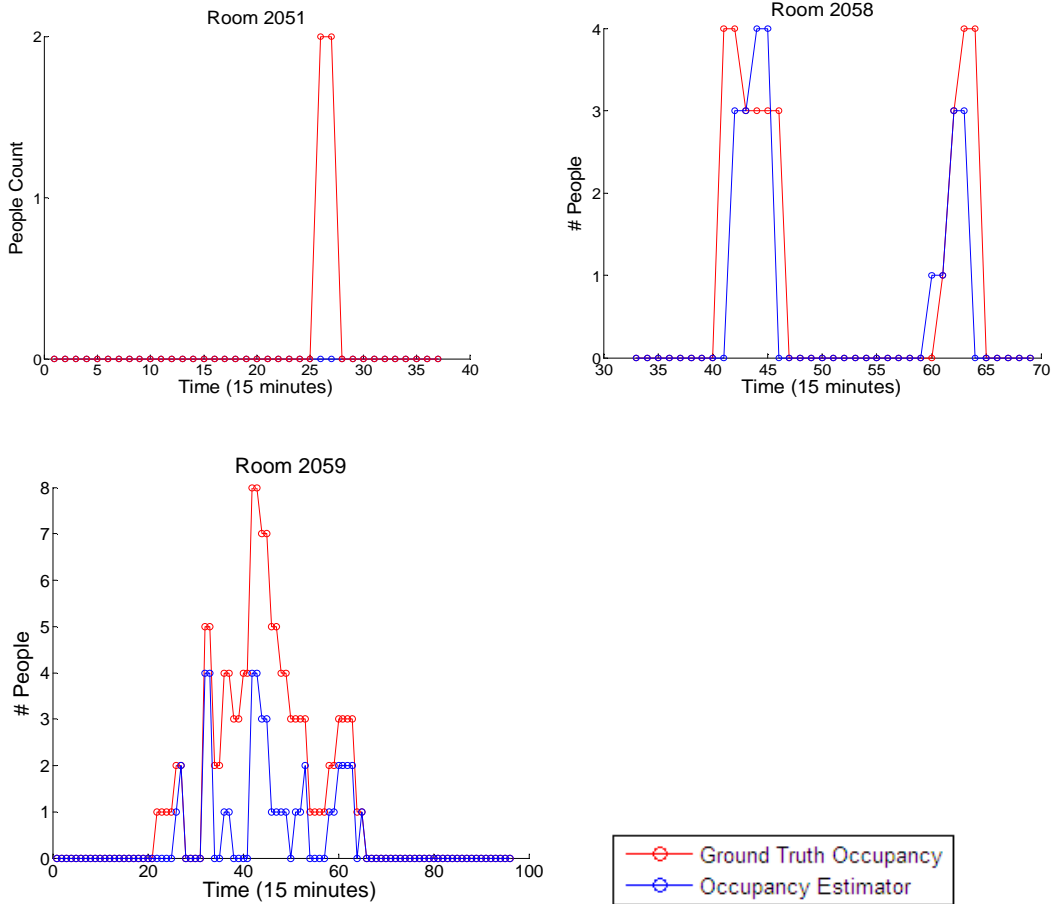
In the project performance objectives, MPE (mean percentage error) was proposed as the metric to measure estimation accuracy. The definition of MPE is listed below:

$$MPE = \frac{1}{n} \sum_{i=1}^n \frac{g_i - o_i}{g_i}$$

The reason that NRMSE is used instead of MPE is that during the project, it has been found that the occupancy levels in some rooms are either very low, or being unoccupied for extended time periods. Therefore, MPE is not well defined for time instances when a room is unoccupied and skewed when the occupancy level is low. For example, if the ground truth occupancy level is 1, and the occupancy estimator is 2, the error can be 100%, which does not reflect the actual impact of the estimation error. Using NRMSE, the mean error for all rooms is 12%, as some rooms have higher accuracy compared with others. It was found that the accuracy depends on the input sensor data and occupancy patterns. The plots below compare the ground truth and estimated occupancy levels for the selected rooms. One room is selected for each zone that has thermostat installed.

Figure2.14 Comparison between ground truth and estimated occupancy level





Appendix E: Development of HVAC Models

This section presents the details and the development of the HVAC models for fans and heat exchangers.

Fan Models

To meet the challenges mentioned above, both the supply and return fan models have been designed with the following inputs and outputs:

- Inputs: volumetric outdoor air flow rate \dot{V}_{OA} and desired supply flow set point \dot{V}_{SA} . Although the latter is an optimization variable, and therefore computed as part of the model predictive control implementation, the former needs to be estimated. The formula used for estimating it is based on a sensible-heat balance for the mixed air where the air density is assumed to constant in the considered temperature range:

$$\dot{V}_{OA} = \dot{V}_{SA} \cdot \frac{T_{MA} - T_{RA}}{T_{OA} - T_{RA}}$$

In the above formula the mixed air temperature T_{MA} is an optimization variable, the outdoor air temperature is extracted from the NOAA forecast and the return air

temperature is estimated based on a zone-return-flow-averaged zone temperature as follows:

$$T_{RA} = 0.64 \cdot T_{Z1} + 0.09 \cdot T_{Z2} + 0.08 \cdot T_{Z3} + 0.02 \cdot T_{Z4} + 0.19 \cdot T_{Z4}$$

The above model for return temperature was built using historical measurement data for all temperature included in the above formula. The coefficients multiplying each zone temperature represent individual zone return portion of the total return flow and are consistent with the values recorded during commissioning.

- Outputs: electrical power consumptions. These are used in the cost function of the optimization problem.

The model considered for the electrical power consumption are polynomials in the input variables whose coefficients were estimated based on least squares approximations using functional test data. These tests have been conducted with various combinations of outdoor damper position, fan speeds and zone dampers. About 5% of the test data was discarded because it did not meet practical criteria such as $\min(T_{OA}, T_{RA}) \leq T_{MA} \leq \max(T_{OA}, T_{RA})$.

Using the mentioned structure and calibration procedure the following models were derived for the two fans:

- $P_{SF} = -0.256 \cdot \dot{V}_{SA}^3 + 3.204 \cdot \dot{V}_{SA}^2 - 11.374 \cdot \dot{V}_{SA} + 0.031 \cdot \dot{V}_{OA}^3 - 0.257 \cdot \dot{V}_{OA}^2 + 0.217 \cdot \dot{V}_{OA} + 13.325$
- $P_{RF} = -0.074 \cdot \dot{V}_{SA}^3 + 0.897 \cdot \dot{V}_{SA}^2 - 3.136 \cdot \dot{V}_{SA} + 0.008 \cdot \dot{V}_{OA}^3 - 0.06 \cdot \dot{V}_{SA}^2 + 0.038 \cdot \dot{V}_{SA} + 3.527$

where the units are: power in [kW] and volumetric flow rate in [$\frac{m^3}{s}$].

The functional test data used to calibrate the models is illustrated in Figures 2.16 and 2.17.

Figure 2.16 Illustration of the damper positions and supply fan speeds for the generated functional test data (there are eight zone damper combinations for each data point, not plotted)

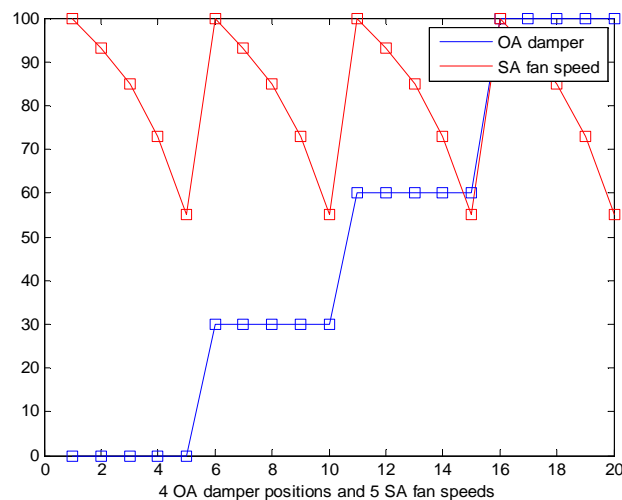
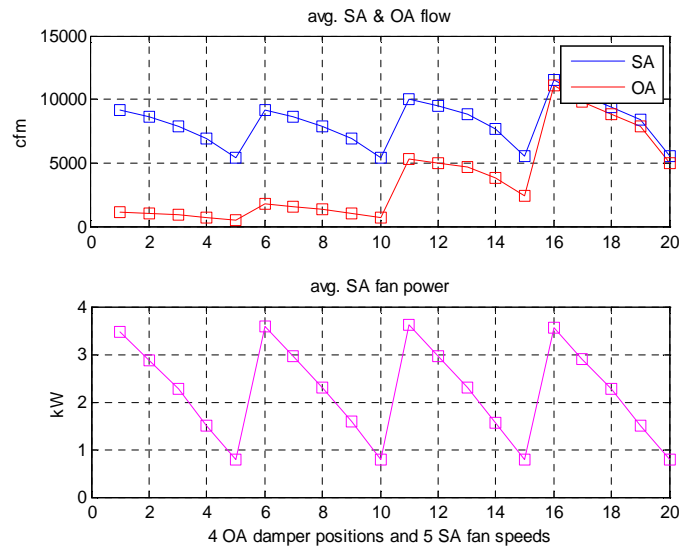


Figure 2.17 Average supply and outdoor air flows, and supply fan power consumption for each set of data illustrated in Error! Reference source not found..



The model errors are plotted in Figures 2.18 and 2.19, illustrating only a few cases when relative error exceeds the selected 20% threshold. These occur at low power levels, below 1kW for the supply fan and below 0.2kW for the return fans, when the uncertainty in the flow estimates increases. Based on this we conclude that the models are adequate for control design.

Figure 2.18 Modeled and measured supply fan power and relative error for functional test cases.

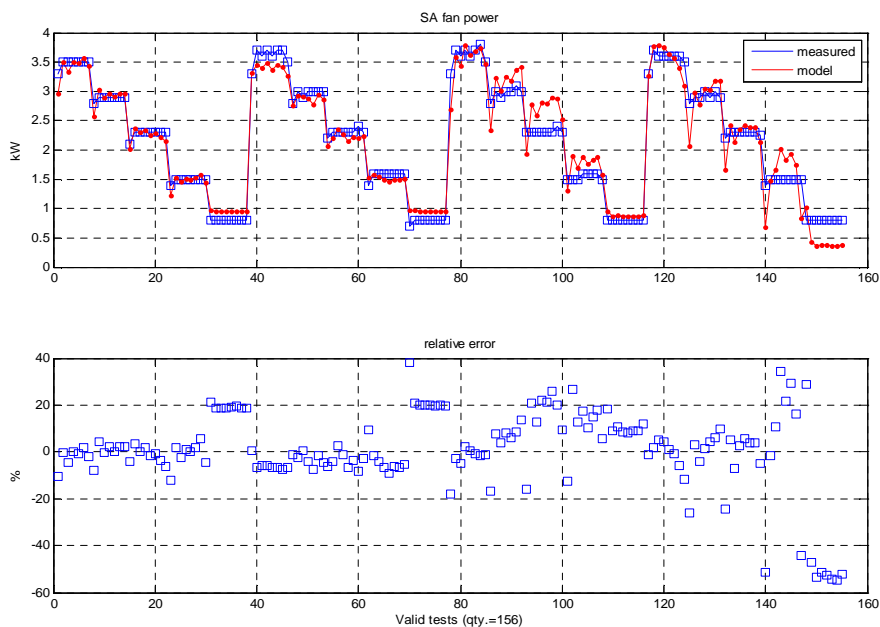
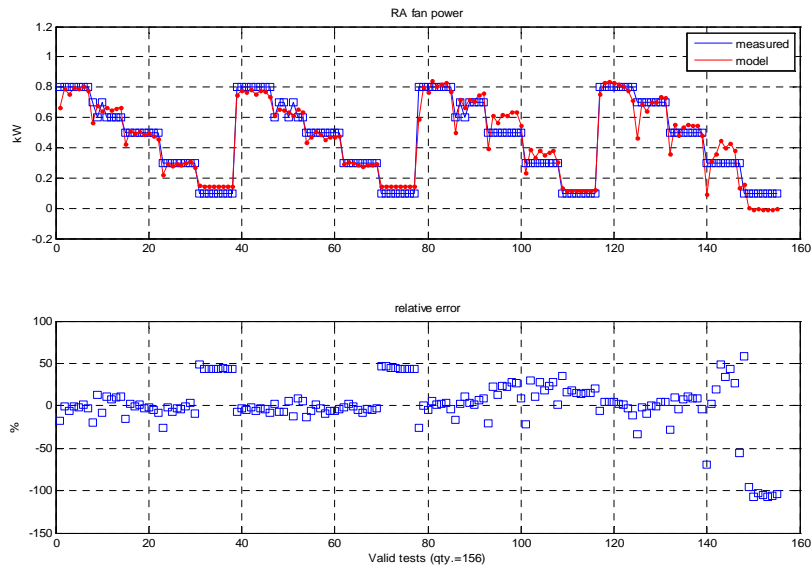


Figure 2.19 Plots of modeled and measured supply fan power and relative error for all the functional test cases.



In addition to modeling the fan electrical power consumptions that are part of the overall optimization cost, one needs to include the constraints imposed by the system operation. Of particular interest is the maximum supply flow and its dependency on the outdoor and mixing dampers. In view of the facts that the two dampers are controlled in a coordinated manner and that the outdoor flow rather than the outdoor damper is part of the model used at supervisory level (see Figure 2.20), we model the maximum supply flow only as a function of the outdoor flow. This dependency is illustrated using the functional test data in Figure 2.21 and 2.22.

Figure 2.20 Illustration of the volumetric supply flow rate with fan speed and outdoor air damper position using all the functional test data sets.

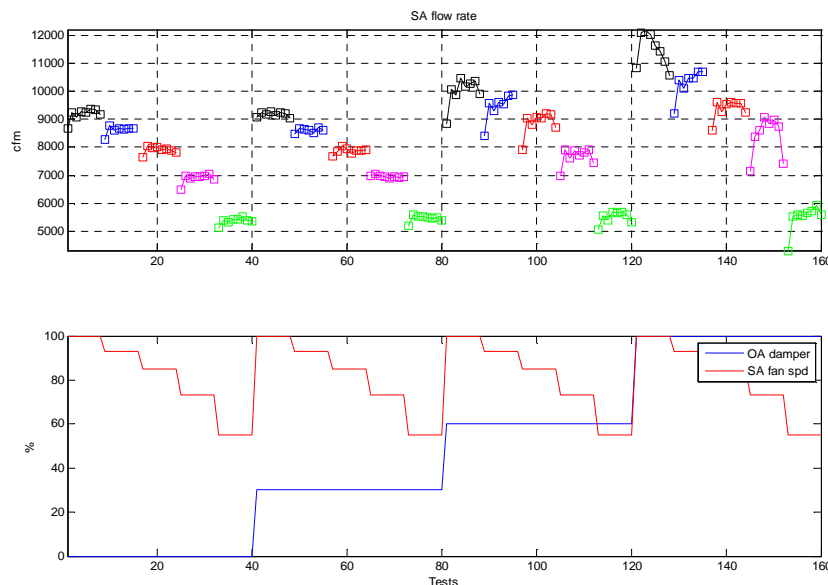
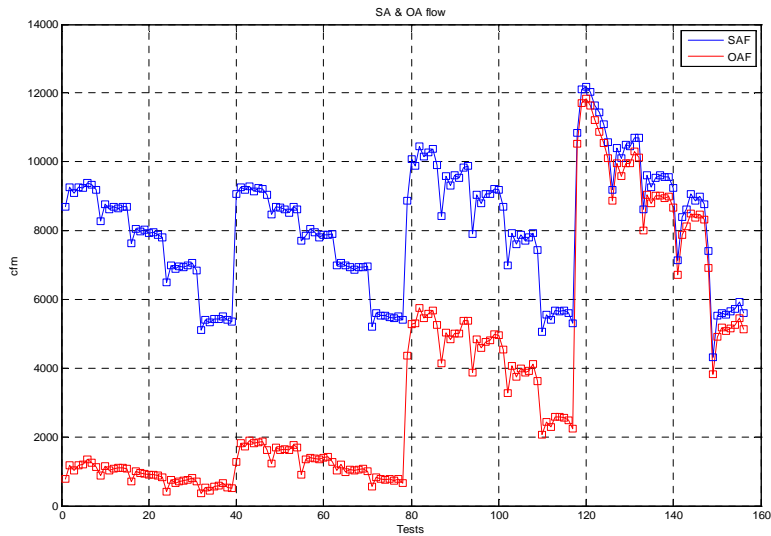
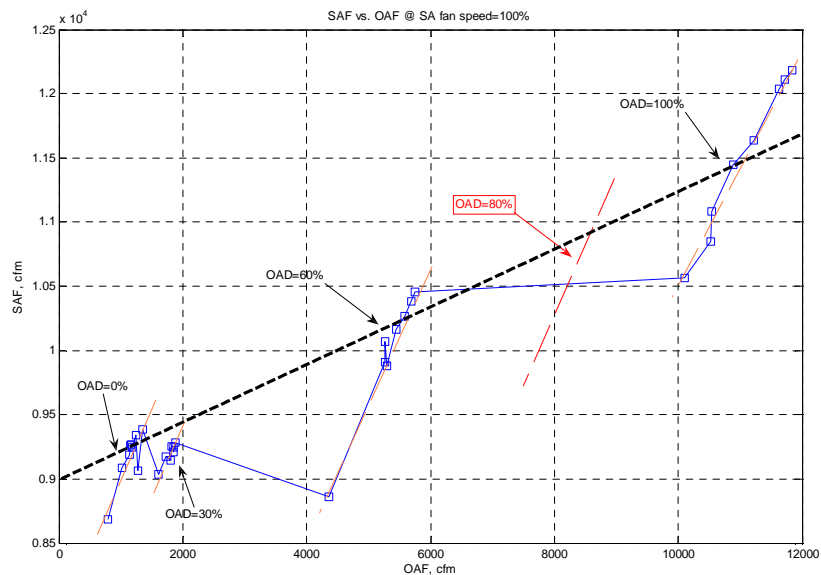


Figure 2.21 Illustration of the volumetric supply and outdoor air flow rates



Using measurement data for the maximum fan speed a linear approximation for the dependency of maximum supply flow rate as a function of the outdoor air flow rate has been generated as a least-squares approximation which is plotted in Figure 2.22: $\dot{V}_{SF}^{max} = 5.094 + 0.227 \cdot \dot{V}_{OA}$ with the units for flows as $[\frac{kg}{s}]$.

Figure 2.22 Illustration of the measured volumetric supply flow rate and outdoor air flow rate for maximum fan speed for different outdoor air damper positions.



Cooling Coil Model

An empirical model of the cooling coil performance was created to allow the maximum cooling capacity of the coil to be computed over the expected range of inlet air temperature and humidity ratio. The HVAC system functional test operating points used to calibrate the model are shown in Figure 2.23 below. The calculated coil power values are calculated simply from the measured

air and water enthalpy differences from inlet to outlet. While the coil thermal cooling power calculated from the water temperature difference and flow rate is always a good match for the value reported by the BTU meter, the air side calculation does not always give such good results. The reasons for this are unknown.

In Figure 2.23, the cooling coil thermal power is plotted against the inlet air humidity ratio for all functional tests in which the airflow over the coil was at maximum and the chilled water valve was fully open. This figure shows that coil total thermal power varies smoothly with inlet enthalpy. An empirical relationship between power and inlet enthalpy was derived in the following form:

$$Q_{Tot,Max} = A_1 \cdot x^2 + A_2 \cdot x + A_3$$

where, $A_1 = 1.29122$; $A_2 = -41.8024$; and $A_3 = 422.483$

A similar relationship was derived between cooling coil latent power and entering air humidity ratio as shown in Figure 2.24.

$$Q_{Tot,Lat} = B_1 \cdot x^2 + B_2 \cdot x + B_3$$

where, $B_1 = 1.53670 \times 10^6$; $B_2 = -2.19985 \times 10^3$; and $B_3 = -34.3187$

These two empirical equations allow the maximum total and latent cooling of the coil to be determined and any valid inlet air condition.

Figure 2.23 Cooling coil thermal power measured by BTU meter compared with values derived from air and water energy balance over a range of test conditions

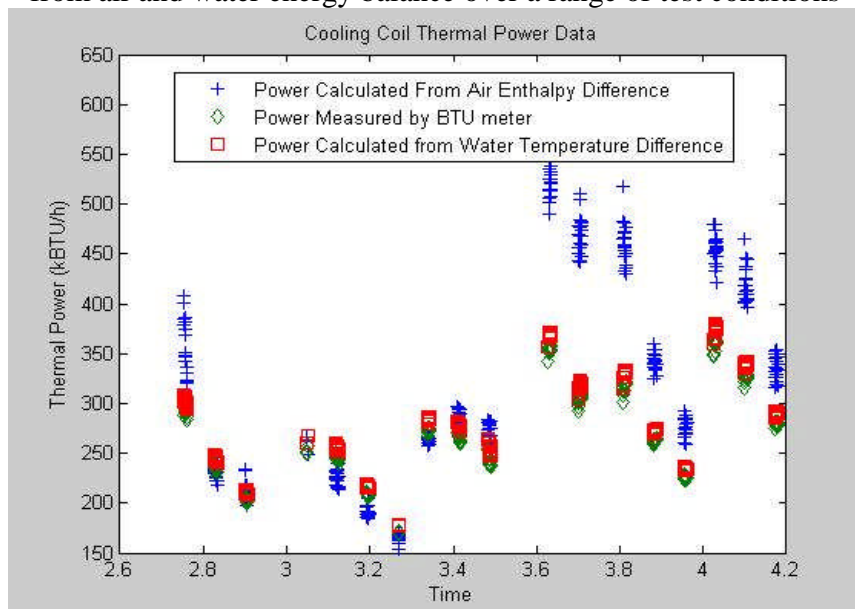


Figure 2.24 Variation of coil total thermal power with entering air enthalpy at full load conditions

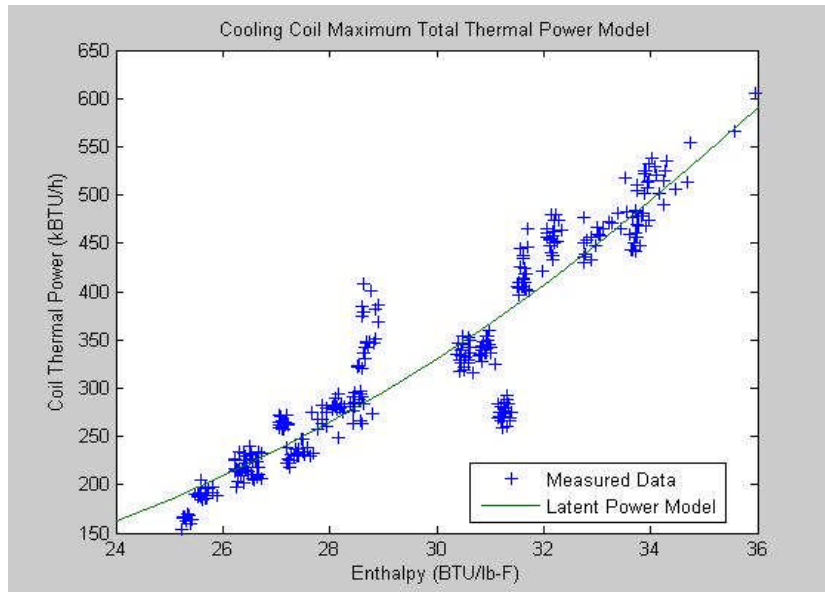
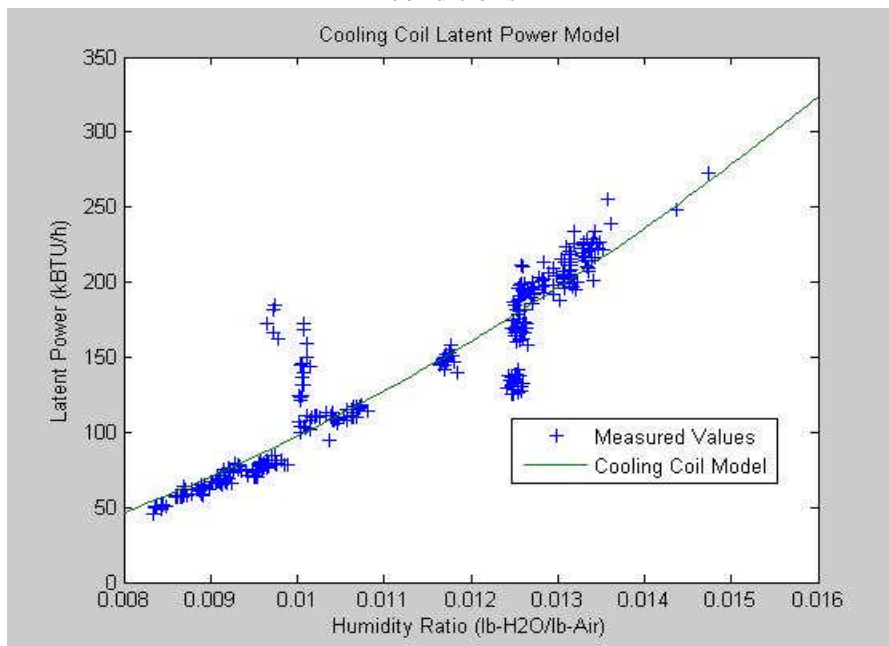


Figure 2.25 Variation of coil latent thermal power with entering air enthalpy at full load conditions



Heating Coil Model

The approach for modeling the heating coil was to assume that the coil performance could be represented by a simple epsilon-NTU formulation. This allows the unknown values of the air outlet and water outlet temperatures to be calculated explicitly in terms of the known air and water inlet temperatures, relative mass flow rates, and the coil effectiveness, which is a

parameter derived from the coil geometry and heat transfer properties. The liquid and air leaving temperatures can be represented as shown in the following pair of equations:

$$\frac{T_{liq,lvq} - T_{liq,ent}}{T_{air,ent} - T_{liq,lvq}} = \varepsilon \cdot \frac{C_{min}}{c_{liq} \cdot \dot{m}_{liq}}$$

$$\frac{T_{air,ent} - T_{air,lvq}}{T_{air,ent} - T_{liq,lvq}} = \varepsilon \cdot \frac{C_{min}}{c_{air} \cdot \dot{m}_{air}}$$

where,

$$\varepsilon = \frac{1 - e^{-NTU \cdot (1-R)}}{1 - R \cdot e^{-NTU \cdot (1-R)}}$$

$$R = \frac{C_{min}}{C_{max}}$$

$$NTU = \frac{UA_{Total}}{C_{min}}$$

$$C_{min} = MIN(c_{air}, c_{liq})$$

$$C_{max} = MAX(c_{air}, c_{liq})$$

and finally,

$$c_{air} = (c_{p,air} \cdot \dot{m}_{air})$$

$$c_{liq} = (c_{liq} \cdot \dot{m}_{liq})$$

In the above formulation, the air and water inlet temperatures can be measured, along with the mass flow rates of the air and water streams. This leaves the values of UA, ε and NTU as unknown parameters reflecting the heat transfer properties of the heating coil; they are expected to vary with \dot{m}_{air} and \dot{m}_{liq} . In practice, the functional dependence of UA on \dot{m}_{air} turns out to be more significant than variation with \dot{m}_{liq} since $C_{min} = c_{air}$ for all reasonable combinations of air and water flow rate for this particular coil.

The value of UA as a function of \dot{m}_{air} , and consequently the values of ε and NTU, was determined by performing a series of functional tests on the heating coil, in which the coil air flow rate and was varied over the expected range of operation of the coil while the coil water flow rate remained fixed. BTU meters and temperature sensors on the water side allowed the heat extracted from the hot water supply to be determined, while temperature and relative humidity sensors upstream and downstream of the coil allowed the heating rate of the coil to the supply air stream to be calculated from conservation of mass and energy. As a result, all the flow variables in the above equations are known measured quantities. UA was assumed to be represented by the following equation:

$$UA = A_1 \dot{m}_{air}^2 + A_2 \dot{m}_{air} + A_3$$

The coefficients in the above equation were determined from the functional test data using a least squares regression. Figure 2.26 shows the result for the coil heat transfer coefficient as a function of coil air flow rate with the coil water flow valve 100% open. This calculation was repeated with the water flow valve 75%, 50%, and 25% open to characterize the part-load performance of the heating coil.

Once the value of UA had been calculated, as in Figure 2.26 above, the predicted coil heat transfer rate could be determined according to

$$\frac{T_{air,ent} - T_{air,lvg}}{T_{air,ent} - T_{liq,lvg}} = \epsilon \cdot \frac{C_{min}}{c_{air} \cdot \dot{m}_{air}}$$

The ratio of heating coil measured thermal output to that predicted from the calculated UA value and its dependence on coil load is shown in Figure 2.27 below. Ideally, this ratio should be unity for a perfect prediction of the coil output. However, since the error seems to increase monotonically as coil output decreases it is possible to use the data in Figure 2.28 to create an additional correction factor to predict the actual coil thermal output. The trend line on the graph is the result of a second order polynomial least squares fit of the data points and it is represented by the equation in the lower right corner of the graph.

Figure 2.26 Heating coil heat transfer coefficient variation with airflow with water flow valve at 100%

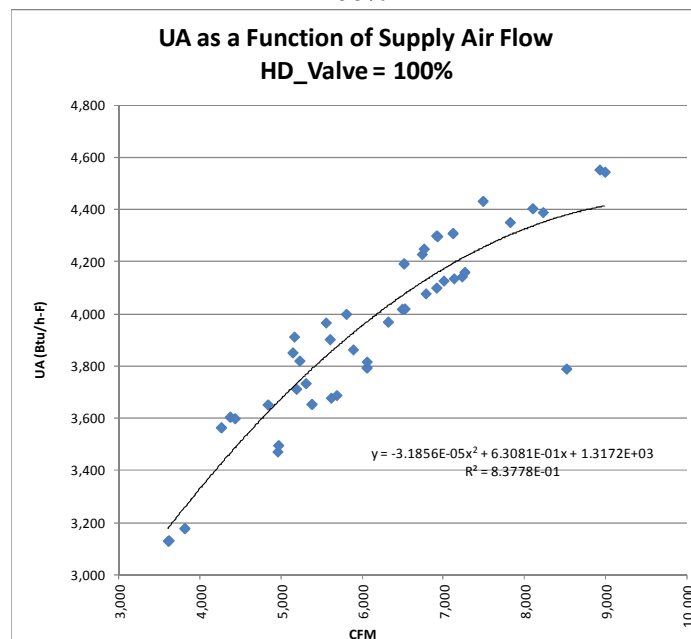


Figure 2.28 is a comparison of the measured heating coil thermal output at several combinations of coil air inlet conditions to the heating coil thermal output predicted from the calculated UA value. The heating coil prediction is shown with and without the capacity correction factor derived from Figure 2.27. As can be seen, the capacity correction improves the coil thermal output prediction significantly over the entire range of coil capacities.

Figure 2.27 Heating coil thermal output correction factor

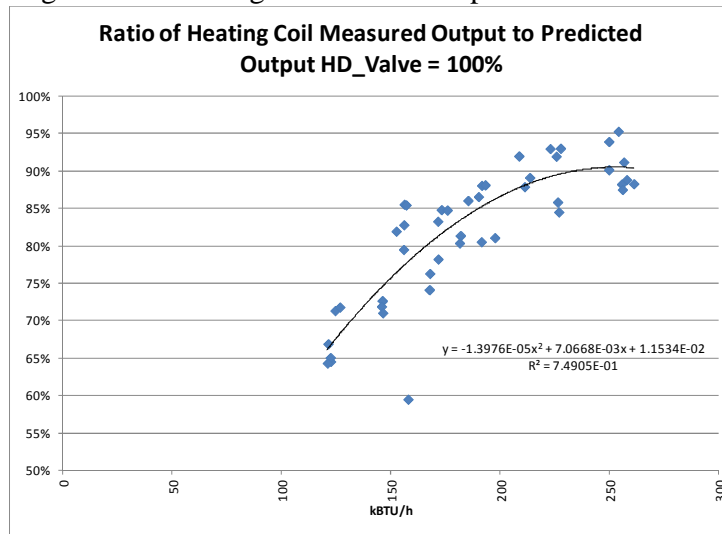
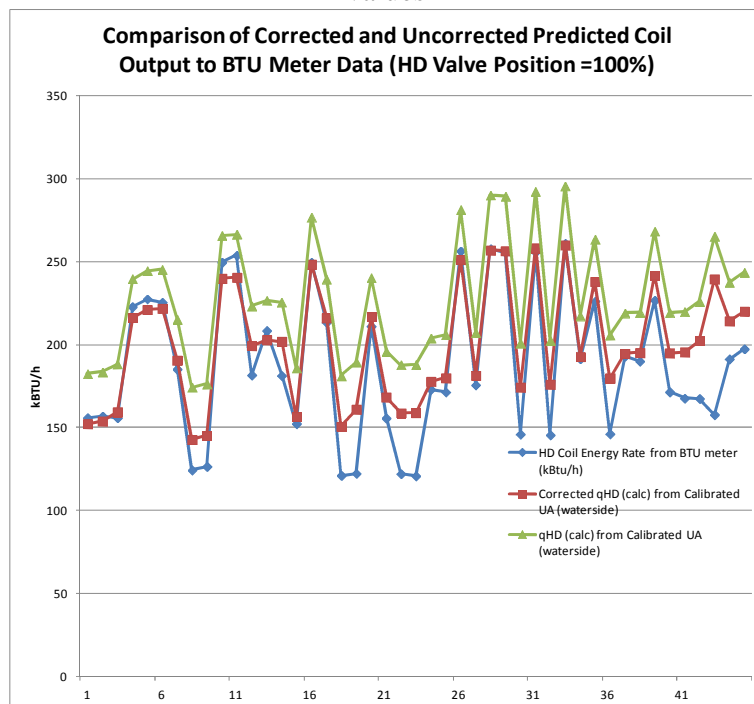


Figure 2.28 Comparison of measured heating coil output to corrected and uncorrected predicted values



Appendix F: Development of Building Thermodynamic Model

The multivariable ARX model considered for each zone has the generic expression given below:

$$A_0 \cdot y(k) + A_1 \cdot y(k - 1) + A_2 \cdot y(k - 2) = B_0 \cdot u(k) + B_1 \cdot u(k - 1) + B_2 \cdot u(k - 2)$$

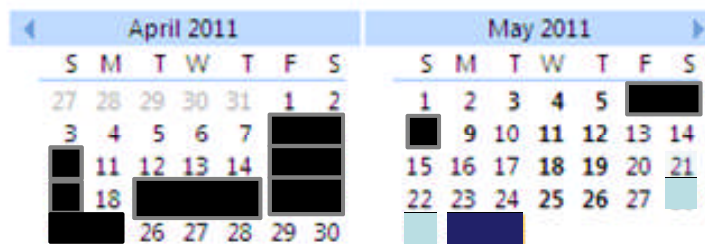
where k is the current time and the sampling time T equals 5[min]. The vector output y and input u of this model are described below.

- Output: is identical to the state described above and consists of the three temperature states: space, plenum and inner roof surface.
- Input: zone supply temperature; total supply flow; product between the zone supply temperature and total supply flow (as a substitute for the energy supplied to the zone); outside air temperature (from NOAA weather forecast); ground temperature (considered constant); solar radiation (from NOAA weather forecast); and plug loads (estimated based on historical data from a Data Acquisition system installed in the building).

The model is used for predicting the zone temperatures for a selected future time interval with all the mentioned inputs, from forecast or estimated based on historical data, and optimization inputs that are generated on-line: supply flow, supply temperature.

Several sets of data were used for calibrating the model as illustrated in the calendar of Figure 2.30. The measurement data set correspond to functional tests for fan and cooling coil, and from post-retrofit system operation available at 15[min] sampling times and that was interpolated at 5[min] intervals.

Figure 2.30 Illustration of the days when data sets were used for: calibration (red and blue) and for validation (grey).



These data sets were used to identify the ARX model matrices using the System Identification toolbox from MATLAB, an engineering technical computational environment. The model calibration and validation results are illustrated below for zone 1 in Figure 2.31 and Figure 2.32, respectively.

Figure 2.31. Comparison between model-based estimation (green) and measurements (black) for space temperature in zone 1 [$^{\circ}\text{C}$].

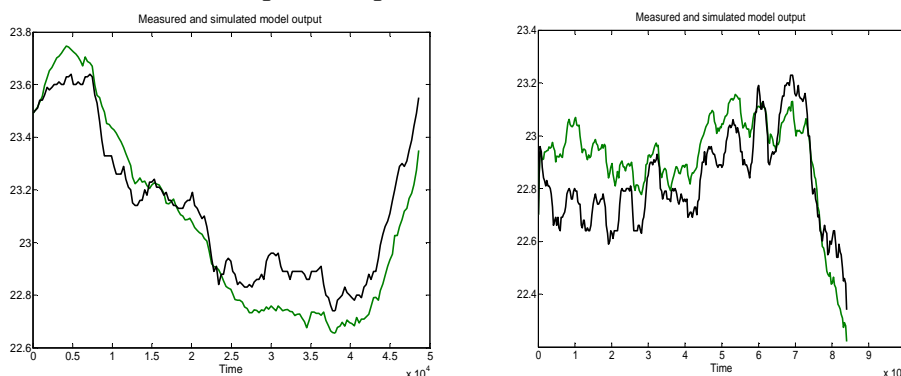
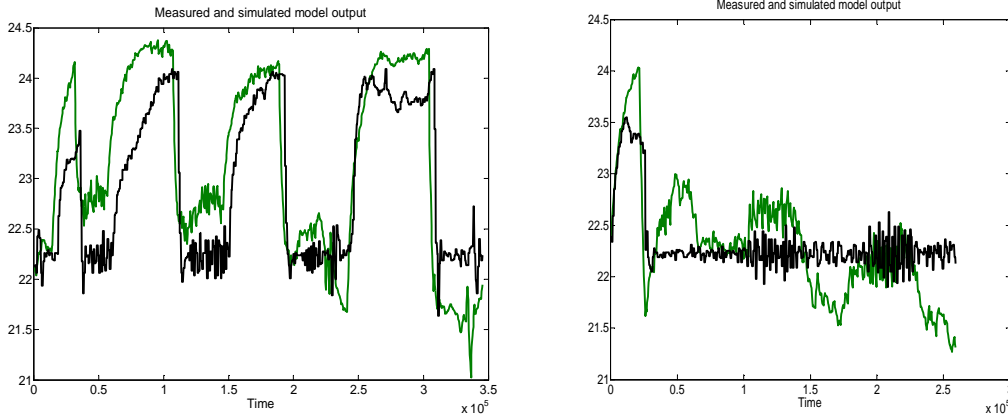


Figure 2.32 Comparison between model-based prediction (green) and measurements (black) for space temperature in zone 1 [°C].



The model validation error is less than 2°C and in most cases it is less than 1°C. These are values that are commonly used. These error levels qualify the model for control design.

Appendix G: Development of Model Predictive Control Algorithm

The following describes the predictive control algorithm formulation and solution approach, involving integration of the system and thermal load models described previously. Combining the HVAC system model from Section 2.2.2.2 and the building thermal model from Section 2.2.2.3, the consolidated model can be expressed as

$$f(x_{k+1|t}, x_{k|t}, u_{k|t}, w_{k+1|t}, w_{k|t}) = 0 \quad \forall k \in \{0, \dots, N-1\}.$$

where $x_{k|t}$ is the value of the state vector at time $t+k\Delta t$ predicted at time t , $u_{k|t}$ is the value of all control inputs at time $t+k\Delta t$ predicted at time t , and $w_{k|t}$ is the value of the disturbance inputs at time $t+k\Delta t$ predicted at time t . The constraints from Section 2.1.2.4 can be expressed as

$$g(x_{k+1|t}, x_{k|t}, u_{k|t}, w_{k+1|t}, w_{k|t}) \leq 0 \quad \forall k \in \{0, \dots, N-1\}.$$

Define the continuous-time one-step cost as

$$J_{k|t}^c = \int_{t+k\Delta t}^{t+(k+1)\Delta t} (r_e P_f + r_e P_c + r_h P_h) d\tau.$$

The integral is approximated according to the trapezoidal discretization. Let $J_{k|t}$ be the discretization of $J_{k|t}^c$.

Model predictive control solves at each time step t the following optimization problem

$$\begin{aligned} & \min_{\mathbf{u}, \mathbf{x}} \sum_{k=0}^{N-1} J_{k|t} \\ & \text{subj. to, } \forall k \in \{0, \dots, N-1\}, \\ & f(x_{k+1|t}, x_{k|t}, u_{k|t}, w_{k+1|t}, w_{k|t}) = 0 \\ & g(x_{k+1|t}, x_{k|t}, u_{k|t}, w_{k+1|t}, w_{k|t}) \leq 0 \\ & x_{0|t} = T_z(t) \end{aligned}$$

where $\mathbf{U} = \{u_{0t}, \dots, u_{N-1t}\}$ is the set of predicted control inputs at time t , $\mathbf{X} = \{x_{1t}, \dots, x_{Nt}\}$ is the set of predicted system states at time t , starting from initial state $x_{0t} = T_z(t)$ and applying the input sequence \mathbf{U} to the system model f .

Let the optimal control input solution at time t be denoted by $\mathbf{U}^\Sigma = \{u_{0t}^\Sigma, \dots, u_{N-1t}^\Sigma\}$. Then, the first step of \mathbf{U}^Σ is input to the system, $u(t) = u_{0t}^\Sigma$. The optimization is repeated at time $t + \Delta t$, with the updated new state $x_{0t+\Delta t} = T_z(t + \Delta t)$ yielding a *moving or receding horizon control* strategy.

The optimization problem has nonlinear cost and nonlinear constraints. In order to solve this optimization problem we use the interior-point nonlinear programming solver Ipopt.

There were three main issues in implementing the MPC algorithm.

1. Real-time optimization calculation speed
2. Guarantees on performance despite model mismatch and prediction uncertainty
3. Convergence to local optima

Issue 1.

Real-time optimization speed was achieved by using a tailored bilinear sparse problem formulation to facilitate gradient calculation, and proper choice of solver to take advantage of sparsity. In particular, we include states as well as control inputs as optimization variables, so the system dynamics are enforced as equality constraints. Additional variables are introduced so that the nonlinear equalities can be expressed in the bilinear form

$$v' C_j v + d_j' v + e_j = 0,$$

where v is a vector that includes all states, control inputs, and auxiliary variables for all time steps, C_j is a square symmetric sparse matrix, d_j is a vector and e_j is a scalar. This tailored bilinear form allows the constraints of the system model to be represented as a set of sparse matrices. The gradients of the constraints, which need to be calculated for the nonlinear programming solver, can hence be computed efficiently by sparse matrix-vector products. Linear inequality constraints are represented in the form

$$Av \leq b,$$

where A is a sparse rectangular matrix and b is a vector.

We initially used the nonlinear programming solver NPSOL but found that as the problem size (number of states, length of prediction horizon) was increased, the convergence speed of NPSOL did not scale well. This is because NPSOL is designed for dense problems; its internal linear algebra operations do not take advantage of sparsity or problem structure. We switched to the solver Ipopt, which is designed for large-scale sparse problems and takes advantage of sparsity in all of its internal linear algebra operations. The performance of Ipopt was orders of magnitude faster than NPSOL for larger problem sizes. Nonlinear inequality constraints due to the coil models were not polynomial functions, so could not be represented using a bilinear form. For these constraints we used Symbolic Math Toolbox to generate analytical gradient functions.

These automatically-generated gradient functions were very lengthy and were observed to be the computationally slowest part of the MPC optimization implementation.

Smart initialization of the solver decreased the number of iterations and hence time required for the optimization algorithm to converge. All of the nonzeros in the matrices C_j were contained in a subset of the rows and columns, corresponding to the control input variables in v . We initialized those variables according to input values from the baseline existing controller. When that subset of variables is held fixed, the equality constraints form a linear system of equations for the remaining variables.

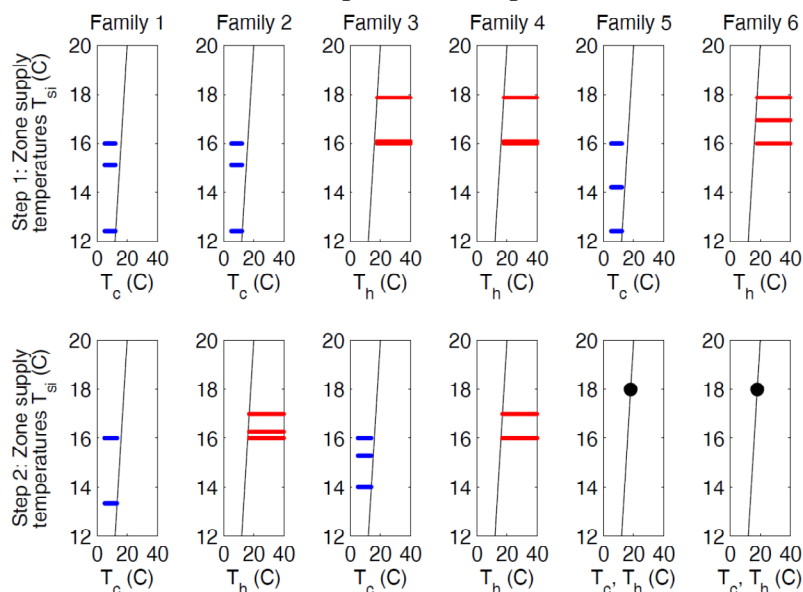
Issue 2.

Model mismatch and prediction uncertainty were not addressed at design and require further investigation for rigorous performance guarantees. We performed extensive simulation to determine the practical sensitivity of our implementation to mismatch and disturbances.

Issue 3.

Because the MPC optimization problem includes nonlinear equality constraints, it is non-convex. Fast nonlinear programming solvers such as Ipopt are not guaranteed to converge to the global optimum solution for non-convex problems. We performed a detailed study on a small simplified instance of the MPC problem with 3 zones and a prediction horizon of 2 steps.

Figure 2.33 Families of local optima for simplified small MPC example



We found 6 distinct families of local optima in this example. At the first time step the locally optimal solutions exhibit two different control modes: a heating mode and a cooling mode. At the second time step, local optima exhibit three different control modes: a heating mode, a cooling mode, and an intermediate mode. Every combination of modes for the first and second time step was feasible, so over the horizon of 2 steps we have six families of local optima. Different local optima belonging to the same family have different heating or cooling coil

setpoints. The cost value, state trajectories, and all other control inputs are equal within a family. The coil setpoints and zone supply temperatures of each family are illustrated in Figure 2.33.

In this example the zones have positive thermal loads so the supply temperatures must be lower than the zone temperatures in order to counteract the loads and remain within the comfort range. Because the zones have different thermal load values, the required supply temperatures will in general be different for each zone. In order for the zone dampers to have enough control authority to meet the required supply temperatures, the heating coil setpoint must be warmer than the highest required supply temperature and the cooling coil setpoint must be cooler than the lowest required supply temperature.

The outside air temperature here is cooler than the zone temperatures so this is an economizer condition. Free cooling is available by using outside air instead of recirculated return air at the AHU, reducing coil energy. The difference between the cooling mode and the heating mode is whether the outside air is cooled or heated before being supplied to the zones. The zones must be cooled in all feasible modes for this example, so the names of the modes here refer only to which coil is active in the AHU.

We hope from this analysis on the simple example we can derive rules that can exclude certain local optima under specific conditions. These rules will apply to all instances of this system model, at every time step, regardless of the number of zones or the length of the prediction horizon. This is a topic of further study.

Appendix H: Procedure for Computation of Quantitative Performance Objective Metrics

Objective 1 – Reduce energy consumption:

Reduction in HVAC electrical energy consumption and demand was driven by implementing the baseline and proposed control strategies on a periodic basis, alternating with each other so as to have weather conditions and building operation very similar during subsequent windows. Further details are provided below.

Calculation –

$$\begin{aligned}
 & \text{kWhbase}_e \\
 &= \sum_{t=1}^b \text{kWhfan}_b \\
 &+ \left\{ \frac{\sum_{t=1}^b \text{MMBtuCC}_b}{(\text{Typical chiller COP})} + \sum_{t=1}^b (\text{MMBtuHC}_b) \right. \\
 & \left. * (\text{Typical boiler eff}) \right\} * mk
 \end{aligned}$$

$$\begin{aligned}
& \text{kWh}_{\text{new}_e} \\
&= \sum_{t=1}^p \text{kWh}_{\text{fan}_n} \\
&+ \left\{ \frac{\sum_{t=1}^p \text{MMBtu}_{\text{CC}_n}}{(\text{Typical chiller COP})} + \sum_{t=1}^p (\text{MMBtu}_{\text{HC}_n}) \right. \\
&\quad \left. * (\text{Typical boiler eff}) \right\} * mk
\end{aligned}$$

$$\text{Savings}_{\text{kWh}_e} = (\text{kWh}_{\text{base}_e} - \text{kWh}_{\text{new}_e}) / \text{kWh}_{\text{base}_e} * 100\%$$

Where:

mk = MMBtu to kWh conversion coefficient

Typical chiller COP = 4.4 (based information from facility manager at CERL of full load power consumption of 0.8 kW/Ton)

Typical boiler eff = 0.75 (information from facility manager at CERL)

t = time step

b = baseline control strategy time frame

p = proposed control strategy time frame

$\text{kWh}_{\text{base}_e}$ = Total fan electrical energy consumption (in kWh) during the time frame when baseline control strategy is being implemented

$\text{kWh}_{\text{new}_e}$ = Total fan electrical energy consumption (in kWh) during the time frame when proposed control strategy is being implemented

$\text{kWh}_{\text{fan}_b}$ = Fan electrical energy consumption (in kWh) at each time step during the time frame when baseline control strategy is being implemented

$\text{kWh}_{\text{fan}_n}$ = Fan electrical energy consumption (in kWh) at each time step during the time frame when proposed control strategy is being implemented

$\text{Savings}_{\text{kWh}_e}$ = Percentage savings in fan electrical energy consumption due to the proposed control strategy

$\text{MMBtu}_{\text{CC}_b}$ = Cooling energy consumption (in MMBtu) at each time step during the time frame when baseline control strategy is being implemented

$\text{MMBtu}_{\text{CC}_n}$ = Cooling energy consumption (in MMBtu) at each time step during the time frame when proposed control strategy is being implemented

$MMBtu_{HC_b}$ = Heating energy consumption at AHU heating-coil (in MMBtu) at each time step during the time frame when baseline control strategy is being implemented

$MMBtu_{HC_n}$ = Heating energy consumption at AHU heating-coil (in MMBtu) at each time step during the time frame when proposed control strategy is being implemented

Objective 2 – Decrease peak electrical power demand:

Same as the assessment method described for Objective 1.

Calculation –

$$kW_{base_e} = \text{Max}(kW_{fan_b} + MMBtu_{CC_b}/(\text{Typical chiller COP}))$$

$$kW_{new_e} = \text{Max}(kW_{fan_n} + MMBtu_{CC_n}/(\text{Typical chiller COP}))$$

$$\text{Savings}_{kW_e} = (kW_{base_e} - kW_{new_e})/kW_{base_e} \times 100\%$$

Where:

kW_{base_e} = Peak electrical power (in kW) during the time frame when baseline control strategy is being implemented

kW_{new_e} = Peak electrical power (in kW) during the time frame when proposed control strategy is being implemented

kW_{fan_b} = Fan electrical power (in kW) at each time step during the time frame when baseline control strategy is being implemented

kW_{fan_n} = Fan electrical power (in kW) at each time step during the time frame when optimal control strategy is being implemented

$MMBtu/hr_{CC_b}$ = Cooling demand (in MMBtu/hr) at each time step during the time frame when baseline control strategy is being implemented

$MMBtu/hr_{CC_n}$ = Cooling demand (in MMBtu/hr) at each time step during the time frame when optimal control strategy is being implemented

Savings_{kW_e} = Percentage savings in peak electrical power due to optimal control strategy

Objective 3 – Decrease CO2 emissions

Same as the assessment method described for Objective 1. The CO2 emissions will be calculated by multiplying the electric and gas usage with CO2 emissions factors.

Calculation –

$$\text{CO2}_{\text{base}} = \sum_{t=1}^b (\text{kWhfan}_b + \frac{\text{MMBtuCC}_b}{(\text{Typical Chiller COP})} * mk) * e_{\text{co2}} + \sum_{t=1}^b (\text{MMBtuHC}_b) * (\text{Typical boiler eff}) * h_{\text{co2}}$$

$$\text{CO2}_{\text{new}} = \sum_{t=1}^b (\text{kWhfan}_n + \frac{\text{MMBtuCC}_n}{(\text{Typical Chiller COP})} * mk) * e_{\text{co2}} + \sum_{t=1}^b (\text{MMBtuHC}_n) * (\text{Typical boiler eff}) * h_{\text{co2}}$$

$$\text{Savings}_{\text{CO2}} = (\text{CO2}_{\text{base}} - \text{CO2}_{\text{new}}) / \text{CO2}_{\text{base}} * 100\%$$

Where

$$h_{\text{co2}} = \text{CO}_2 \text{ emissions for natural gas (120.593 lbs/MMBtu) [13]}$$

$$e_{\text{co2}} = \text{CO}_2 \text{ emissions for electricity (1.16 lbs/kWh for Illinois) [14]}$$

Objective 4 – Decrease in sensor installation cost:

For the section of the building selected for this project, the data related to costs of wireless sensors and their installation and commissioning will be compared with the costs of equivalent wired sensor network and its installation. The costs of wired sensors network and its installation will be obtained as quote from the same vendor who would install the wireless sensors. The costs would consist of sensors costs, installation cost, and commissioning costs.

Calculation –

$$\text{Costs}_{\text{base}} = \text{Costs-wired sensors (\$)} + \text{Costs-wired sensors installation (\$)} + \text{Costs-wired sensors commissioning (\$)}$$

$$\text{Costs}_{\text{new}} = \text{Costs-wired sensors (\$)} + \text{Costs-wired sensors wiring (\$)} + \text{Costs-wired sensors installation (\$)} + \text{Costs-wired sensors commissioning (\$)}$$

$$\text{Savings}_{\text{costs}} = (\text{Costs}_{\text{base}} - \text{Costs}_{\text{new}}) / \text{Costs}_{\text{base}} * 100\%$$

Objective 5 – Maintain/Improve Temperature Regulation:

The occupancy sensor data for each zone will be reduced to create a binary value indicating whether that zone is occupied or not. The temperature regulation error (absolute value) will be integrated during the periods of occupancy on a weekly basis. This calculation will be repeated for baseline control operation & operation with the MPC control strategy. The two values will be compared to ensure that temperature regulation performance is not sacrificed when realizing the energy savings.

Calculation –

Zone_occupancy = 0 or 1 based on occupancy sensor data (PIR, CO₂ and PC sensors) and occupancy estimator output

$$\text{Temperature_error} = \sum_{\text{all zones}} \sum_{\text{occupied time in a week}} |T_{\text{measured}} - T_{\text{setpoint}}| \Delta t_{\text{sampling}}$$